UNIVERSITÉ DE BOURGOGNE

Ecole Doctorale Environnement - Santé / STIC (E2S)

THÈSE

Présentée par

Mohammad IQBAL

pour obtenir le grade de

Docteur de l'Université

Discipline Instrumentation et Informatique de l'Image

Polarization Stereoscopic Imaging Prototype

Soutenue le 2 Novembre 2011

Jury

Fabrice MERIAUDEAU	Professeur	Directeur de thèse
Sarifuddin MADENDA	Professeur	Rapporteur
Abdelaziz BENSRHAIR	Professeur	Rapporteur
Samia AINOUZ (ZEMOUCHE)	Maître de conférences	Examinateur
Olivier MOREL	Maître de conférences	Encadrant de thèse

For my Parents, my wife and my children…

If all the trees on earth become pens, and the sea replenished by seven more seas were to supply them with ink, the Words of God would not be exhausted. He is indeed Most Mighty, Most Wise... (Luqman 27)

Acknowledgements

Thanks to God because only with God's help and permission I can finish this thesis in time. This thesis work has been performed at Laboratoire Electronique, Informatique et Image (LE2I) – IUT Le creusot, Université de Bourgogne, France with financial support from National Education Department of Republic of Indonesia in *Beasiswa Unggulan* program and Universitas Gunadarma, Jakarta, Indonesia.

With all of my modesty, I want to take this opportunity to thank everyone who has helped me in one way or another during this thesis work period.

My deepest gratitude is to my supervisor Fabrice Mériaudéau and co-advisor Olivier Morel, for their effort, guidance, support and patience that allowed me to finish this thesis.

I am also grateful to Prof. Dr. E.S.Margianti, SE., MM., as Head of Gunadarma University and Prof. Dr. Suryadi Harmanto,SSI, MMSI as 2nd Assistance of Head of University that give me a valuable advice support and encourage. Appreciations are also expressed to Prof. Dr. Sarifuddin Madenda, Prof. Dr. Djati Kerami, Mrs. Trini Saptariani, Mrs. Peni Sawitri, Mrs. MS. Harlina, Mrs. Rini Tesniwati and Dr. Yuli Karyanti for their remarkable support.

Of my colleagues in LE2i-IUT Le Creusot, I want to express particular thanks to Abd-el-rahman Shabayek and Rindra Rantoson, for a lot of assistance to refresh my knowledge in programming and mathematics. Deep thanks to helpful friends who have delivered valuable time and effort in my study ; Youssef, Ouadi, Ahlam, Bushra, Souhail, Nicholas, Intuon, Pierre and Alban. Also friends from master VIBOT ; Adhiguna, Arun, Arsalan, Naveed, Moazzam, Ruddy JS, and friends from Master of Computer Vision ; Kassem, Ali Mirzae, Diou, and Amine Mahiddin for sharing idea and for our fun time.

I am blessed with wonderful friends that I could not stated one by one here in many ways, my successes are theirs, for mas Aries, mbak Cut, mbak Ira, Fitrin, Dian,

Debyo, Musa, Imam Ahmad and Franco-Indo family such as mbak Agnes and Jean Louis, mbak Yati and Serge, Bang Ujai and Briggitte, Julia, Zooran, Inez, and also Vicky, for their support and to teach me how to live in Dijon and Le Creusot. Also for all brothers from Association Musulmane et Cultuelle Du creusot - Sheik Larabi Basyir and from Communaute Islamique De Milli Gorus Section de le Creusot - Sheik Mohamed.

To my parents, Mohammad Rais Ahmad and Sri Astuti Rais, Prof. Dr. AM Saefuddin and Ati Surtiati, my sister Ummu Najiyah (Allahu yarham), Ani Khairani, Ibrahim Fajri and all of my big family, I greatly appreciate for their taken care of my wife and children when I was absent during my research time and the sincere prayer that never stops to strengthen my spirit here.

Most importantly, I want to express thanks to my wife Dina Diana who has stayed long far away from me with our lovely children. She had difficult period, but still she ensured the ideal and warm atmosphere for me here. To all my children Alwan Muhammad Zaidan, Maryam Rif'atul Afifah and Nusaibah Karima Zuhda, the hope and your smiling was a great motivation to me to finish this research, and I dedicate this thesis to you all. What I am today, it cannot be happened without their love, support, and sacrifice.

Finally, thanks for all the others that have contribution to this work and cannot be mentioned one by one. I realize that there are no perfect things in this world, same as this thesis. Therefore, I am looking forward to get some encouraging critics, advices and suggestions from anyone to make it better. It is wonderful and proudly if all people can use and take advantage of this thesis.

Abstract

The polarization of light was introduced last ten years ago in the field of imaging system is a physical phenomenon that can be controlled for the purposes of the vision system. As that found in the human eyes, in general the imaging sensors are not under construction which is sensitive to the polarization of light. These properties can be measured by adding optical components on a conventional camera. The purpose of this thesis is to develop an imaging system that is sensitive both to the stereoscopic and to the state of polarization. As well as the visual system on a various of insects in nature such as bees, that are have capability to move in space by extracted relevant information from the polarization. The developed prototype should be possible to reconstruct three-dimensional of points of interest with the issues associated with a set of parameters of the state of polarization.

The proposed system consists of two cameras, each camera equipped with liquid crystal components to obtain two images with different directions of polarization. For each acquisition, four images are acquired: two for each camera. Raised by the key of main capability to return polarization information from two different cameras. After an initial calibration step; geometric and photometric, the mapping of points of interest process is made difficult because of the optical components placed in front of different lenses. A detailed study of different methods of mapping was used to select sensitivity to the polarization effects. Once points are mapped, the polarization parameters of each point are calculated from the four values from four images acquired. The results on real scenes show the feasibility and desirability of this imaging system for robotic applications.

Keywords: Stereo Vision, Stereo Matching, Polarization Imaging, feature extraction

Resumé

La polarisation de la lumière, phénomène physique parfaitement maîtrisé, a été introduit depuis une dizaine d'années seulement dans le domaine de l'imagerie. En effet, tout comme l'oeil humain, les capteurs ne sont pas, par construction, sensible à la polarisation de la lumière. Cette propriété particulièrement intéressante ne peut être obtenue qu'en ajoutant des composants optiques aux caméras classiques. L'objectif de ce travail de thèse est de développer un système à la fois stéréoscopique et sensible à l'état de polarisation. En effet, de nombreux insectes dans la nature, comme les abeilles par exemple, ont la capacité à s'orienter dans l'espace et à extraire des informations pertinentes issues de la polarisation. Le prototype ainsi développé doit permettre de reconstruire en trois dimensions des points d'intérêt tout en associant à ces points un ensemble de paramètres relatifs à l'état de polarisation.

Le système proposé ici est constitué de deux caméras équipés chacune de deux composants à cristaux liquides permettant d'obtenir deux images avec des orientations de polarisation différentes. Pour chaque acquisition, quatre images sont obtenues : deux pour chacune des caméras. Le verrou majeur soulevé ici est la possibilité de remonter à des informations de polarisation à partir de deux caméras différentes. Après une première étape de calibration géométrique et photométrique, la mise en correspondance des points d'intérêt est rendue délicate en raison des composants optiques placés devant les objectifs. Une étude approfondie des différentes méthodes de mise en correspondance a permis de sélectionner la méthode la moins sensible aux effets de polarisation. Une fois les points mis en correspondance, les paramètres de polarisation de chacun des points sont calculés à partir des quatre valeurs issues des quatre images acquises. Les résultats obtenus sur des scènes réelles montrent la faisabilité et l'intérêt d'un tel système pour des applications robotiques.

Mots clés : imagerie polarimétrique, stéréovision, mise en correspondance, reconstruction 3D

Table of Contents

List of Tables

List of Figures

Chapter 1
Introduction

This chapter will give a brief outline of the research, which consists of:

1. *A brief background of this study.*
2. *Overview of this study in general.*
3. *The research contribution to research of stereo vision and polarization imaging.*
4. *Organizational thesis, the overview of contents of each chapter.*

The main function of polarization imaging camera is to perform fixed quantity analysis of the polarization of light. In the last decades, polarized light has been widely used in optical devices and displays in the computer vision field. Polarization imaging permits to infer information about the orientation/direction of vibration/oscillations as well as a measure of the amplitude (brightness) and wavelength (color) which are familiar qualities, to many researcher. In nature, details about the source of light and the reflecting surface can be ascertained from the polarization state of light. It fact is widely believed that insects, such as some species of ants and bees, use polarized light to determine the position of the sun, position of their nests and identify flowers [Wehner (2001)]. The important advantages of polarization can be easily applied in it simplest form, by just adding a polarizer in front of a camera, leading to various application in the various areas of computer vision, such as 3D reconstruction of shape, object recognition and so on.

Beside polarization vision ability, in the nature, some insects also make use of the two eyes to see and identify object. Meaning they also utilize a stereo vision system besides their ability to extract polarization information from the light. The stereo vision

system is a well known technique for obtaining depth information from different view in a pair of images. The one challenge is to find correspondences between two images. Once the correspondences between the two images are known, the depth information of the objects in the scene can be easily obtained by triangulation. This is the motivation of our research, we aim at developing an imaging system able to extract polarization information based-on a stereo system.

1.1 Background

The polarized light is the light in which there is a preferred direction for the electric and magnetic field vectors in the wave. In unpolarized light, the waves come with electric and magnetic field vectors in random directions. In linearly polarized light, the electric field vectors are propagating all along in oneline. So are the magnetic field vectors that are perpendicular to the electric field vectors. Most light sources emitt unpolarized light, but there are several ways to polarize it. There are three main ways for the light to become polarized:

1. Polarized light by reflection. When Light reflects from a surface, it will tend to be polarized, with the direction of polarization (the electric field vectors) being parallel to the plane of the surface.
2. Polarized light by selectively absorbing light. Some materials can absorb light polarized in one direction, but do not absorb light polarized perpendicular to that direction. These materials are known as dichroic materials. If the material is thick enough to absorb all the light polarized in one direction, the emerging light from the material will be linearly polarized.
3. Polarized light by scattering. Light scattered off atoms and molecules in the atmosphere is un-polarized if the light keeps traveling in the same direction, but becomes linearly polarized if scattered in a direction perpendicular to the incident direction.

1.1.1 *Polarization Vision*

The use of polarization light as a vision system can be found in nature. Since the late 1940's, the researchers attempted to look for Polarization-vision elsewhere and found it in an extraordinary range of animals, including fish, octopuses, arthropods and amphibians. These animals can see and use the polarization of light not only as a compass for navigation, but also to detect surfaces alike water, to enhance visual ability (similar to colors recognition), and even to communicate between each other. There are special instruments on animals that make them be able to see the extra dimension of reality, something mostly invisible to human without the aid of optical instrument. Early in this study, Karl von Frisch, the Austrian ethologist in 1944, discovered that honey bees could sense the polarization state as well as sense the earth's magnetic field and have a unique behaviour movement called "*waggle waggle dance*". These dances based on gravitational cues and knowing the location of the sun as the key reference point (the sun sense and the polarization sense were found to be closely related) and can be used to give directions to other honey bees, to indicate where a distant food source may lie. Incredibly, they have been found to use this dance when a food source is located 100 meters or more away from the hive.

The human's eyes have a minor sensitivity to see polarized light. Human is able to distinguish polarized from non-polarized light only very mildly without the aid of other visual/optical instrument. Polarization state will appear as a small yellow and blue bowtie image in the center of the visual field, called Haidinger's Brush-- as discovered by Haidinger in 1846. However, if the polarization filter could be assembled on the human eye, it will be easier to distinguish it.

The use of polarized light by the human goes back to the Vikings era. In 1967, a Danish archaeologist, Thorkild Ramskou, suggested that the Vikings might have used the polarization of the skylight for orientation when clouds were hiding the sun position by use of crystalline "sunstone" called "saga" for navigational purposes. This fact was affirmed also in 1995 by Gabor Horvath from Budapest university [Horvath (1995)], who demonstrated that Vikings might have required some kind of devices, other than just the naked eye, to accurately guess the position of the sun on cloudy days. Hovart also gives

an illustration about what has been seen by Vikings in the sky as a guide direction through a crystal. Crystals are known as one of optical instrument to produce a polarized light. This instrument could have been used to gather the position of a light source, moreover for some kinds of crystals such as quartz, tourmaline, or cordierite, they could be used to indicate the angle of incoming sunlight through changing color and brightness, and that could indicate the position of the sun, indirectly through polarized sunlight patterns in the sky.

The progress research a polarization of light in the computer vision literature was introduced by the work of Koshikawa in 1979, who tried to take advantage from the linear polarization. Since then, research has been growing faster, to get even more advantages of the polarization of light, thus until now, more extensive application of Polarization Vision was developed, such as image identification, Shape estimation, dielectric or metal discrimination, navigation of autonomous vehicle and other.

In the computer vision field, difficulties and challenges in polarization can be identified as follows:

1. How to capture good/high quality Polarized light image?
2. How to improve quality of image from poor polarized light image?
3. How to extract polarized light information features to obtain the polarization template?
4. How to classify or verify polarization information of an object in a scene ?

1.1.2 *Stereo Vision*

Stereo vision systems estimate the values directly from stereo pairs of images. The main task involves to solve two sub-problems: The correspondence problem and the reconstruction problem. This research uses stereo pairs of images to calculate, through triangulation, the depth of corresponding pairs of points from each image. These corresponding points, known as conjugate pairs, are determined by a search process that utilises image cues, such as contrast and texture, to find matching points.

The correspondence problems have some difficulties, such as texture, shading, and depth occlusion. Texture and shading are useful cues when searching for

corresponding points. It relies on the assumption that appearance of the objects is consistent between stereo views, but this can be erroneous, when observing surfaces exhibiting specular reflection. On the other hand, when the feature is visible to one camera, but not to the other, it occurs the occlusion. This condition caused by areas of the same object or by other objects that are closer to the camera and lie along the same line of sight. Solving the correspondence problem gives a set of disparities (distances between corresponding point), which is termed as the disparity map. Reconstruction of 3D models is possible through use of the disparity map and knowledge of the geometry of the system.

1.1.3 *Scope and Objective*

This research is focused on building a prototype of stereo imaging system with polarization sensitivity and developing a simple and fast polarization imaging algorithm based-on stereo vision to be implemented on smart camera devices. The algorithm will combine the advantage from polarization imaging and stereo vision system and it will be based-on correspondence stereo to extract polarization information. For testing and performance evaluation, we create a simple data sets and the algorithm were developed and simulated using Matlab programming. This research attempts to answer the following questions :

1. How to develop an imaging system that can accommodate Polarization imaging system and Stereo vision system computation?
2. How to develop an algorithm to extract polarization information from founded feature matching in stereo vision system that are adaptable to implementation using smart camera device?

Therefore, the objectives of this research are, (1) to obtain Stereo Imaging system setup with ability to sensing polarized light (2) to obtain simple (hardware adaptable, low complexity) polarization information extraction algorithm from stereo vision system and properly implement them on smart cameras.

1.2 Research Overview

This thesis starts with an introduction into imaging polarimetry and stereo vision, an efficient technique for measuring light polarization from stereo images, and moves onto some tests and evaluations to present improved results from a polarization stereoscopic imaging prototype. The final aim is to develop a simple and low cost polarization sensitive imaging system setup with parallel acquisition using a stereo system.

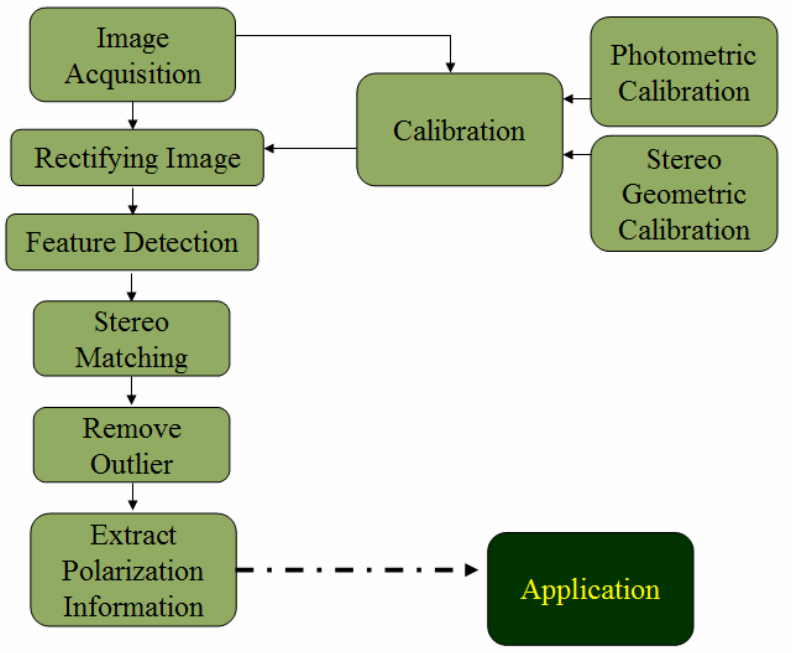

Figure 1.1 Flowchart system

1.2.1 *Polarization Imaging from Stereo Vision*

This research will deal with many techniques borrowed from stereo vision and polarization imaging. As seen in Figure 1.1, Stereo vision system steps consist of:

1. Images acquisition techniques, including stereo imaging system setup scheme.
2. Geometric calibration to obtain camera internal and external parameter of stereo imaging system.
3. Rectifying images technique and epipolar geometry.
4. Feature detector, stereo Matching and removing outliers.

And Polarization imaging steps consist of :

1. Images acquisition techniques, including polarizer filter setup in stereo imaging system.
2. Polarization Calibration
3. Extracting polarization information

1.2.2 *Experimental Evaluation*

In the experiment, a number of algorithms concerning stereo vision and polarization imaging part are developed. In this research, apart from choosing the best stereo matching score algorithm that can accommodate polarized images, we also determine the best stereo polarization imaging system installation. From here, the performance of the imaging system and the extracted polarization information algorithm are obtained and tested with comparison the polarized information extracted from our system and a ground truth (known polarization).

1.3 Contribution

The major contribution of this thesis is a proposed scheme of stereo imaging system, capable of extracting polarization information and with a simple but reliable algorithm. The main contributions of this project include :

- A review of the state-of-the-art polarization with stereo vision techniques.
- The demonstration of imaging system with capabilities of being polarized light sensitive and an investigation of its applicability in using stereo vision tasks.
- Arrange the best stereo camera and polarizer setup and develope an algorithm capable to make a selection of interest points on a stereo rectified image and display the stereo correspondences on the other images computing using the best local matching scores for polarization images.
- Analysis of different local stereo matching techniques to determine the optimal approach for uses in polarization imaging.

1.4 Thesis Organization

This thesis is organized as follows :

Chapter 1 Introduction, presents the background, scope and objective, research overview as well as contributions of this thesis.

Chapter 2 Polarization Imaging, explains the background theory related to the polarization of light and polarization imaging. It concludes with an overview the basic theory related to the proposed scheme.

Chapter 3 Polarization Imaging Toward a Physical-based Robotics Vision, This chapter contains a state of the art techniques or methods that were developed to represent polarization information. It consists of bio-inspiring polarization sensitive ability possessed by animals, the development of the system producing the polarization, and the application associated with the skills needed in robotic vision.

Chapter 4 Polarization Imaging Using Stereo Vision, addresses the problem definition of polarization Imaging with stereo vision and its associated difficulties. It consists of a presentation of background theory related to stereo vision system, and the detail discussion of the proposed polarization stereoscopic imaging setup as well as the performance evaluation of the proposed scheme.

Chapter 5 Conclusion and Perspectives, concludes the thesis with the summary of this thesis as well as suggestions for future enhancements.

Chapter 2
Polarization Imaging

This chapter discusses about theoretical background of polarization imaging. It consists of :

1. *Polarization light model.*
2. *Mathematical representation of polarization.*
3. *Polarization in outdoor scenes, polarization generator instrument and simplified polarization imaging.*
4. *Visual Representation of polarization images.*

2.1 Polarization Light Model

Polarization is a common property to all types of vector waves including electromagnetic (EM) waves. The light is also an EM wave, and the polarization state of the light can be determined by analyzing only the electrical field strength (E).

In nature scenes, the vibrations of each light beam have different orientations without any specified direction. In some cases, however, all the waves in rays beam can vibrate in parallel planes in the same direction. The light is polarized, because it has a directional characteristic. More specifically, the light is also said to be linearly polarized, or circularly or elliptically polarized light (it will be discussed later). Most of the light sources such as the sun, bulb or a candle provide un-polarized light. Thanks to reflection, refraction, transmission, and scattering the light can become partially polarized.

2.1.1 *Plane Waves*

The electric field in the plane waves can be decomposed into components parallel and perpendicular to the plane of incidence. Their behaviour during reflection and refraction phenomena are independent. So, the EM field can be treated as a superposition of two plane-polarized waves, which can form a basis for generating any other polarization state.

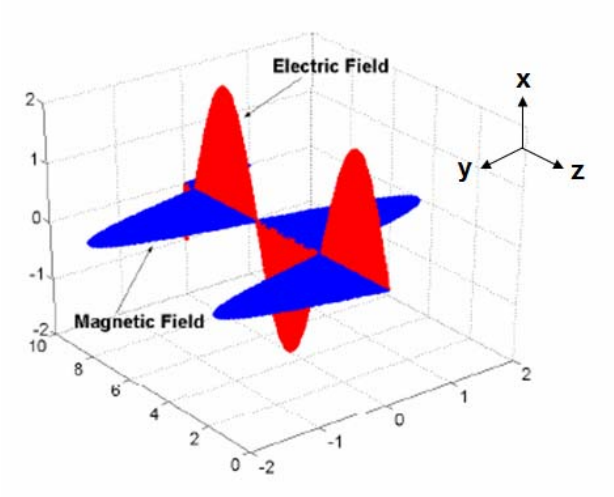

Figure 2.1 Plane Propagation of Waves

The polarization state can be obtained from analyzing the electric field only. As Illustrated in Figure 2.1, all EM light waves are composed of an electric (E) and a magnetic (B) field vectors that are mutually orthogonal to each other and to the direction of propagation. It is assumed that the direction of propagation, $\vec{k}$, is in the z direction. Polarization states arise from relationships between the magnitude and phase of the orthogonal components of $\vec{E}$ (i.e. $\vec{\mathrm{E}}_{\mathrm{x}}$ and $\vec{\mathrm{E}}_{\mathrm{y}}$). In general, $\vec{E}$ can be described mathematically by :

$$\vec{\mathrm{E}} = \vec{\mathrm{E}}_{\mathrm{x}}(\mathrm{z},\mathrm{t}) + \vec{\mathrm{E}}_{\mathrm{y}}(\mathrm{z},\mathrm{t}) \tag{2.1}$$

where $\vec{\mathrm{E}}_{\mathrm{x}}$ and $\vec{\mathrm{E}}_{\mathrm{y}}$ are given by

$$\vec{\mathrm{E}}_{\mathrm{x}}(\mathrm{z},\mathrm{t}) = \vec{\mathrm{E}}_{0\mathrm{x}} \cos(\tau + \delta_x) \tag{2.2}$$

$$\vec{\mathrm{E}}_{\mathrm{y}}(\mathrm{z},\mathrm{t}) = \vec{\mathrm{E}}_{0\mathrm{y}} \cos(\tau + \delta_y) \tag{2.3}$$

where $\tau = \omega t - kz$ is the propagation term and ω is the angular frequency :

$$\omega = 2\pi f \tag{2.4}$$

where f is the temporal frequency and k is the wave number :

$$k = \frac{2\pi}{\lambda} \tag{2.5}$$

and t is time, δ_x and δ_y are the phase angles of $\vec{E}_x$ and $\vec{E}_y$ respectively, and $\vec{E}_{0x}$ and $\vec{E}_{0y}$ are the peak magnitudes in the x and y directions. The complete equation is

$$\vec{E}_x(z,t) = E_{0x}\cos(kz-\omega t+\delta_x)\,\vec{x} \tag{2.6}$$

$$\vec{E}_y(z,t) = E_{0y}\cos(kz-\omega t+\delta_y)\,\vec{y} \tag{2.7}$$

2.1.2 *Types of Polarization*

The most general form of polarized light is the elliptical polarization. Linear and circular polarizations are simply special degenerate cases of elliptical polarization. The type of polarization is determined by the relative magnitude and phase difference between the two orthogonal components of vector E.

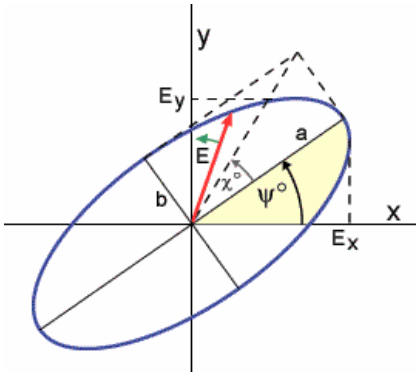

Figure 2.2 The Polarization Ellipse

Figure 2.2 represents the electric vector $\vec{E}$ of a complete polarized wave in the x-y plane in the ellipse form. It can be represented by four quantities ; size of minor axis "b", size of major axis "a", orientation angles "ψ", and sense of ellipticity "χ" (Clock Wise, Counter Clock Wise). From equation (2.6) and (2.7), the equation of the ellipse can be found to be :

$$\left(\frac{E_x}{E_{0x}}\right)^2+\left(\frac{E_y}{E_{0y}}\right)^2-2\frac{E_x}{E_{0x}}\frac{E_y}{E_{0y}}\cos\,\delta=\sin^2\,\delta \tag{2.8}$$

where

$$\delta=\delta_y-\delta_x \tag{2.9}$$

Any instant of time the points spot described by the optical field as it propagates in ellipse form can be described by Equation (2.8).

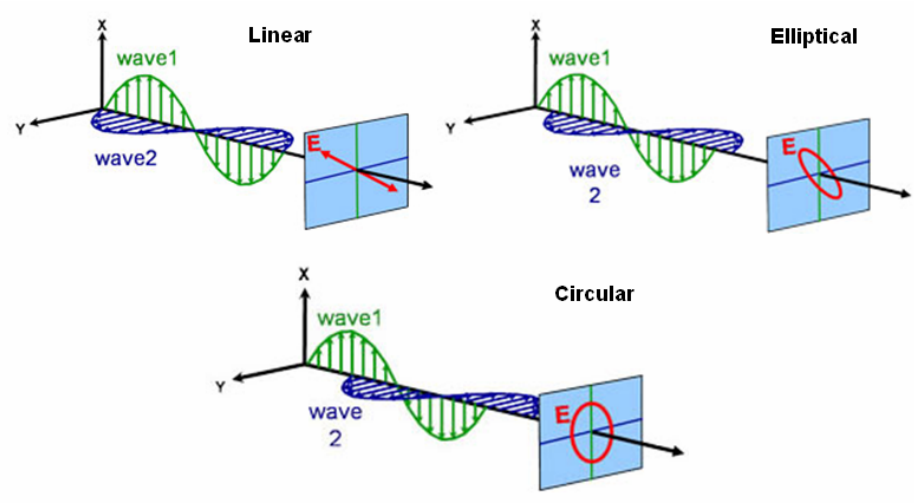

Figure 2.3 Polarization Classification [Woollam (2011)]

If two plane waves of different amplitude are related in phase by 90°, or if the relative phase is other than 90° then the light is said to be elliptically polarized. If the electric field of light remains in a fixed plane and the vibration are confined to a single plane, then the light is said to be linear polarized. If light is composed of two plane waves of equal amplitude by differing in phase by 90°, then the light is said to be circularly polarized.

2.1.2.1 Linear polarization

Linear polarization occurs when the two orthogonal plane waves have the same phase but possibly different amplitudes. The transverse electric field wave is accompanied by a magnetic field wave as illustrated in Figure 2.4.

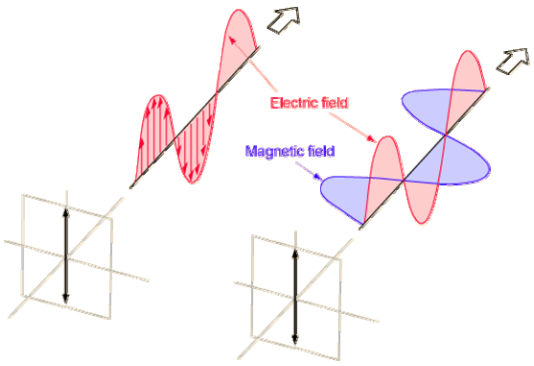

Figure 2.4 Linear Polarization (picture courtesy of Department of physics and astronomy Georgia State University)

For light to be linearly polarized, the following condition has to be true

$$\delta = \delta_x - \delta_y = 0 \tag{2.10}$$

Substituting it, into equations (2.2) and (2.3), and the results in cosine terms for $\vec{E}_x$ and $\vec{E}_y$ put in equation (2.1), the equation becomes

$$\vec{E} = (\vec{E}_{0x} + \vec{E}_{0y})\cos(\tau + \delta) \tag{2.11}$$

If there is no amplitude in x ($\vec{E}_{0x} = 0$), there is only one component, in y (vertical), it called linear vertically polarized light, otherwise if there is no amplitude in y ($\vec{E}_{0y} = 0$), it called linear horizontally polarized light. If there is no phase difference ($\delta = 0$) and $\vec{E}_{0x} = \vec{E}_{0y}$, then $\vec{E}_x = \vec{E}_y$, will cause the light become linear polarized at 45º.

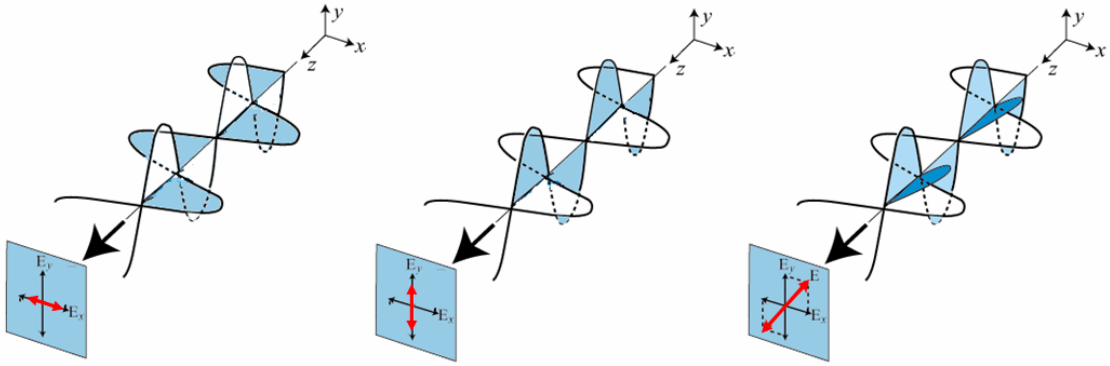

Figure 2.5 Light Polarized Linear vertical, horizontal and 45° (picture courtesy of Department of physics and astronomy Georgia State University)

2.1.2.2 Circular polarization

Circular polarization is a polarization state in which the two perpendicular components of the electric field have equal amplitude and a 90-degree phase difference. In this case, the tip of the electric field vector traces a circle on a plane that is perpendicular to the wave propagation direction.

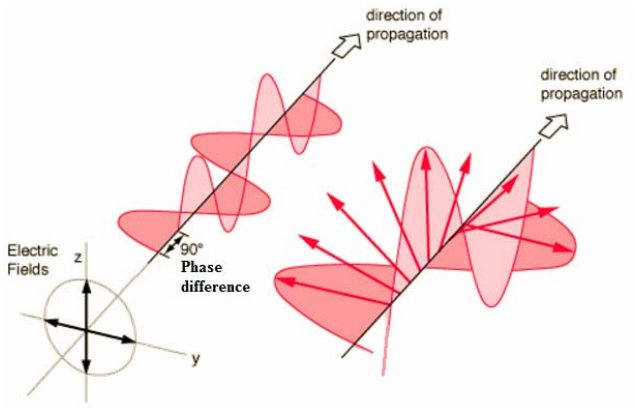

Figure 2.6 Circular Polarization (picture courtesy of Department of physics and astronomy Georgia State University)

As seen on Figure 2.6, the arrow shows the electric field in a plane perpendicular to the direction of propagation. Circular polarization occur under the following conditions:

$$\begin{aligned} &\vec{E}_{0x} = \vec{E}_{0y} = \vec{E}_0 \\ &\delta = \frac{\pi}{2} + 2m\pi \rightarrow where(m = 0, \pm 1, \pm 2, ...) \end{aligned} \tag{2.12}$$

Then equation (2.2) and (2.3) become:

$$\begin{aligned} \vec{E}_x(z,t) &= \vec{E}_{0x}\cos(\tau) \\ \vec{E}_y(z,t) &= \vec{E}_{0y}\sin(\tau), \end{aligned} \tag{2.13}$$

Combining equation (2.13) in equation (2.1), then obtained:

$$\vec{E} = \vec{E}_0(\cos(\tau) + \sin(\tau)) \tag{2.14}$$

In this situation, the magnitude of $\vec{E}$ remains constant while the direction of E is time varying. This is the opposite than the situation of linear polarization. The tip of the electric field vector is moving in a circle as it approaches the observer. If the electric vector of the light, from the source coming toward the observer appears to be rotating

counterclockwise (or clockwise), the light is said to be right-circularly polarized (or left-circularly polarized light).

2.1.2.3 Elliptical Polarization

Elliptical polarizations are characterized by their ellipticity "χ" and orientation "ψ", (Figure 2.2). Linear and circular polarizations are limiting cases of elliptical polarizations, with $\chi = 0$ for linear and $\chi = 45°$ for circular polarizations.

In the case of Elliptical polarization, both the magnitude and direction of electric wave (E) are time varying. The polarization in the two orthogonal components of the electric field will have unequal magnitudes and a non-zero phase difference (ideally 90°). The definition applies to fully polarized waves, where the tip of the electric field vector traces an ellipse on a plane that is perpendicular to the wave propagation direction (Figure 2.7).

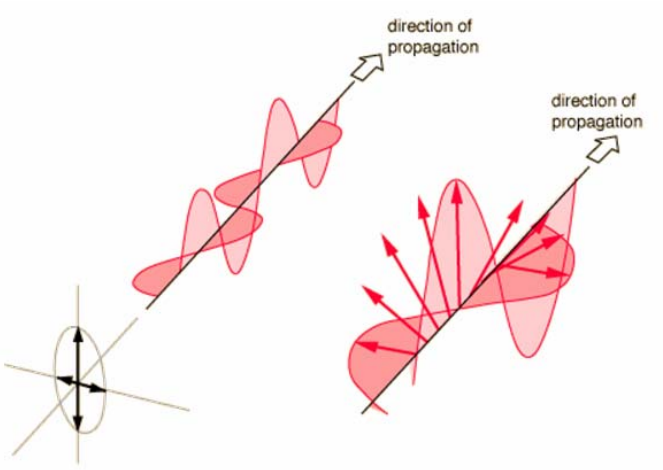

Figure 2.7 Elliptical Polarization (picture courtesy of Department of physics and astronomy Georgia State University)

Equation (2.8) shows that the elliptical polarization can be characterized in terms of parameter $\vec{E}_{0x}$, $\vec{E}_{0y}$ and δ. The auxiliary angle $\alpha(0 \le \alpha \le \pi/2)$ for the polarization ellipse defined by:

$$\tan \alpha = \frac{\vec{E}_{0y}}{\vec{E}_{0x}}, \tag{2.15}$$

and the relationship between parameter $\vec{E}_{0x}$, $\vec{E}_{0y}$ and δ with ψ is:

$$\tan 2\ \psi = \frac{2\vec{E}_x \vec{E}_y \cos\delta}{\vec{E}_{0x}^2 - \vec{E}_{0y}^2} = \frac{2\tan\alpha\cos\delta}{1-\tan^2\alpha}, \tag{2.16}$$

then, relationship between ψ, α, and δ is:

$$\tan 2\ \psi = (\tan 2\alpha)\cos\delta \tag{2.17}$$

For $\delta = 0$ or π (in linear polarization), the angle of rotation from equation (2.17) is:

$$\psi = \pm\alpha \tag{2.18}$$

For $\delta = \frac{\pi}{2}$ or $\frac{3\pi}{2}$ (in circular polarization), the angle of rotation from equation (2.17) is $\psi = 0$, indicating there is no rotation, this shows that the circle is rotationally symetric.

Another important parameter in the polarization ellipse is the angle of ellipticity, χ, defined by:

$$\tan\chi = \frac{\pm b}{a}, -\frac{\pi}{4} \le \chi \le \frac{\pi}{4} \tag{2.19}$$

It can be seen that in linearly polarized light, b=0, and $\chi = 0$ and for circularly polarized light b=a, so $\chi = \pm\pi/4$. The "a" and "b" represents the major and minor axis of ellipse, that are given by:

$$\begin{aligned} a &= \sqrt{E_{0x}^2\cos^2\psi + E_{0y}^2\sin^2\psi + 2E_{0x}E_{0y}\cos\psi\sin\psi\cos\delta} \\ b &= \sqrt{E_{0x}^2\sin^2\psi + E_{0y}^2\cos^2\psi - 2E_{0x}E_{0y}\cos\psi\sin\psi\cos\delta} \end{aligned} \tag{2.20}$$

2.2 Mathematical Representation

This section focuses on exploring the representation and extraction of the polarization information methods. There are three main methods to represent the polarization state of the light :

1. A method using coherency matrix (Wolff and Kurlander in 1990) [Wolff and Kurlander (1990)]. The 2 x 2 coherency matrix represents polarizations and determine the degree of polarization of light using quasi-monochromatic fields. Partially polarized light can be decomposed into polarized and un-polarized

components and expressed using coherency matrices. Thus the state of the polarized portion of light can be extracted from the coherency matrix even when light is partially polarized.

2. Jones calculus, introduced in 1941 by American physicist, R. Clark Jones (1916–2004) who studied at Harvard University. Jones vector represents a polarized light and Jones matrices represents linear optical elements. The Jones calculus describes the polarization of the optical field in terms of amplitudes and phases, and work only for fully polarized light. In this calculus, the fields are described in terms of coherency functions and arranged in 2 x 2 matrices [Shamaraz and Masroor (2005)].
3. Mueller calculus, developed in 1948 by the German physicist, Hans Mueller to solve problems involving wide-band partially polarized light, using 4x4 matrices (Mueller matrix). This theory can be used in a wide area of representation of polarized light and various optical elements. The Mueller-Stokes matrix calculus describes the polarization in terms of intensities. In the Mueller calculus, the Stokes vector S is used to describe the polarization state of a light beam, and the Mueller matrix M to describe the polarization components. Mueller calculus expresses the Stokes parameters developed by Stokes (1852 -1903) as a 1 x 4 column matrix and expressed the polarizer, wave plate, and rotator as 4 x 4 matrices.

In this thesis, only stokes and Mueller calculus will be discussed because currently, this later method is the most comprehensive in representing all the polarization states and it also enables to describe the optical properties of objects.

2.2.1 *Stokes Formalism*

In 1852 Sir George Stokes, introduced the comprehensive scheme of polarized light beam represented in four parameters. This scheme is based on the measurement of intensities by using ideal polarization components. The equations for Stokes column S for completely polarized light in terms of electric field and intensity is defined as:

$$\left(E_{0x}^2+E_{0y}^2\right)^2-\left(E_{0x}^2-E_{0y}^2\right)^2-\left(2E_{0x}E_{0y}\cos\delta\right)^2=\left(2E_{0x}E_{0y}\sin\delta\right)^2$$

$$S=\begin{pmatrix}S_0\\S_1\\S_2\\S_3\end{pmatrix}=\begin{pmatrix}I\\Q\\U\\V\end{pmatrix}=\begin{pmatrix}E_{0x}^2+E_{0y}^2\\E_{0x}^2-E_{0y}^2\\2E_{0x}E_{0y}\cos\delta\\2E_{0x}E_{0y}\sin\delta\end{pmatrix}=\begin{pmatrix}\text{Intensity}\\I_0-I_{90}\\I_{45}-I_{-45}\\I_{RCP}-I_{LCP}\end{pmatrix} \quad (2.21)$$

The first Stokes parameter (S_0) represents the total intensity (I_0+I_{90}) of the field. The measurement of the total intensity is performed without any polarizing component. The three other parameters describe the state of polarization. S_1 and S_2 represent a linear polarization difference between intensity respectively at 0° and 90° and at 45° and -45°. S_3 represented a circular polarization difference between right (RCP : Right Circular Polarization) and left (LCP : left Circular Polarization). All these measurements, together, allow the determination of the Stokes parameters S_0, S_1, S_2, S_3.

The properties of polarized light can directly obtained from intensity measurements and represented by four elements of S related by the expression:

$$\begin{aligned}&\textit{Linear Polarization} \Rightarrow s_1 \textit{ and } s_2 \text{ see Table 2-1, } s_3=0\\&\textit{Circular Polarization} \Rightarrow s_1=0, s_2=0, s_3\neq 0\\&\textit{Fully Polarized light} \Rightarrow s_0^2=s_1^2+s_2^2+s_3^2\\&\textit{Partially Polarized light} \Rightarrow s_0^2\geq s_1^2+s_2^2+s_3^2\\&\textit{Un-polarized light} \Rightarrow s_1=s_2=s_3=0\end{aligned} \quad (2.22)$$

The degree of polarization is given by comparing the total intensity with the sum of the ones measured with polarizers. The direction of the polarization ellipse can be found by analyzing the measurements with linear polarizers, carried out under different angles of the polarizer. The different polarization states can also be described in term of amplitude and phase and it can be seen at Table 2-1.

Table 2-1 Representation of equation & stokes parameter of polarization states

Polarization State	**Amplitude**	**Phase**	**Equation**	**Stokes Parameter**
Linear Polarization Horizontal [H]	$E_{0y} = 0$ $E_0 = E_{0x}$	$\delta = \pm n\pi$ $n = 0,1,\ldots$	$E = E_x + E_y = E_x$ $E_x(z,t) = iE_0\cos(kz - wt)$	$\begin{pmatrix}1\\1\\0\\0\end{pmatrix}$
Linear Polarization Vertical [V]	$E_{0x} = 0$ $E_0 = E_{0y}$	$\delta = \pm n\pi$ $n = 0,1,\ldots$	$E = E_x + E_y = E_y$ $E_y(z,t) = jE_0\cos(kz - wt)$	$\begin{pmatrix}1\\-1\\0\\0\end{pmatrix}$
Linear Polarization +45° [P]	$E_{0y} = E_{0x} = E_0$	$\delta = \pm n\pi$ $n = 0,1,\ldots$	$E = E_x + E_y = E_y$ $E(z,t) = (i+j)E_0\cos(kz - wt)$	$\begin{pmatrix}1\\0\\1\\0\end{pmatrix}$
Linear Polarization -45° [M]	$E_{0y} = E_{0x} = E_0$	$\delta = \pm n\pi$ $n = 0,1,\ldots$	$E = E_x + E_y$ $E(z,t) = (i-j)E_0\cos(kz - wt)$	$\begin{pmatrix}1\\0\\-1\\0\end{pmatrix}$
Right Circular [R]	$E_{0y} = E_{0x}$	$\delta = \pm n\pi/2$ $n = 1,2,\ldots$	$E = E_0\left[i + E_0\cos(kz - wt)\right.$ $\left. + jE_0\sin(kz - wt)\right]$	$\begin{pmatrix}1\\0\\0\\1\end{pmatrix}$
Left Circular [L]	$E_{0y} = E_{0x}$	$\delta = \pm n\pi/2$ $n = 1,2,\ldots$	$E = E_0\left[i + E_0\cos(kz - wt)\right.$ $\left. - jE_0\sin(kz - wt)\right]$	$\begin{pmatrix}1\\0\\0\\-1\end{pmatrix}$

The Stokes formulation is only valid for light that is incoherent. Light that is coherent could potentially interfere at the detector plane causing the Stokes representation not to be valid. This requires that the coherence time of the wave front

being measured be much shorter than the integration time of the instrument. In other words, the Stokes vector is only valid to describe a light wave in time-averaged sense. It measures a statistical average of the polarization of an instantaneously changing light wave that is fluctuating much faster than the measurement time.

2.2.1.1 Stokes Representation for Polarized light

This section describes how the stokes parameters are used to represent three types of polarized light, which are the un-polarized light, completely polarized light and the partially polarized light.

2.2.1.1.1 Un-polarized light

An un-polarized EM wave does not have a consistent pattern of its polarization ellipse, and one example is a pure noise signal. According equation (2.6) and (2.7), when δ varies in a random manner with time, the light is said to be un-polarized. Related to Stokes vector approach, for an un-polarized wave, the mean value of the last three Stokes parameters, S_1, S_2 and S_3 are zero and the degree of polarization is zero (see equation (2.24)).

2.2.1.1.2 Completely Polarized (or Fully polarized) light

A Completely polarized light can be elliptically polarized, circularly, or linearly polarized and it has a constant ellipticity and orientation angle. A complete polarized light can be designed by using ellipticity χ, orientation angles ψ and by Stokes vector. With S_0 representing the power of the wave, the 4-element Stokes vector becomes:

$$\begin{pmatrix} S_0 \\ S_1 \\ S_2 \\ S_3 \end{pmatrix} = \begin{pmatrix} S_0 \\ S_0 \cos 2\chi \cos 2\psi \\ S_0 \sin 2\chi \cos 2\psi \\ S_0 \sin 2\chi \end{pmatrix} \tag{2.23}$$

For a completely polarized wave, only three elements of the Stokes vector are independent, since $S_0 = \sqrt{S_1^2 + S_2^2 + S_3^2}$. Note that the last three elements of the Stokes vector represent the cartesian coordinates of the polarized part of the wave.

2.2.1.1.3 Partially polarized light

A partially polarized wave is an electromagnetic wave that is not fully polarized. The wave does not have a constant polarization ellipse; and its degree of polarization is less than one. Waves that contain noise, or that have a time varying ellipticity and orientation are examples of partially polarized waves.

A partially polarized wave can be described by a completely polarized component and an un-polarized component. Stokes vector can easily describe a partially polarized light. This can be thought of as combinations of several mutually incoherent beams of different polarizations. The combination can be obtained by addition of the intensities, which are represented by the individual elements of the Stokes vector. As the total power is greater than the fully polarized component, the Stokes vector elements can be expressed in relation $s_0^2 \geq s_1^2 + s_2^2 + s_3^2$.

A measure for partially polarized light can be the parameter ρ, given by:

$$\rho = \frac{I_{pol}}{I_{tot}} = \frac{\sqrt{s_1^2 + s_2^2 + s_3^2}}{s_0} \leq 1 \text{ or } \frac{I_{\parallel} - I_{\perp}}{I_{\parallel} + I_{\perp}} \tag{2.24}$$

which is called the degree of polarization, where I_{pol} and I_{tot} represent the polarized intensity and total intensity, $I_{\parallel}$ and $I_{\perp}$ designated an intensity parallel and perpendicular to the surface plane. The degree of polarization ρ is equal to 1 for fully polarized light and equal to 0 for non-polarized (natural) light. Stokes vector with a degree of polarization between 0 and 1 represents partially polarized light beams. To find the parameters of the ellipse of the polarized component, the expression of parameters of the Stokes vector can be written in different forms:

$$\begin{pmatrix} S_0 \\ S_1 \\ S_2 \\ S_3 \end{pmatrix} = \begin{pmatrix} I_{tot} \\ I_{pol} \cos 2\varphi \\ I_{pol} \sin 2\varphi \cos \delta \\ I_{pol} \sin 2\varphi \sin \delta \end{pmatrix} \tag{2.25}$$

where δ is the polarization phase and φ is the angle of polarization. Based-on equation (2.25), it can be written as

$$\delta = \arctan\frac{S_3}{S_2},\ \varphi = \frac{1}{2}\arccos\frac{S_1}{\sqrt{S_1^{\,2} + S_2^{\,2} + S_3^{\,2}}} \tag{2.26}$$

From equation (2.23) an ellipticity χ and orientation angles ψ can be written as:

$$\chi = \frac{1}{2}\arcsin\frac{S_3}{\sqrt{S_1^{\,2} + S_2^{\,2} + S_3^{\,2}}},\ \psi = \frac{1}{2}\arctan\frac{S_2}{S_1} \tag{2.27}$$

Another equation to compute the degree of polarization can be seen in the following equation:

$$\begin{aligned} &\text{Degree of linear polarization } = DOLP = \frac{\sqrt{s_1^2 + s_2^2}}{s_0} \\ &\text{Degree of circular polarization } = DOCP = \frac{s_3}{s_0} \end{aligned} \tag{2.28}$$

2.2.2 *Mueller Formalism*

Hans Mueller at 1943 was the first to determine the description of the E field polarization status of light by matrice for the polarizer, wave plate, and rotator. The use of matrices to deal with complex polarization problems was a significant breakthrough with respect to carrying out the difficult calculations. When light travels through space, scatters through a medium, reflects from a surface, or propagates through optical components, its Stokes vector is modified. The output Stokes vector is a function of the initial state and the interactions modelled by Mueller matrices that occurred during propagation.

The Mueller matrix provides the full characterization of a polarization element [Shurcliff (1980)]. That is describing the light beam is simply the four-parameter Stokes vector, described as before. The bandwidth (wave length range) of the light is assumed to be broad enough that the light may, for example, be un-polarized, and narrow enough that the optical devices in question may be regarded as achromatic within this range. The package can describe the effects of linear optical systems (polarizers, wave plates, or reflecting surfaces). Equation (2.29) shows the standard Mueller matrix representation of

a transformation from an original state (on the right-hand side) to a modified state (on the left-hand side), both of the state represented by the Stokes vector.

$$\left[\text{Stokes Vector}\right] = \left[\text{Muller matrix}\right]\left[\text{Stokes Vector}\right]$$

$$\begin{pmatrix} S_0' \\ S_1' \\ S_2' \\ S_3' \end{pmatrix} = \begin{pmatrix} m_{11} & m_{12} & m_{13} & m_{14} \\ m_{21} & m_{22} & m_{23} & m_{24} \\ m_{31} & m_{32} & m_{33} & m_{34} \\ m_{41} & m_{42} & m_{43} & m_{44} \end{pmatrix} \begin{pmatrix} S_0 \\ S_1 \\ S_2 \\ S_3 \end{pmatrix} \tag{2.29}$$

2.2.2.1 The Mueller Matrix of a Polarizer

A polarizer is an optical element that attenuates the orthogonal components of an optical beam unequally; that is, a polarizer is an anisotropic attenuator. Mueller Matrix for a linear polarizer inclined with an angle α and with transmission coefficient τ is:

$$M_{pol}(\alpha) = \frac{\tau}{2}\begin{pmatrix} 1 & \cos 2\alpha & \sin 2\alpha & 0 \\ \cos 2\alpha & \cos^2 2\alpha & \cos 2\alpha \sin 2\alpha & 0 \\ \sin 2\alpha & \cos 2\alpha \sin 2\alpha & \sin^2 2\alpha & 0 \\ 0 & 0 & 0 & 0 \end{pmatrix} \tag{2.30}$$

From the general equation above, Mueller matrix of a linear polarizer such as horizontal, vertical, 45°, and circular polarizer (left hand and right hand) can be computed.

2.2.2.2 The Mueller Matrix of a Retarder

A retarder is a polarizing element which changes the phase of the optical beam. Strictly speaking, its correct name is a phase shifter. However, historical usage has led to the alternative names retarder, wave plate, and compensator. Mueller matrix for retarder with fast axis at angle θ and phase shift retardation δ is:

$$M_{pol}(\theta,\delta) = \begin{pmatrix} 1 & 0 & 0 & 0 \\ 0 & \cos^2 2\theta + \sin^2 2\theta \cos\delta & (1-\cos\delta)\sin 2\theta \cos 2\theta & -\sin 2\theta \sin\delta \\ 0 & (1-\cos\delta)\sin 2\theta \cos 2\theta & \sin^2 2\theta + \cos^2 2\theta \cos\delta & \cos 2\theta \sin\delta \\ 0 & \sin 2\theta \sin\delta & -\cos 2\theta \sin\delta & cos\,\delta \end{pmatrix} \tag{2.31}$$

From the general equation above, Mueller matrix of retarder such as quarter wave retarder and half wave retarder can be computed. Mueller Matrices for some optical elements are given in Table 2-2.

Table 2-2 Mueller Matrix for Optical Elements

No	Optical Element	Mueller matrix	No	Optical Element	Mueller matrix
1.	Horizontal Linear polarizer	$\frac{1}{2}\begin{pmatrix}1&1&0&0\\1&1&0&0\\0&0&0&0\\0&0&0&0\end{pmatrix}$	5.	Quarter wave plate fast axis vertical	$\begin{pmatrix}1&0&0&0\\0&1&0&0\\0&0&0&-1\\0&0&1&0\end{pmatrix}$
2.	Vertical Linear polarizer	$\frac{1}{2}\begin{pmatrix}1&-1&0&0\\-1&1&0&0\\0&0&0&0\\0&0&0&0\end{pmatrix}$	6.	Quarter wave plate fast axis horizontal	$\begin{pmatrix}1&0&0&0\\0&1&0&0\\0&0&0&1\\0&0&-1&0\end{pmatrix}$
3.	Linear polarizer with with a transmission axis at +45°	$\frac{1}{2}\begin{pmatrix}1&0&1&0\\0&0&0&0\\1&0&1&0\\0&0&0&0\end{pmatrix}$	7.	Homogeneous right circular polarizer	$\frac{1}{2}\begin{pmatrix}1&0&0&1\\0&0&0&0\\0&0&0&0\\1&0&0&1\end{pmatrix}$
4.	Linear polarizer with with a transmission axis at -45°	$\frac{1}{2}\begin{pmatrix}1&0&-1&0\\0&0&0&0\\-1&0&1&0\\0&0&0&0\end{pmatrix}$	8.	Homogeneous left circular polarizer	$\frac{1}{2}\begin{pmatrix}1&0&0&-1\\0&0&0&0\\0&0&0&0\\-1&0&0&1\end{pmatrix}$

2.3 Polarization in Outdoor Scenes

A commonly physical phenomenon that can produce a polarized light consists of reflection and scattering, where the reflection is related to diffraction, absorption and refraction. Generally, this phenomenon can occur in natural environment or created by humans with certain optical instruments. Therefore, in this section will be discussed on these two optical processes and the next section will explain the various other processes in terms of optical devices made by humans.

2.3.1 *Polarization by Reflection of Light*

The polarization of light by reflection occurs when a light beam strikes a surface. Polarization is dependent upon the material that the surface is made of and upon to the angle of the light approaching the surface. Non-metallic surfaces such as asphalt roads, snow and water, reflect light such that there is a large concentration of vibration. The reflected beam will be linearly polarized and the direction of polarization is parallel to the plane of the surface. There is a specific angle of incidence that satisfies this condition which is known as the Brewster angle (the angle of incidence required to produce a linearly-polarized reflected beam), is given by:

$$\tan\theta_B = \frac{n_2}{n_1} \tag{2.32}$$

This expression can be derived using Snell's law and the law of reflection. Figure 2.8 below shows some of the geometry involved, and the Brewster angle can be generated by using Snell's law:

$$\begin{aligned} \theta_i &= \theta_r \\ n_1 \sin\theta_i &= n_2 \cos\theta_t \end{aligned} \tag{2.33}$$

This gives the Brewster relationship:

$$\frac{\sin\theta_i}{\cos\theta_t} = \frac{n_2}{n_1} \Rightarrow \tan\theta_B = \frac{n_2}{n_1} \tag{2.34}$$

For un-polarized light incident on the surface at Brewster's angle, the reflected light is polarized perpendicular to the incident plane, or parallel to the surface. At other angles, the reflected light will be partially polarized.

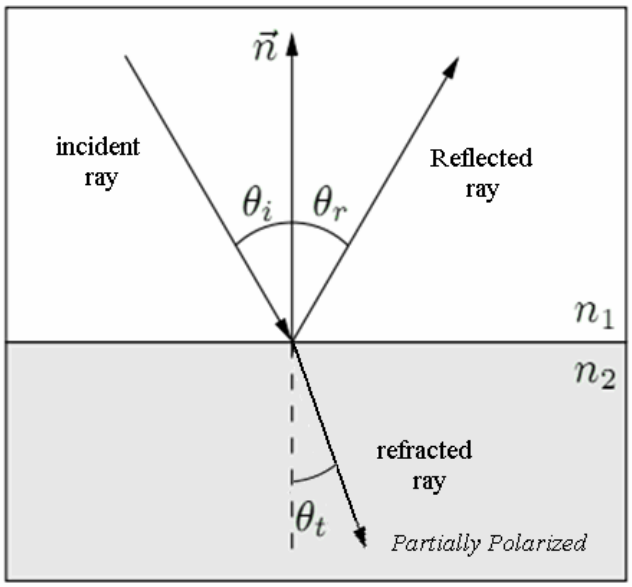

Figure 2.8 Snell's Law Illustration for Polarization by Reflection

The Fresnel equations can establish the ratios between the amplitude of the incident light ray and the amplitude of the reflected light ray, along the orthogonal projections and parallel to the incidence plane. If $A_\perp$ and $A_\parallel$ are the amplitudes of the incident light, and $R_\perp$ and $R_\parallel$ are the amplitudes of the reflected light, it can be written as:

$$f_\perp = \frac{R_\perp}{A_\perp} = \frac{-\sin(\theta_i - \theta_t)}{\sin(\theta_i + \theta_t)}$$
$$f_\parallel = \frac{R_\parallel}{A_\parallel} = \frac{\tan(\theta_i - \theta_t)}{\tan(\theta_i + \theta_t)} \tag{2.35}$$

The reflectivity coefficients $F_\perp$ and $F_\parallel$, are also determined from the Fresnel coefficients and are given by equation:

$$F_\perp = |f_\perp|^2, F_\parallel = |f_\parallel|^2 \tag{2.36}$$

Mueller's model description of a reflective surface is given by multiplying of Mueller matrix of a linearly polarizer and a retarder.

$$M_{refl} = M_{pp}(F_\perp, F_\parallel) \cdot M_{ret}(\delta, 0)$$
$$where \quad \delta = \arg(f_\parallel - f_\perp) \tag{2.37}$$

Then, Mueller matrix for reflection can be written as:

$$M_{refl} = \frac{1}{2}\begin{bmatrix} F_\perp + F_\parallel & F_\perp - F_\parallel & 0 & 0 \\ F_\perp - F_\parallel & F_\perp + F_\parallel & 0 & 0 \\ 0 & 0 & 2\sqrt{F_\perp F_\parallel}\cos\delta & 2\sqrt{F_\perp F_\parallel}\sin\delta \\ 0 & 0 & -2\sqrt{F_\perp F_\parallel}\sin\delta & 2\sqrt{F_\perp F_\parallel}\cos\delta_\parallel \end{bmatrix} \tag{2.38}$$

2.3.2 *Polarization by Scattering of Light*

Most of polarization effect by scattering in outdoor scene occur in the air or in the water. Briefly, scattering phenomenon can be explained as follows : When light hits the atoms of a material, it will regularly set the electrons of those atoms into vibration. Some electromagnetic wave is produced from that vibrating electrons, propagating outward in all directions and hits the neighboring atoms and forces their electrons to the vibrations at the same frequency. This phenomenon occurs continuously, so that the process absorption and reemission of waves causes the light to be scattered about the medium. The quantity of light scattered (termed Rayleigh scattering) depends upon the wavelength of light and the size of the molecules, and it will proportional to $1/\lambda^4$ (λ is wavelength), as demonstrated by Lord Rayleigh in 1871.

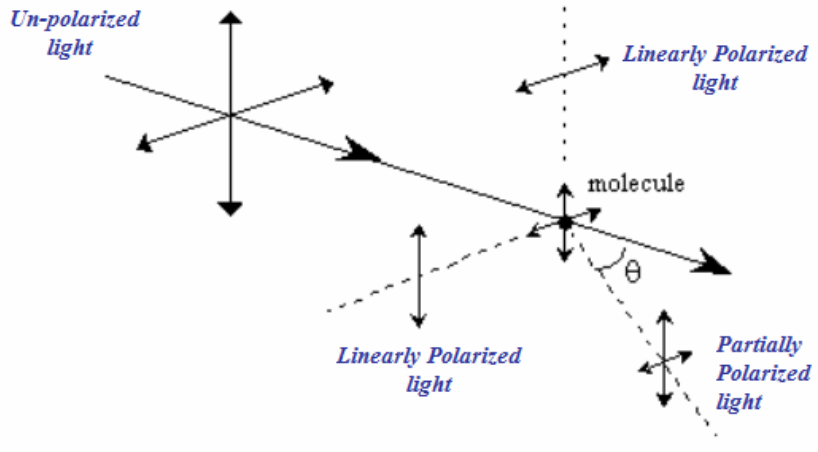

Figure 2.9 Polarization by Scattering of Light

The Rayleigh scattering Phenomenon in the air, or called atmospheric polarization is observed as light passes through our atmosphere. It is responsible for the blue colour of the sky or red colour of sun during sunrise and sunset. This is can be explained as follow, when the sun light strikes the molecules of atmosphere, some components of the light become scattered and produce linearly polarized light in the plane perpendicular to the incident light. That scattered light it self becomes partially polarized (see Figure 2.9). The rayleigh scattering is strongly dependent on the colour of the light, for instance, the shorter wavelengths, such as violet and blue, will scattered more effectively than the longer wavelengths of light, such as red, orange, and yellow. The blue light ($\lambda \approx 425$nm) scatters about 5.5 times than red light with $\lambda \approx 650$nm [Liou (1980)], then the molecules scatter light at the blue end much more than light at the red. It is the reason why the sky appears blue.

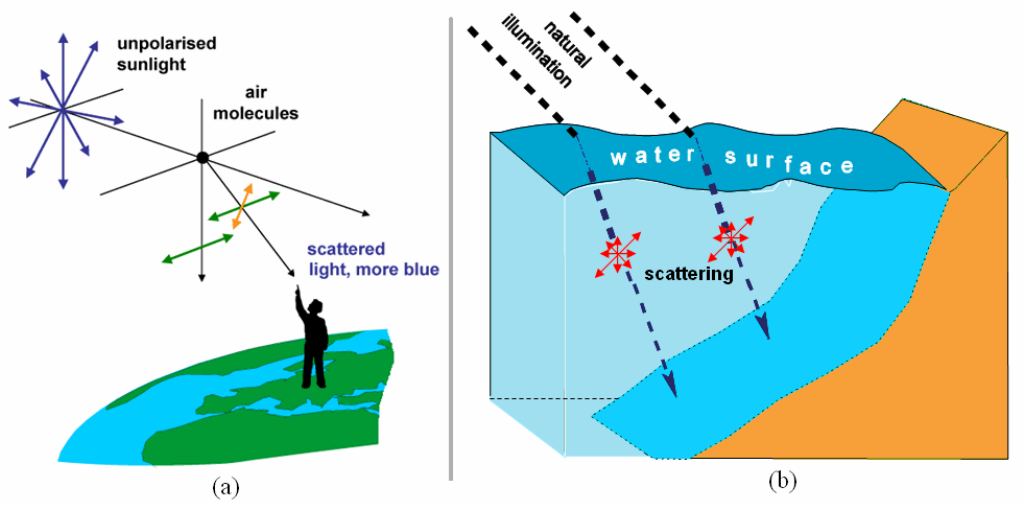

Figure 2.10 Scattering in the Air (a) and Water (b)

At mid day, when the Sun positions in the shortest distance to the observer, the Sun looks yellow because every colors from light source are represented almost equally. This is caused by a small quantity of light scattered in thin layer of atmosphere. But on the other hand, when the sun is near the horizon (at sunrise or sunset), the light from the Sun has to pass through much more atmosphere layer to reach the observer (see Figure 2.10.a). Then, at the time, most of the light with colour blue end of the visible spectrum ray is scattered in other directions, but much less of the light with colour red is scattered.

It make the Sun appear to be orange or near red. The same thing is also happening in the natural water scene, scattering of un-polarized light passing through a fluid will produce the scattered light partially or completely polarized.

2.4 Polarization Instrument

A device which creates polarized light when natural incident light is passing trough it, is called a polarizer. Polarizers work by one of four methods: reflection, birefringence (double refraction), selective absorption (dichroic) and scattering.

2.4.1 *Basics Polarizer*

The polarizers always select a particular polarization state and discards all others. The simplest polarizer is a wire-grid polarizer and consists simply of a number of closely spaced parallel wires.

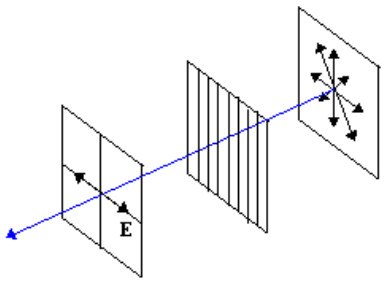

Figure 2.11 Wire grid Polarization

The electric field parallel to the wires causes electrons in the wires to oscillate backwards and forwards in a current. This energy is dissipated by Joule heating and the parallel component of the field is effectively absorbed. Thus only the component of the field perpendicular to the wires is transmitted. Clearly for light the spacing between wires must be very small (microwaves can be polarized with electrical wires).

At this moment, a common way to produce a polarization is by using a linear polarizer. In practice, to use this device for producing polarization from un-polarized light, is by installing polarizer in front the imaging system.

2.4.2 *Birefringent material*

Birefringent phenomenon is the property of optically anisotropic materials, such as crystals, of having the phase velocity of propagation dependent on the direction of measurement of propagation or polarization. For example, in liquid crystals material, this is due to the alignment and the shape of the molecules. In other words, birefringent material does not have the same optical properties in all directions.

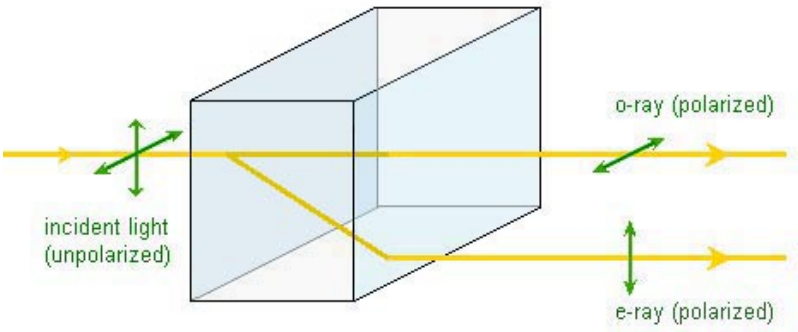

Figure 2.12 Light traveling through a birefringent medium

Substance in birefringent material has two different refractive indices. This can arise from a difference in electrons force in the atoms bound to their nucleus in the crystal structure, causing them to have a different resonance frequency. Certain crystals have this birefringent property. As seen at Figure 2.12, when light enters a birefringent material, the process is modeled in terms of the light being split up into the fast axis (called the ordinary ray/o-ray) and slow axis (called the extraordinary ray/e-ray) components. Because the two components travel at different velocities, the waves have a difference of phase. When the rays are recombined as they exit the birefringent material, the polarization state is changed because of this phase difference.

To separate two rays in a crystalline material, a lot of methods have been designed which make use of birefringence phenomenon, such as : Nicol prism, Wollaston prism (another variant of this crystalline type is the Rochon, Sénarmont prisms and the Nomarski prism, which have a similar method but use different optical axis orientation) and Glan-Foucault prism (another variant of this crystalline type is the Glan–Thompson prism and Glan–Taylor prism).

2.4.3 *Dichroic material*

The dichroic material can achieve polarization by selective absorption. It is made from some materials which have different absorption for perpendicular incident planes of light. If un-polarized light passes through a polarizer, the intensity of the transmitted light will be half from what it was entering the material. If linearly polarized light passes through a polarizer, the intensity of the light transmitted is given by the Malus' law.

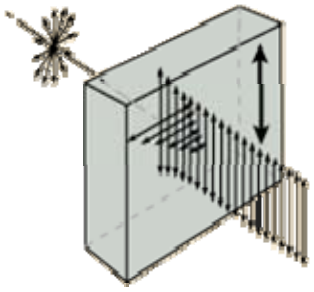

Figure 2.13 Dichroic material Principle [Nave (2011)]

The Dichroism work principle is to do a selective absorption from the two orthogonal polarization components (x,y) of an incident light. A dichroic polarizer produces a preferential absorption of one field component while being essentially transparent to the other. The simplest form of a dichroic polarizer is a grid of parallel conducting wires. Physically, dichroic material have anisotropic properties, there are also certain materials which are due to the anisotropy which exist in their crystal structure. It is the mineral tourmaline (refers to a class of boron silicates). A tourmaline crystal has a unique optic axis, and any electric field vector which is perpendicular to that axis is strongly absorbed.

Certainly, for now, the most famous polarizer with dichroic material is the polaroid. It was invented by Edward Land at Harvard in 1928 that employed from synthetic substance herapathite. The Polaroid sheet typically transmits less than 1% of incident light rays which are parallel with it surface and it may transmit more than 80% of light in the perpendicular plane. The polaroid widely used for the manufacture of polarizer sunglasses or polarizer filters for photography.

2.4.4 *Polarizer Component in Optical Industry*

The optical industry produces various type of polarization components. This is also related to the demand from downstream industry or from the researchers needing specific optical equipments for supporting their work. In this section, the discussion will focus on common polarization components offered by the optical industry. Based-on some catalog offered by optical instrument manufacturers (Melles griot and Edmund optics), the polarization components are divided into several parts, namely:

1. Polarizer for special function/special purpose, included in this type is Stacked plate polarizers, near infra-red polarizer, high contrast polarizers and depolarizer.
2. Polarizer for multipurpose, in particular :
   - Dielectric polarizers: Polarization of the light beam by reflection is much more effective in the case of dielectric optical coatings. Two basic kinds of thin film layer dielectric polarizers are used:
     a) Plate polarizers: The Polarizer from a plane parallel glass plate with multilayer dielectric coating on the optical surface. It adjusted in optical beam at Brewster angle.
     b) Cube polarizers: Beam splitter cubes, the cube dielectric polarizers consist of two cemented right angle prisms with dielectric multilayer coating inside.
   - Birefringent polarizers: Operate on the basis of space separation of the ordinary and extraordinary rays. Example: Glan-Thompson polarizers, Glan-Taylor polarizers, Wollaston polarizers, Rochon polarizers and Beam displacing polarizers.
   - Retardation plates (phase shifter): Working alike birefringent, but operates on the basis of velocity difference between the ordinary and extraordinary beams, without space separation and operate as elements changing the state of polarization of optical beams.
   - Dichroic sheet polarizer: Made of from a plastic dichroic polarizing sheet sandwiched between selected strain free glass plates. Usually used to subject with

polarization from strong absorption, suited for low power application and use in the visible spectrum of light.

In addition, the production component of polarization is also categorized based on the structure of light such as visible light, infra red, ultraviolet or laser (standard or high power). Then, categorization can also based-on the type of material of polarization components. It will consist of prism, thin film sheet and crystal. Finally, polarization component in application level can be divided based-on its function, such as Polarization rotator, beam splitter, waveplate, Retardation plates and depolarizer.

2.4.5 *Liquid crystal component*

Since the liquid crystal is widely used for various application, many researches were conducted to study and produce new liquid crystal materials, characterize their physical properties, and evaluate their potential as active components of optoelectronic and photonic devices. In the computer vision field, Liquid crystal tunable filters (LCTFs) based on cholesteric and nematic liquid crystal are gaining wide acceptance.

The liquid crystal is a state observed between the crystalline (solid) and isotropic (liquid) phase. There are many phase behaviour of liquid crystal, and it can be characterized according to the material. The molecules inside the liquid crystal (called *mesogens*) are to point along a common axis, called the *director*. This type of molecules is very different from the molecules in the liquid phase, which have no order to any translational area and in the solid state, that the molecules are already ordered and have only a little translational freedom. Hence, the liquid crystals are fluids formed order by molecules with one-or two-dimensionally anisometric shapes such as rod-like (calamitic) or disk-like (discotic) molecular structure. They have rigidness of the long axis, and strong dipoles and can easily caused polarization of light.

This section will explain the phase behaviour of the most widely implemented liquid crystal materials in the optoelectronics to support computer vision research, namely nematic and cholesteric liquid crystal.

2.4.5.1 Nematic Crystal component

The nematic liquid crystal phase is characterized by molecules that have no positional order but tend to point in the same direction along the director. The twisted nematic represents the first successful application of liquid crystals, introduced by Schadt and Helfrich in 1971. In optoelectrical device, usually the liquid crystal is set up between crossed polarizers (the polarizer and the analyzer) and the birefringence is controlled electrically (see Figure 2.14).

The Crossed polarizers part used together transmit light differently depending on their relative orientation. For example, when the polarizers are arranged in a state where a planes of polarization are perpendicular to each other, the light is blocked. Then in the other side, when the analyzer as the second filter is parallel to the polarizer, all of the light passed by the first filter is also transmitted directly.

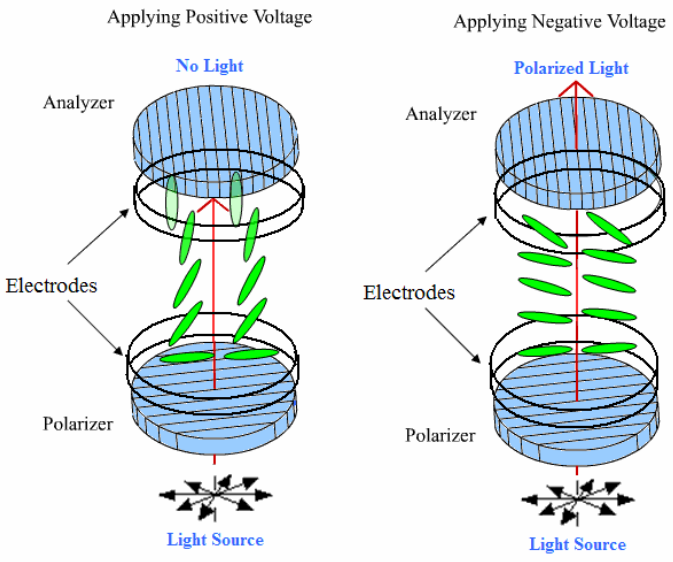

Figure 2.14 Twisted Nematic device geometry

The surfaces of the transparent electrodes in contact with the LC are coated with a conductive coating thin layer of polymer (such as indium tin oxide/ITO), which has been rubbed or brushed in one direction. The nematic LC molecules tend to orient with their long axes parallel to this direction. When a voltage is applied to the electrodes, the liquid crystal molecules tend to align with the resulting electric field E (Figure 2.14 left side), each polarizer molecules are oriented with its easy axis parallel to the rubbing direction

of the adjoining electrode, and made a dark state of LC cell. In other words, the polarizer and analyzer are crossed. Otherwise, when the electric field is turned off, the nematic director encounter a 90 degree twist within the cell and the LC State cell becomes transparent. Un-polarized light pass through into the first polarization filter and become polarized in the same plane with the local orientation of LC molecules. Then, twisted LC molecules will act as optical wave guides and rotates the polarization plane by 90°, so that the light can pass through the second polarizer (see Figure 2.14 right side)

2.4.5.2 Ferroelectric Liquid Crystal (FLC) component

Ferroelectric liquid crystals belong to cholesteric phase liquid crystals and are known as chiral nematic devices. In the cholesteric phase (when each of molecule is rotated individually and move helically throughout the plane), orientation of molecules in the different layers is in a slight angle relative to each other, rather than parallel along direction axis as in the nematic liquid crystal (see Figure 2.15). Ferroelectric liquid crystals can switch very quickly under a electric DC field, because of it electrical polarization properties.

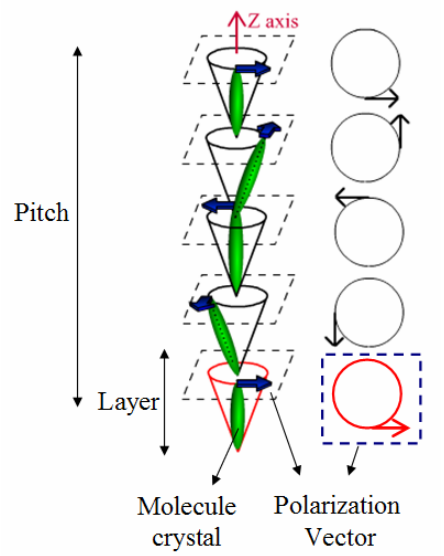

Figure 2.15 Ferroelectric Liquid crystal Structure (picture courtesy of the Case Western Reserve University, US)

The most common configuration for a ferroelectric liquid crystal device is the Surface Stabilized Ferroelectric Liquid Crystal (SSFLC) configuration, in which the natural twist of the material is suppressed by the surface conditions [Shtykov and Vija (2003)]. This SSFLC system is installed by putting the cell between linear crossed polarizers with one polarizer parallel to one of the two possible directions of the director. The state with the director parallel to the polarizer is non transmissive (down state) while the other allows light to cross the cell. Briefly, SSFLC technique can be explain as follows. The molecules are arranged in a layered geometry. The rubbing direction or alignment direction of the cell, make the tilted with respect to the layer normal. The unique property of SSFLC is the coupling between the collective molecular tilt and a spontaneous polarization perpendicular to the plane of the tilt angle. By using external electric field, the direction of spontaneous polarization will reverse, and flips all molecules to the other side, away from the alignment direction. For example, as seen Figure 2.16 left side, applying a DC voltage will make a state of polarizer in the dark state because the polarization of the incident light are aligned to direction of molecules.

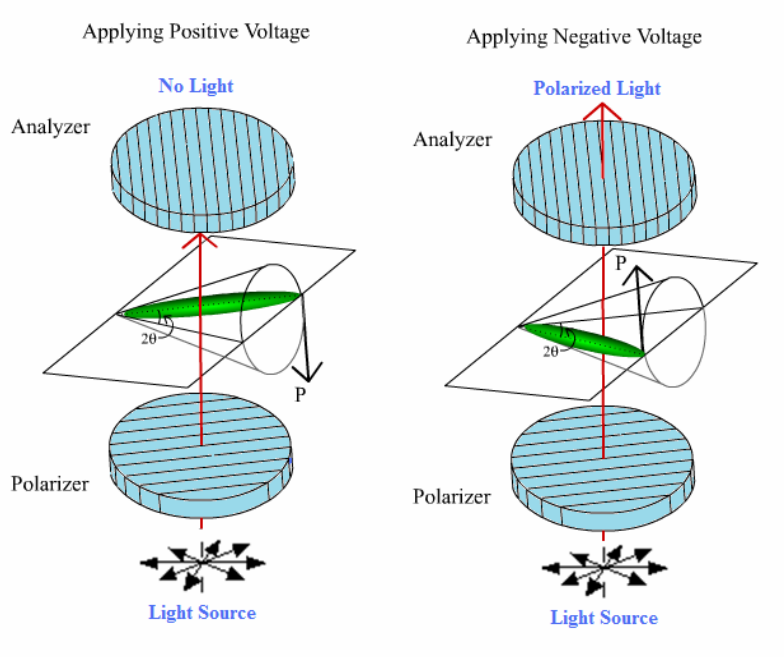

Figure 2.16 Polarizer with Ferroelectric Device

In the up state (when is voltage no applied), one component of the polarization has been retarded by 180 degrees and the director is no longer parallel to the incident of

polarizer light allowing the light to pass through the analyzer outside the FLC system (see Figure 2.16 right side). The intensity of the light across the cell is dependent on the cone angle, cell thickness and wavelength of the light.

Briefly, liquid crystal can be used to create polarization rotator, phase retarders, Polarization State Generator, Radial Polarization converter and so on, which can be found in [Arcoptix (2009)].

2.5 Simplified polarization imaging

To describe a partially linearly polarized light, not all the Stokes parameters need to be estimated since the ellipticity component is assumed to be zero. The optical devices that can measure the polarization parameters of a partially linearly polarized light can be called simplified polarization imaging systems.

2.5.1 *Principle*

In the case of partially linearly polarized light, the ellipticity χ of polarized component (represent by Stokes parameter S_3) is zero and the major axis of the ellipse is oriented in the same orientation with the angle of polarization ($\psi = \varphi$). The Stokes vector of partially linearly polarized wave can be written as follows:

$$\begin{aligned} S_0 &= I_{tot} \\ S_1 &= \rho I_{tot} \cos 2\varphi \\ S_2 &= \rho I_{tot} \sin 2\varphi \\ S_3 &= 0 \end{aligned} \tag{2.39}$$

The polarization state of a partially linearly polarized wave, need to be determined by three parameters: Stokes (S_0, S_1, S_2) or (I_{tot}, ρ, φ), I_{tot} represents the total intensity of the light, ρ is the degree of polarization and φ is the angle of polarization of the linearly polarized component.

The intensity of light is the quantity perceived by human vision and captured by imaging sensors as time averaged energy. Whereas the other two parameters are the enhancement of the sensory over human vision. The degree of polarization which is also

referred to as partial polarization could be defined as the relative proportion of the linearly polarized component in a partially linearly polarized light. It varies from zero to one corresponding to completely un-polarized and completely linearly polarized light respectively. The orientation of the polarized component in a partially linearly polarized light with respect to a certain reference (say horizontal) is referred to as the angle of polarization. It varies from 0 to a maximum value of 180 degrees.

2.5.2 *Simplified polarization imaging Using Rotating Polarizer*

The polarization state of partially linearly polarized light can be determined using a rotating linear polarizing filter in front of a camera setup (see Figure 2.17) [Morel (2005)]. It can be generated according by the equation (2.39) and using the Mueller matrix of the polarizer filter defined in equation (2.30). A relationship between light intensity I_p as seen by the sensor, and rotation angle of polarizer filter is:

$$I_p(\alpha) = \frac{1}{2}(S_0 + S_1 \cos 2\alpha + S_2 \sin 2\alpha), \tag{2.40}$$

Then, by introducing i_{min} and i_{max} (minimum intensity and maximum intensity polarization), the equation (2.40) can be written:

$$\begin{aligned} I_p(\alpha) &= \frac{I_{\max} + I_{\min}}{2} + \frac{I_{\max} - I_{\min}}{2} \cos(2\alpha - 2\varphi), \\ I_p(\alpha) &= \frac{I_{tot}}{2}(1 + \rho \cos(2\alpha - 2\varphi)). \end{aligned} \tag{2.41}$$

From this step, computation of intensity and degree of polarization can be written as:

$$I = I_{\max} + I_{\min}, \quad \rho = \frac{I_{\max} - I_{\min}}{I_{\max} + I_{\min}}, \tag{2.42}$$

and the angle of polarization is given by the phase of the sinusoid.

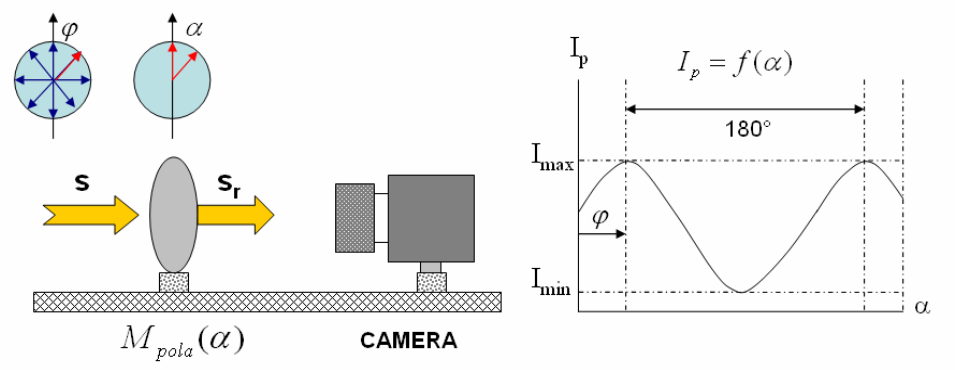

Figure 2.17 Polarizer Setup and variation the intensity I_p of angle α

In practice, to calculate the three parameters of polarization state, the image acquisition step must take at least three images with different orientation of the polarizing filter. This is following the work of Wolff and Andreou in 1995 [Wolff and Andreou (1995)], three different intensity measurements (I_0, I_{90} and I_{45}) were taken at 0^0,45^0 and 90^0. Saito in 1999 [Saito et al. (1999a)] offers another way to calculate the parameters. 36 pictures are taken, in which corresponding to 36 rotations of the polarizing filter, in the range from 0° to 180° with 5° steps. By keeping the minimum and maximum intensity of each pixel and applying the formulas of equations (2.42), I and ρ are calculated. φ is obtained by keeping the angle of α corresponding to the maximum intensity. This method provided an easy way to determine intensity and degree of polarization, but it is very sensitive to noise on the value of the angle of polarization. Another method commonly used, relies on the approximation in the sense of linear least mean squares.

2.5.3 *Simplified polarization imaging Using Twisted Nematic Liquid Crystal*

Wolff et al. in 1997 [Wolff et al. (1997)] developed a polarization sensitive camera using two liquid crystal cells twisted nematic synchronized with the sensor. The structure of twisted nematic liquid crystal rotates the linear polarization at a pre determined angle. When an voltage is applied to the LC component, the molecule crystal will stops to being "twisted" and the linear polarization is not rotated. The un-polarized component is not affected by the component.

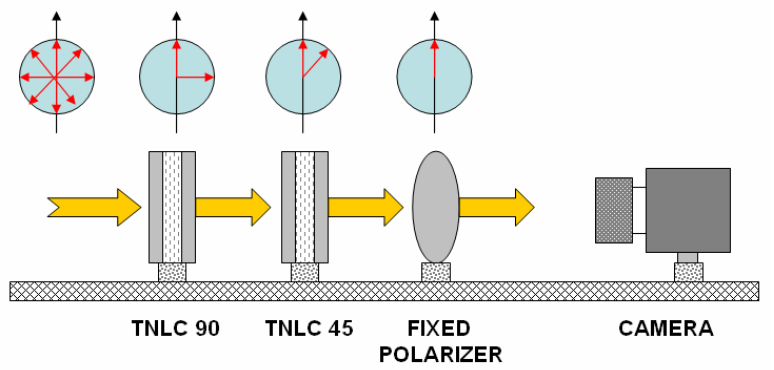

Figure 2.18 TNLC Setup for simplified polarization imaging computation (Wolff et al., 1997)

Two twisted nematic liquid crystals are used: one set at 45° and the other at 90°. A linear polarizer filter oriented at 0° is placed between the two cells and the camera (Figure 2.18). The acquisition of the image corresponding to I_0 obtained by supplying the two components with electricity voltage (in this case, the polarization is not rotated). The acquisition of I_{45} and I_{90} is obtained by cutting off only the power of the cell set at 45° or 90°.

2.5.4 *Simplified polarization imaging Using Liquid Crystal Variable Retarder*

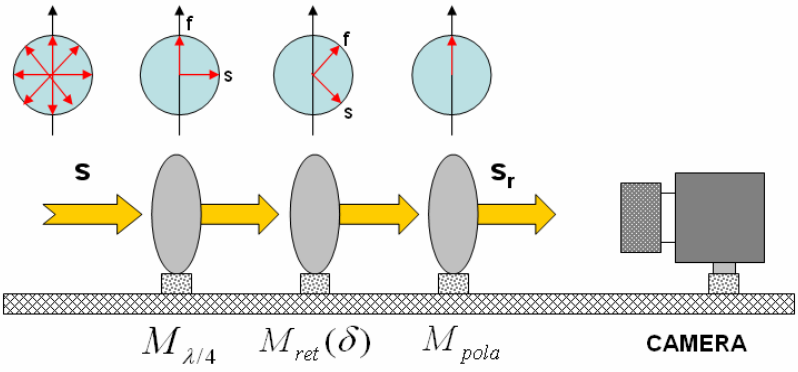

Figure 2.19 LCVR Setup for simplified polarization imaging computation

Setup for simplified polarization imaging using a Liquid Crystal Variable Retarder (LCVR) can be seen at Figure 2.19. The imaging system is composed of a quarter wave plate oriented at 0°, a variable retarder at 45° and a linear polarizing filter oriented at 0°. This setup allows to acquire multiple images with different orientations of

polarization and it is possible to apply the method of linear least squares to obtain polarization parameters. However, the acquisition time is longer than the previous method, because the cell of LCVR is slower to stabilize. If M_{pola}, $M_{ret}(\delta)$ and $M_{\lambda/4}$ are Mueller Matrix for linear polarizer, variable retarder (where $\delta = 2\alpha$) and quarter wave plate respectively then, the Mueller matrix of this setup can be given by:

$$M(\delta) = M_{\lambda/4}.M_{ret}(\delta).M_{pola} = \frac{1}{2}\begin{pmatrix} 1 & \cos\delta & \sin\delta & 0 \\ 1 & \cos\delta & \sin\delta & 0 \\ 0 & 0 & 0 & 0 \\ 0 & 0 & 0 & 0 \end{pmatrix} \tag{2.43}$$

The Intensity I_p can be measured by the camera, as:

$$\begin{aligned} I_p(\delta) &= \frac{1}{2}(S_0 + S_1 \sin\delta + S_2 \sin\delta), \\ I_p(\delta) &= \frac{1}{2}(1 + \rho\cos(\delta - 2\varphi)). \end{aligned} \tag{2.44}$$

2.6 Visual Representation of the Polarization Parameter

Polarization states produce captured images that are not familiar in the sense of human vision. To ease their representation, scheme polarization vision into colour vision was used by [Wolff et al. (1997)]. The three components of polarization are mapped into color space. In this schema, the angle of polarization φ, degree of linear polarization ρ and intensity I of partially linearly polarized light mapped by the hue, saturation and brightness, respectively, using the following transformation:

$$\begin{aligned} 2\varphi &\rightarrow H, \\ I &\rightarrow L, \\ \rho &\rightarrow S. \end{aligned} \tag{2.45}$$

The coloured pixels is represented polarized light, whereas colourless pixels indicate un-polarized light. The variety colour of angle of polarization indicated by hue multiplied by two to make it can reach up to entire 360^0 (see Figure 2.20).

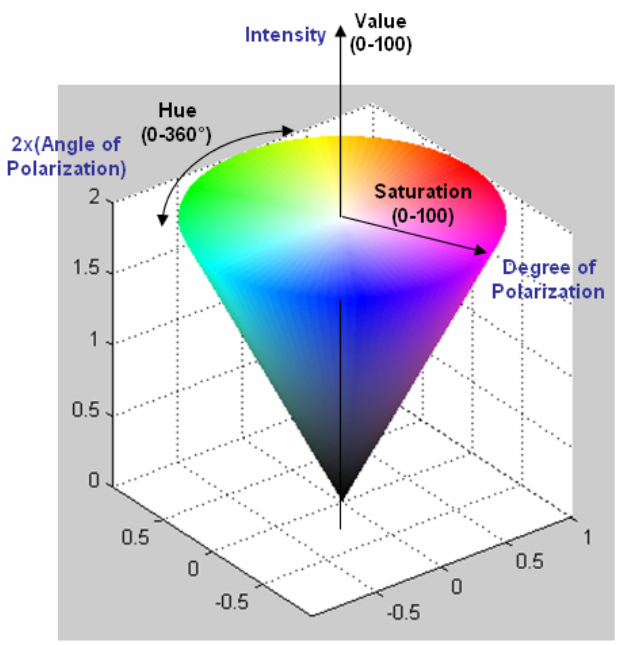

Figure 2.20 Representation of polarization parameter on HSV colour space

2.7 Conclusion

This chapter has described a review about polarization imaging. The discussion starts from the description of polarization light model, which is the one of electromagnetic wave and deeper in description of the polarization type, which consists to three types, such as elliptical polarization as the basics form, and linear and circular polarization as derivatives form. This chapter also outlines a method to measure the polarization state (known as the polarization imaging system).

In addition, two important discussions about the main cause of polarization is also described in a comprehensive manner. First, a discussion about polarization light in outdoor environment and the second is about the instruments that can produce and control the polarization. Polarization light in nature occurs mostly due to the reflection and scattering.

Related to main research topics, this chapter also discusses about the liquid crystal components that are used as one of the material of imaging system. There are two main types of liquid crystal which are most widely used in computer vision, they are nematic and ferroelectric liquid crystal.

The next chapter will describe various efforts undertaken bt the research community in investigating the phenomenon of polarization, especially in visual ability. Starting from the study of animal vision capabilities that can be used as bio-inspiration in creating a machine or robot vision that is sensitive to polarization, to the creation of various imaging techniques and polarization sensors.

Chapter 3

Polarization Imaging Toward a Physical-based Robotics Vision

This chapter discusses about a polarization imaging to be used in robotic vision. It consists of:

1. *Bio-inspiring polarization sensitive ability possessed by animals,*
2. *The development of the system producing the polarization, from polarization instrument to embedded polarization sensors,*
3. *The application associated with the skills needed in robotic vision.*

3.1 Bio Inspiring from Animal Vision A Wonderfull technique from the Nature

Using the polarization of light is an everyday behaviour for many creatures of the Earth. Several types of animals using the polarization information as navigation tool for detecting food, nest or the presence of predators that could threaten their life. Some other animals are able to exploit the polarization of light for camouflage to avoid predators and even to communicate with each other. The brief history that explains this wonderful phenomenon in nature, are detailed in the comprehensive study by [Andreou and Kalayjian (2002)] and [Hovarth (2003)].

In nature, the light coming from the sun is essentially un-polarized. But in the transmission toward the object on earth, this natural light fields normally contain a complex pattern of partially linearly polarized light (in most of research called e-vector), produced by reflection from dielectric surfaces (such as water) or by scattering in the air

and water. This pattern, or aspects of it, can be visualized by some animal species, including terrestrial animal and the majority of marine invertebrates.

3.1.1 *Polarization sensitivity of Terrestrial Animals*

In addition to their ability to sense Earth's magnetic field, the bees also have Polarization sensitive ability. This can be understood from the fact that bees have a unique behaviour based-on the position of the sun and the earth's gravity called *the swaggle waggle dance of bees*. A review from [Srinivasan (2011)] gives a complete illustration about bee's visual cell. The surface of compound eye of bee is shown on Figure 3.1 A. These facet lenses, consist of approximately 5500 units a little eyes called *ommatidium*. The longitudinal cross section of one *ommatidium* is showed on B, this part consists of a small lens (diameter ~15-20μm) which focuses light into nine *photoreceptors*. Each *ommatidium* collects light from the world and accepts incoming light from a cone-shaped. Figure 3.1.C illustrates a structure of one of the *photoreceptor* cells, and shows the *microvilli* that contains the *photopigment*; the ability to absorb and read polarization information and process as array together with other *ommatidium*.

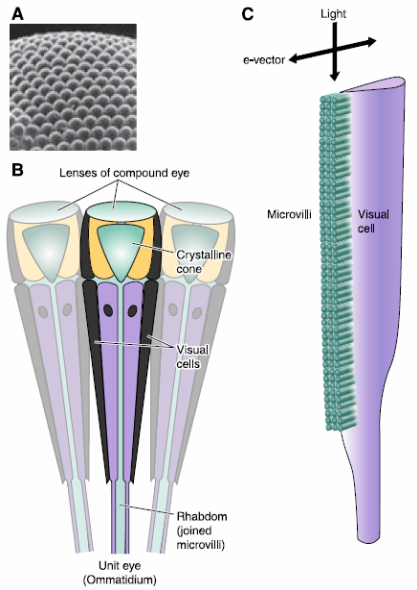

Figure 3.1 Bee Visual System [Srinivasan (2011)]

Karl Von Frisch in 1967 indicates that the *photopigments* of bees contribute to the polarization sensitivity and can perceive polarized light distinctly in the Ultraviolet range.

[Srinivasan (2011)] also showed that the perception of polarized light by bees can still be efficient in a partially cloudy sky which would support this idea.

The *swaggle waggle dance* is the moving pattern of bees that indicates a cue to the distance of food. There is an α angle, which indicates the angle between the sun position and the direction of flight to be taken. From this fact, Von Frisch concludes that for the bees, the sky reveal a pattern of polarized light from the sun.

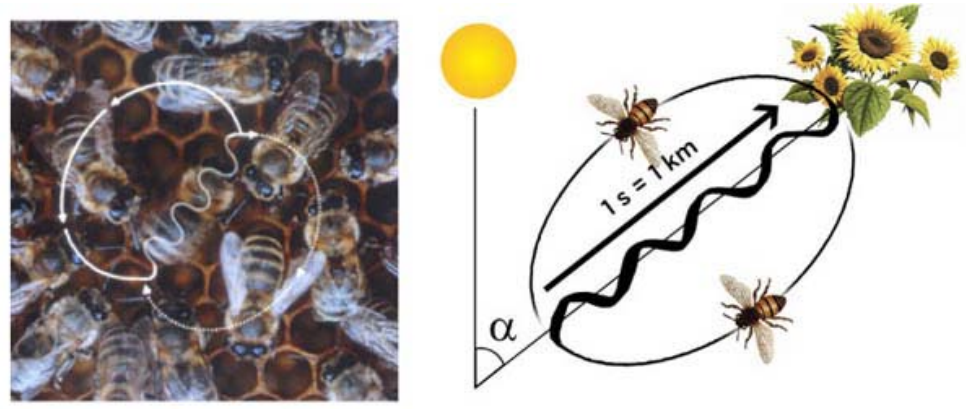

Figure 3.2 Unique movement of honeybees based-on the sun position sense ability

Based-on review of [Andreou and Kalayjian (2002)], other terrestrial animals such as dragonflies and waterstrides use the polarization of reflected light to detect water. The insec alike beetles, flies, and also some reptile such as salamanders and lizards are able to sense and use polarization in their environments.

3.1.2 *Polarization sensitivity of Marine Animals*

The differences between the polarization properties of marine and terrestrial environments have a direct influence to the sensitivity of the Polarization receptors in animals that live in that habitat. According to [Cronin and Shashar (2001)], unlike in air environment, the water region generally have a light intensity (ultraviolet light is considered as an object that can be sensed by marine animal sensor) relatively low because of absorption and scattering of light, even in quite clear water. They showed that the degree of polarization of light in water increases steadily with wavelength above 450 nm. The relatively low polarization values in water must challenge the polarization sensitivity vision of marine animals.

Many species of marine fishes such as rainbow trout and goldfish [Hawryshyn (2000)] perceive the submarine light field for orientation. Hawryshyn has identified the presence of two differentially sensitive classes of UV polarization sensitive cone mechanisms in trout fishes. The polarization vision depends on the possession of at least two differentially sensitive receptor (cone) mechanisms. The cephalopods (one kind of squid) have more unique capability to sense polarization of light. They can respond and reflect the patterns of polarized light at once. The interesting fact is, the cephalopods are colorblind, but their eyes have photoreceptors and corresponding hair-like *microvilli* which expand their surface area, and can enhanced ability to selectively perceive linearly polarized light [Shashar and Cronin (1996)]. In the recent research, it was shown that the cuttlefish (one species of cephalopod) have ability to manipulate the reflected pattern of polarization in their skin. They can use its ability for camouflage and also for enhancing the visibility of their prey. They also induced polarization patterns in their skin for communication between male and female during copulation time [Shashar et al. (2000)].

The Octopus used polarization information to increase visual contrast [Shashar and Cronin (1996)]. The interesting part is, the stomatopod has a unique colour-vision system that is able to register a change, located in the mid-band region of the eye. The mid-band may therefore be involved in communication in both colour and polarization space [Marshall and Shashar (1999)].

The mantis shrimp have a hyperspectral eyes with crystalline structure of their *microvilli* which perceive from the infra-red, visible to UV range. They can also perceive linearly and circularly polarized light [Chiou et al. (2009)]. In the mantis shrimp retina there are specialized cells that work like a nearly perfect quarter-wave retarders, much better than the best synthetic retarders made by humans. They can convert incoming circular polarized light into opposite angles of linear polarized light and can emit circular polarized light from their tail.

Based on the facts derived from various studies that have been done on the visual modality on terrestrial and marine animals, suggesting to researchers that the ability to utilizes the polarization of light existed on them. The animal ability to sense the polarization of light, came as a wonderful gift and can be addressed as a good source for

human to enhance their visual capabilities, by mean of creating a bio inspired machine vision or robotics.

3.1.3 *Polarization In Nature*

Naturally, human are unable to sense polarization, but humans have still been able to measure and analyze polarization in our environment and using it for many applications. This chapter contain summary of the main evolution of ideas and the invention of the light polarization phenomena.

The first observation of a polarization related phenomenon in nature was made by Erasmus Bartolinus in 1669, concerning the double-refraction of light through an Iceland spar, but in this time, he was not yet aware of the polarization phenomenon [Coulson (1989)]. Then, the polarization of light by reflection was formulated by a French engineer, Étienne Louis Malus (1775-1812) in 1808. He found that the two images obtained by double refraction of calcite crystal from reflection of direct sunlight, varied in relative intensities when the crystal was rotated about the line of sight. The Malus law explained about the proportionality of the intensity of light transmitted by a polarizer to the square of the cosine of the angle of direction of the transmission axis for linearly polarized incident light. However, Malus has not interpreted this phenomenon, but Malus experiment can be applied as first the "polarization of light". One year later, the polarization of light in the clear blue sky was discovered by French physicist Dominique Francois Jean Arago (1786-1853) in 1809. He found the first neutral point of the firmament and the skylight polarization established maximum at 90° from the sun.

In 1815 Scottish physicist, David Brewster (1781-1868) issued the relationship between the refractive index of a medium and the angle of incidence, called the Brewster angle. In 1869, the Irish physicist John Tyndall (1820-1893), made some observations on smoke particles, and found the fact that the polarization of light scattered by particles changes strongly with the dimensions of the particles. Then, more detail about the light, the Scottish physicist, James Clerk Maxwell (1831-1879) at 1873 has surmised that light is an electromagnetic wave based-on theoretical considerations. Several years later, at

1888, Heinrich Hertz (1857-1894), the German physicist verified Maxwell theory by direct experiments, and give a proof that light is an electromagnetic wave.

The study of polarization phenomenon in different wavelength of light is still continuing. For example, [Wolff et al. (1998)] analyzed the degree of polarization in the infrared wavelengths. In 2004, [Barta and Horváth (2004)] investigate the insect perception of skylight polarization for orientation in the ultraviolet (UV) wavelength.

[Hovarth (2003)] made a comprehensive research about polarization characteristics of the Sky, by doing a lot of measurement of polarization effect in several places in the world and characterized the fourth neutral point in the sky.

[Sabbah et al. (2006)] performed a series of measurements of the polarization of skylight transmitted through Snell's window into water. Sabbah investigated the spectral distribution of this polarization, and figured out predictions concerning the polarization information, that are available to underwater animals and summarized the potential animals adaptations for utilizing these information.

The two recent researches above show that the polarization measurement method strongly supports another field such as physics and biology in the sky and marine research. The information obtained from that, can be used for further research in biology-related behaviors or other animals for example.

3.2 Research for Measuring Polarization of Light

One of the milestones for acceleration of polarization imaging related research, in the field of computer vision was due to Lawrence B. Wolff in his thesis about Polarization methods in computer vision in 1991. After that, many implementations in the vision field have been discussed and realized. Since 1980's, and more intensively from 1990's until now, different kinds of imaging polarimetry have been developed to measure the polarization patterns of objects and natural scenes in a wide field of view, and the polarimetric devices have been invented to filter, quantify, modulate or even to separate polarized light.

3.2.1 *Toward Polarization sensor and camera technology*

In the early 1990's, to measure partial linear polarization, the polarization cameras used a monochrome CCD camera mounted with a mechanically rotating linear polarizer (called analyser – see Figure 3.3) which is rotated to three different orientations [Wolff (1989)], [Wolff (1990a)]. This is an easy set up but which suffers from many drawbacks such as time involvement, repetitive, distortion, which an explained in chapter 2, were solved by the used of active component such as nematic liquid crystal [Ferraton et al. (2008)], [Morel et al. (2005)], [Rantoson et al. (2009)] or Ferro electric liquid Crystal [Shtykov and Vija (2003)].

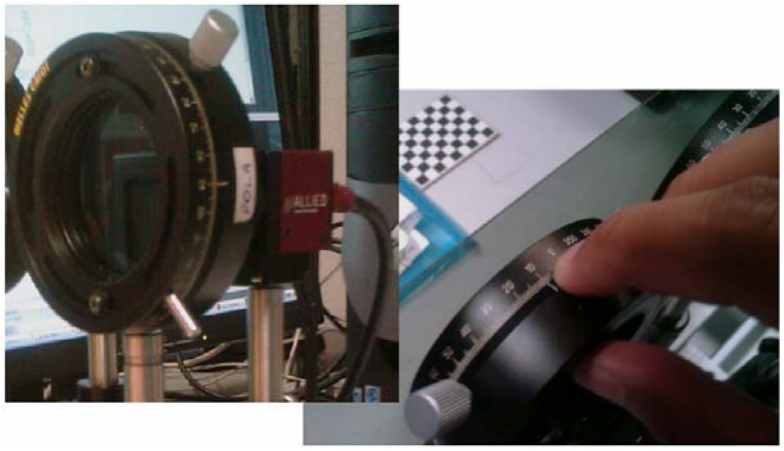

Figure 3.3 Polarizer mechanical rotator

Later on, the research community has used the polarization information to infer other information (3D geometry, colour, texture, etc) about the controlled scene.

3.2.1.1 Polarization and Stereo Imaging

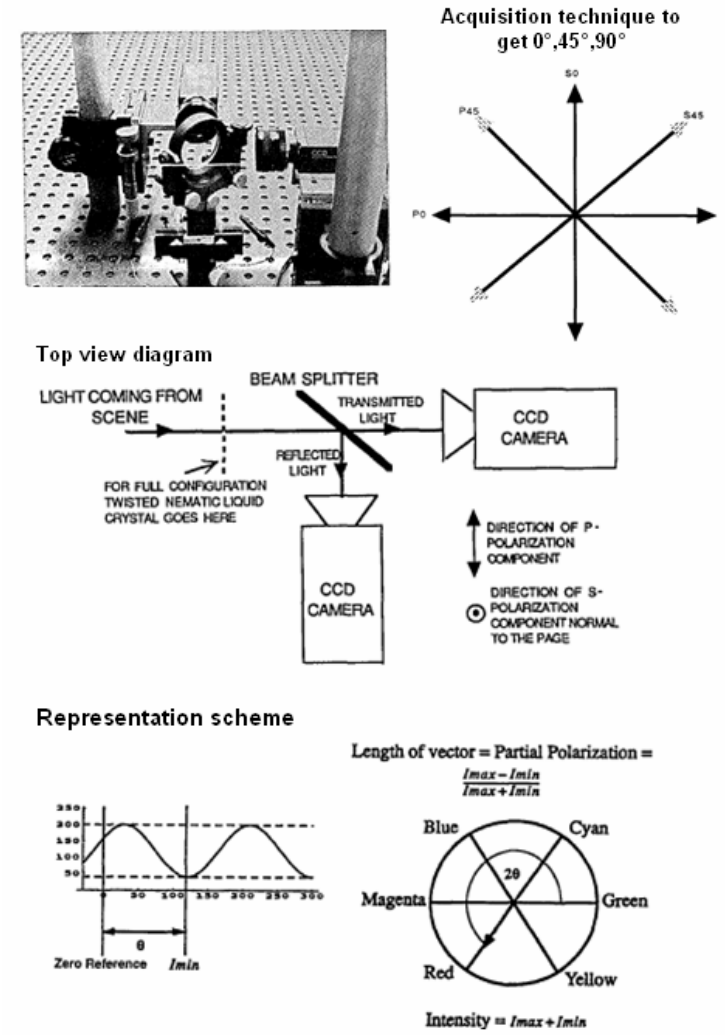

Figure 3.4 Polarization Stereo using beamsplitter and liquid crystal [Wolff (1994)], [Wolff and Andreou (1995)]

[Wolff (1990b)] made the first effort to merge the polarization data from more than one view. In order to estimate the orientation of the plane, Wolff designed a imaging systems based on a beam splitter enabling to measure the polarization components simultaneously directly from two CCD cameras. To accelerate the measurement time, Wolff in 1994 [Wolff (1994)] as well as Wolff and Andreou in 1995 [Wolff and Andreou (1995)] utilized twisted nematic liquid crystal in front of the beamsplitter to rotate

automatically the polarization angle of the transmitted light. The polarization information are obtained in pixel resolution and visualized in the hue-saturation-brightness scheme.

In 1997, Lin [Lin and Lee (1997)] proposed a specularity detection method based on a synergistic integration of color and polarization information from multiple views. Their approach fuses color and polarization histogram spaces and compares multiple-view data in the fused space without spatial correspondence with Color Histogram Differencing (CHD) technique and performs well in detecting specularities for a surface with spatially varying color under complex illuminations.

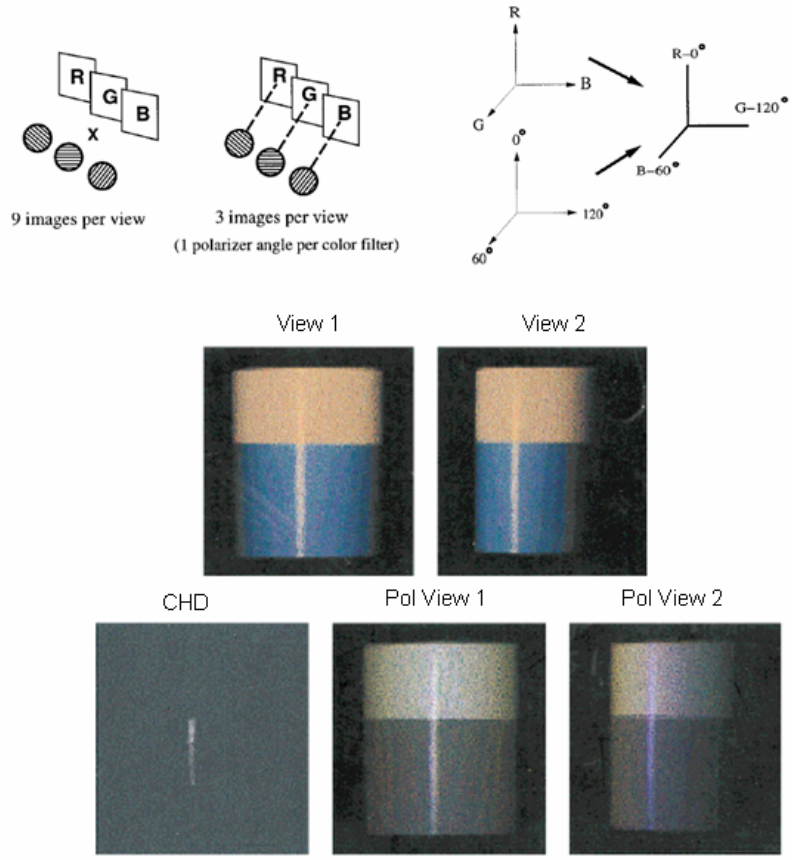

Figure 3.5 Polarizer filter pairing with colour (top left), merged space of polarization and colour space (top right) and result [Lin and Lee (1997)]

Image acquisition is done by choosing 0°, 60° and 120° as polarization-space angles, to promote differences in attenuation of polarized light. A fixed-angle polarizer is employed with each color filter not only to facilitate the use of the merged color/polarization space (see Figure 3.5 top left). But also to reduce the amount of image

data, from nine image planes per view to three, and potentially allowing quick image capture by obviating the need for polarizer rotation. This configuration is called color/polarization histogram differencing (CPHD).

In 2000, Terrier [Terrier and Devlaminck (2000)] proposed a method for precisely determining the angle of polarization φ based on self-calibration techniques. He merged the polarization information with the classical intensity information of the light in order to generalize the information content of a standard image. The advantage of his methods is that it is not necessary to exactly know the rotation angles θ of the polarizer.

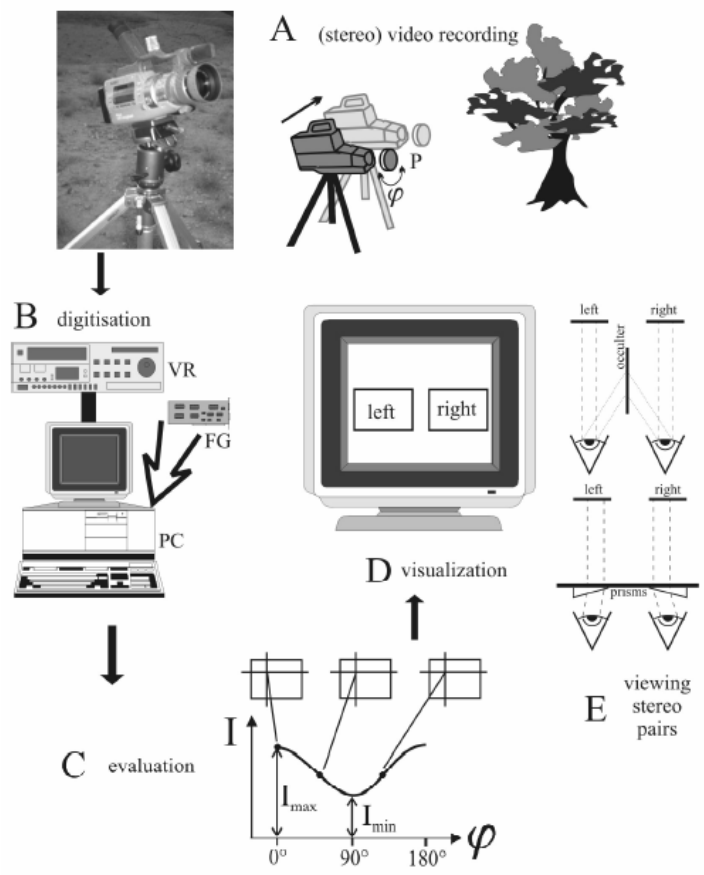

Figure 3.6 Schematic of the technique of rotating-analyzer stereo video polarimetry [Mizera et al. (2001)]

In 2001, Mizera et al [Mizera et al. (2001)] designed a stereo video polarimetry to measure and visualize in three dimensions the polarization patterns in nature scene. In 2005, Atkinson [Atkinson and Hancock (2005)] developed a surface reconstruction technique that uses polarization information from two views. Finding correspondences

between pixels on each image is a common problem on many multiple view techniques. Atkinson resolve these problem by exploiting the spontaneous polarization of light caused by reflection to recover surface normals. Polarization information is using to analyze the topographical surface structure and to perform patch matching in order to present correspondence.

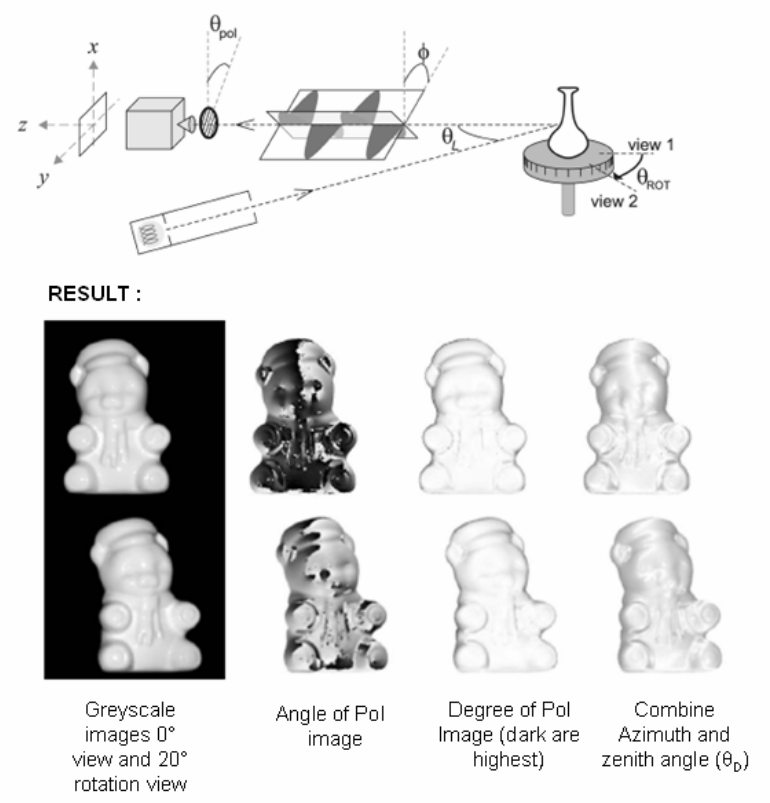

Figure 3.7 Schematic of a two view polarization image acquisition system for shape estimation and the result [Atkinson and Hancock (2005)]

To compute the angle and degree of polarization, Atkinson performed two images acquisition step, in the first view, images were captured with the polarizer oriented at 5° intervals. The second view obtained by rotating the object by 20° from initial state 0° (see Figure 3.7 first row). The images from each view are converted into two angle images and two degree of polarization images by applying a Levenberg-Marquardt least squares fitting algorithm to observed pixel brightnesses (see the result in Figure 3.7 second row). Then next step is to make a selection of potential point correspondences based-on polarization information above. Needle map integration to form depth map using the

Frankot-Chellappa algorithm was generated after disambiguation of azimuth angles. Finally, Atkinson using the mean of an estimated reflectance functions from the shading information to improve the accuracy of the surface normal estimates.

In 2009, Sarafraz [Sarafraz et al. (2009)] proposed the integration of polarization analysis with stereovision for enhancing visibilities images in scattering media in underwater imaging application. Acquisition principle is using two images are taken simultaneously with different polarization filter setting, which is one image is typically brighter than the other. The computation of degree of polarization is perform from the ratio of the difference between the two images and taking into account to the backscatter component (see figure Figure 3.8 first row). In the experiment, scattering level (related to water turbidity) was varied by adding a known volume of low-fat milk to clear water, namely quarter (for low concentration) and half (for high concentration).

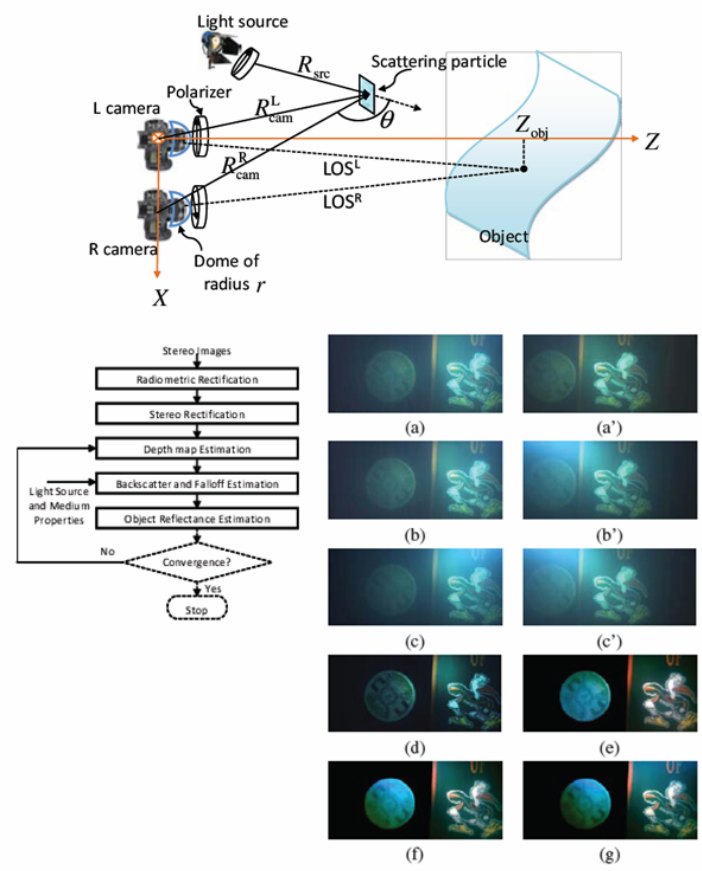

Figure 3.8 Polarization Stereo Imaging Setup for Enhancing underwater visibility, flowchart and result [Sarafraz et al. (2009)]

As seen on Figure 3.8, the data results from medium concentration scene can be explained as follows. Images in (a,a') are raw data left and right stereo using polarizers on both cameras with orientation that minimizes the backscatter effect, images in (b,b') is came from polarizer filter only on the left camera, (c,c') are images with no polarizer in both camera. (d) is left image in clear water (d) use as comparison image to the reflectance maps estimated by Sarafraz method. The images in (e-g) are left images de-scattered results that correspond to the data in (a-c) respectively.

3.2.1.2 Polarization and Wide Angle Camera

Generally, the field of view of an imaging system depend on the optical device that is used. For instance, in common photographic and video cameras, the lens system has a field of view of about 30°-50° for horizontal view and 20°-40° for vertical view. The uses of wide angle camera are depending on the focal length and the aperture of camera. Many applications of polarimetry require a wider field of view, for example to observe polarization effects in the sky or in the autonomous vehicle navigation system. One of the ways to extend the common field of view to wider field of view is by decreasing the focal length. It can be given by using a fisheye lens mounted onto a normal photographic camera to ensuring a conical field of view with an aperture angle of 180°, therefore it can capture the whole hemisphere of the optical environment.

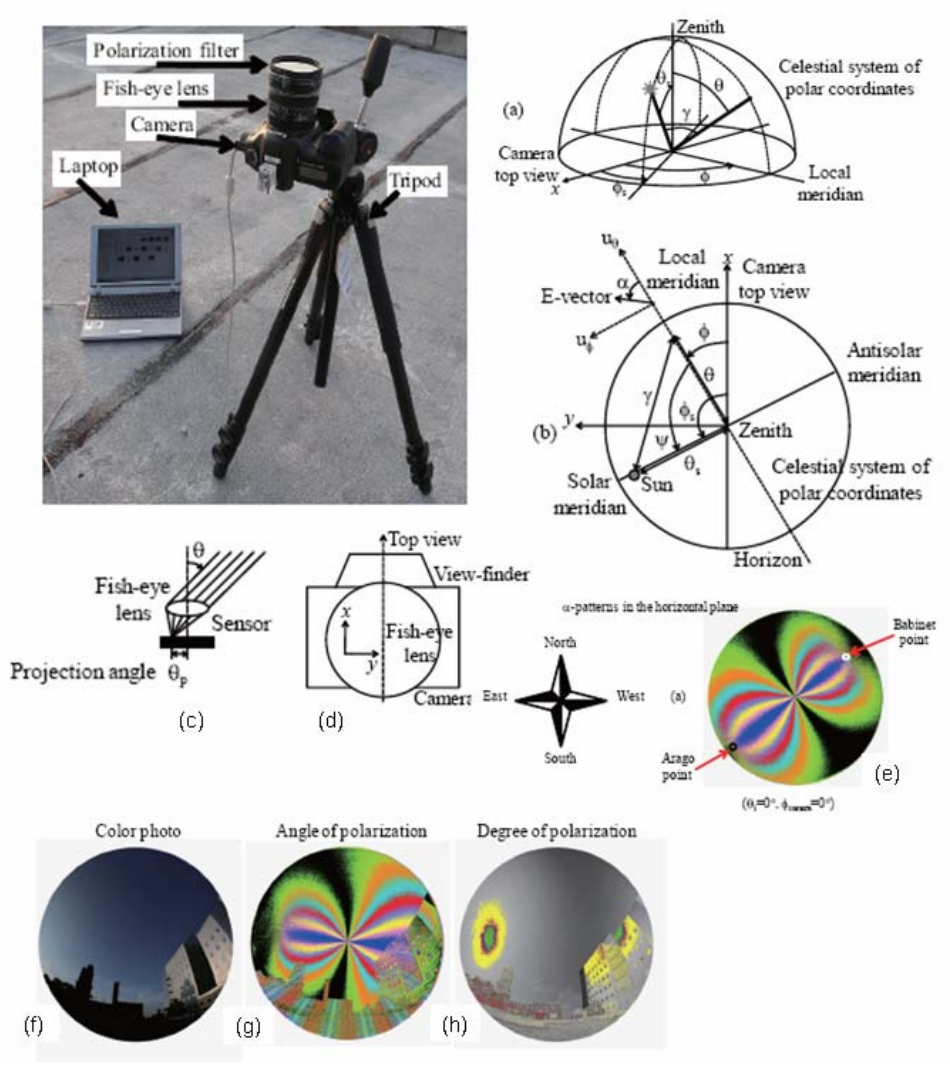

Figure 3.9 Miyazaki setup, representation and result polarimetry of sky using fish eyes lens [Miyazaki et al. (2009)]

In 2009, Miyazaki [Miyazaki et al. (2009)] proposed a measurement system based on a fish-eye lens, with CCD camera and linear polarizer to analyze transition of sky polarization patterns in 180°. To validate the measurement of overcast skies, Miyazaki compared the results measured with celestial polarization patterns calculated using the single-scattering Rayleigh model. The system setup and the result of Miyazaki can be seen in Figure 3.9.

Another alternative technique of wide angle camera system to provide a 180° field-of-view is by using a mirror with a 180° field of view. This is technically known as

a catadioptric system. Catadioptric is an unusual construction of acquisition technique using combination of mirrors (catoptric) and lenses (dioptric).

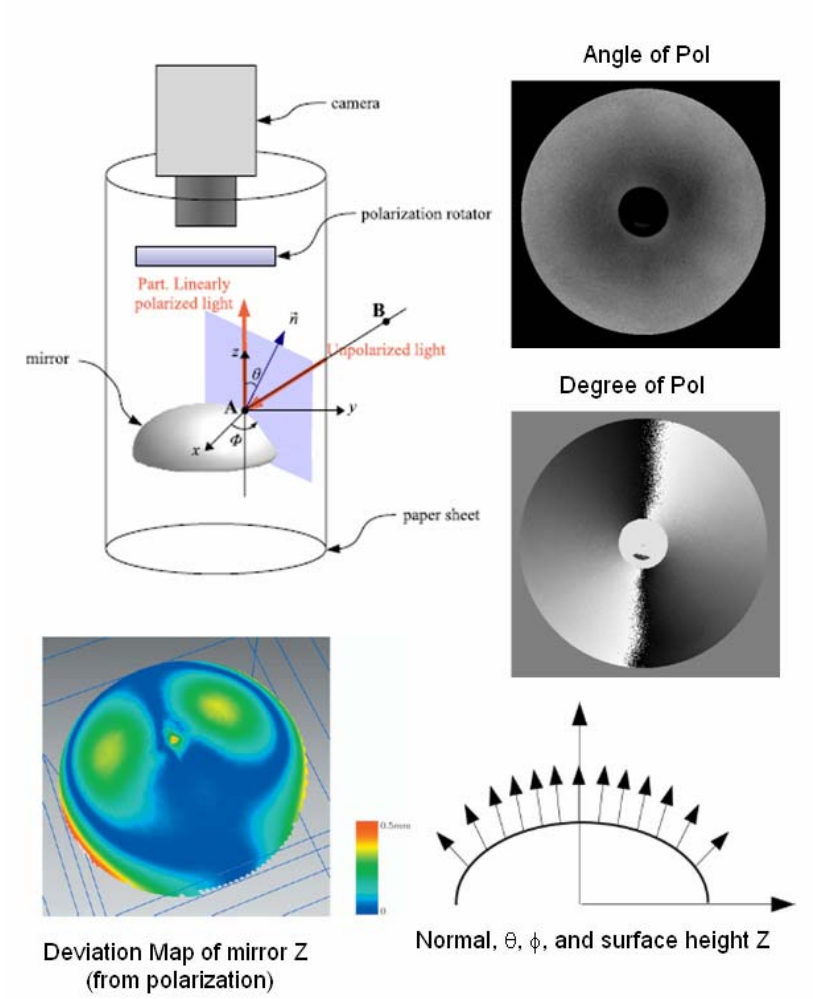

Figure 3.10 Calibration of camera catadioptric by polarization [Morel et al. (2007)]

In 2007 Morel [Morel et al. (2007)] proposed an efficient method based on an accurate measurement of the three-dimensional parameters of the catadioptric mirror through polarization imaging for calibration of catadioptric sensors. Using Morel's method, the camera is automatically calibrated without any calibration patterns, while inserting a rotating polarizer between the camera and the mirror (see Figure 3.10 top left). Morel implemented a polarization imaging to calibrate the catadioptric sensor based-on principle of the "shape from polarization" technique (to compute the normals from the angle polarization φ that is linked to azimuth angle ϕ and degree of polarization ρ that is

linked to zenith angle θ). Then, three-dimensional surface of the mirror (see Figure 3.10 bottom left for illustration of 3D map model) can be computed from the surface normals. To perform a calibration, Morel uses the generic calibration concept that considers an image as a collection of pixels, and each pixel measures the light along a particular 3D ray. The calibration conducted from determination of all projection rays and their correspondence with pixels. The Experimental results provide that the sensor is properly calibrated.

According to the two examples describe before, it can be concluded that the utilization of wide angle camera is ideal to study the polarization patterns of the full sky, and to obtain three-dimensional parameter of surrounding area or study of the reflection-polarization patterns of dielectric or specular surfaces.

3.2.2 *Polarization Cameras*

A polarization camera has more general capabilities than standard intensity cameras by adding component capable to make possible to sense the complete set of electromagnetic parameters of the light incident onto the camera. The next section will give step by step development of polarizational camera research ranging from experimental to commercial camera.

3.2.2.1 Experimental Polarization Camera

Research of Wolff et al in 1997 [Wolff et al. (1997)] exploited the principles of liquid crystal technology to fully automate the process of resolving polarization components, and added ability to visualize a scheme for mapping partial linear polarization states into hue-saturation-intensity color space in the end of his system.

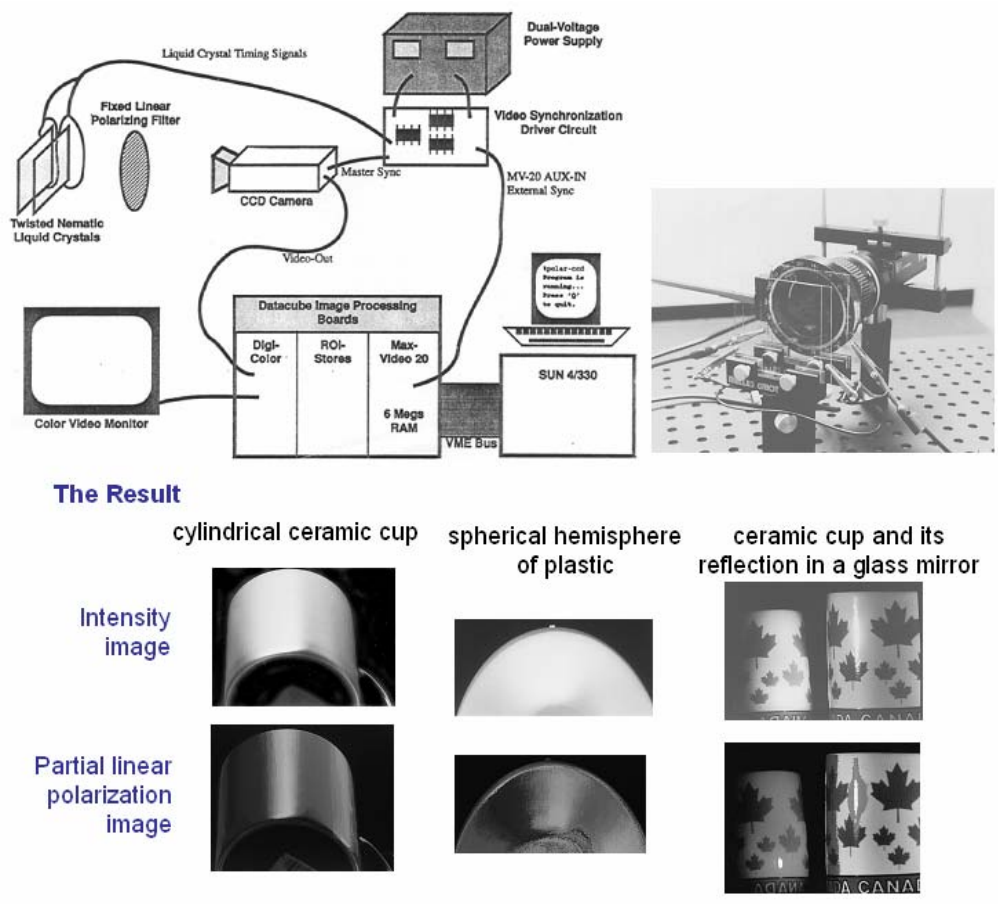

Figure 3.11 Complete schematic diagram of the liquid crystal polarization camera interfaced with digital hardware and the captured images (Wolff, 1997) [Wolff et al. (1997)].

Cronin et al. in 1994 [Cronin et al. (1994)] tried to build a portable version of the imaging polarimeter of Wolff (1993). He constructed a portable polarimeter that analyses the linear polarization characteristics on a single camera basis and using LC as automatic rotation polarizer. Two configurations are presented (see Figure 3.12):

1. The autonomous sensor, uses a small camcorder for recording images, and analyzed polarization at a later stage. This configuration consist of two twisted nematic LC (TNLC) and fix polarizer filter are mounted in front of the camcorder lens. The TNLC rotate light by 0°, 45° or 90° with controlling circuit and the 9 V batteries are placed on a board to hold the camcorder with its protecting housing.

2. The on-line sensor that uses a digital camera connected to a personal computer which controls and analyses the information directly. Two TNLCs and a fixed polarizer filter are connected to an monochrome digital camera, the images are transferred to a personal computer for polarization analysis and also working as controller for switching of the TNLCs.

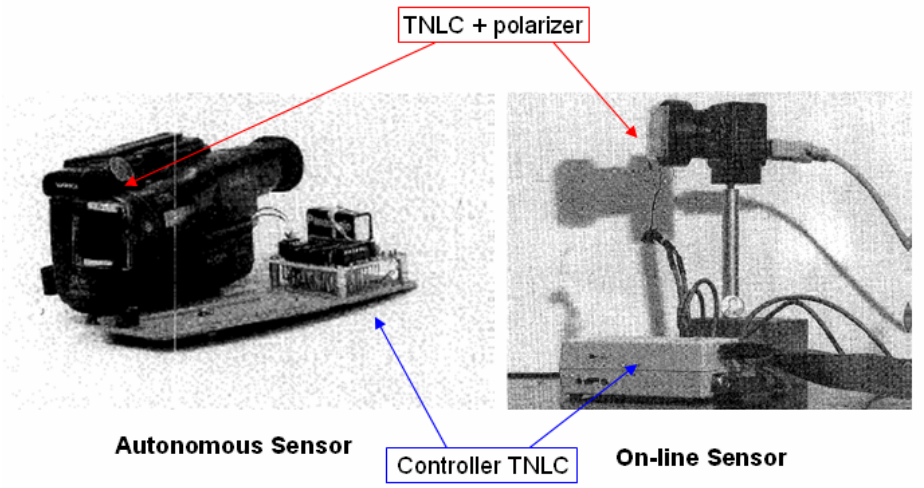

Figure 3.12 Two Configuration Polarization LC camera by Cronin [Cronin et al. (1994)]

Cronin et al. used their portable and on-line Polarization LC camera to record polarization patterns occurring in a tropical rain forest.

In 1999, Hanlon et al. [Hanlon et al. (1999)] designed a simultaneous video camera polarimeter from a standard three-tube camera. Three-tube camera is a video camera with a special device called a beam splitter prism, that separate the incoming light (usually is white) from the lens into the 3 separate colors for the color tubes in the camera [Bensinger (1981)]. The individual color signals from the tubes are then mixed electronically by a matrix and added to the luminance signals generated by a separate luminance tube (see Figure 3.13). In Hanlon configuration, this prism is replaced with a neutral prismatic beam-splitter made from dichroic material. A linear polarizer (small disc Polaroid) is placed in front of each camera tube to distribute a different part of polarization sensitivity (with direction of the transmission axis of the polarizers is 0°, 45° and 90° from the vertical) to the three channels.

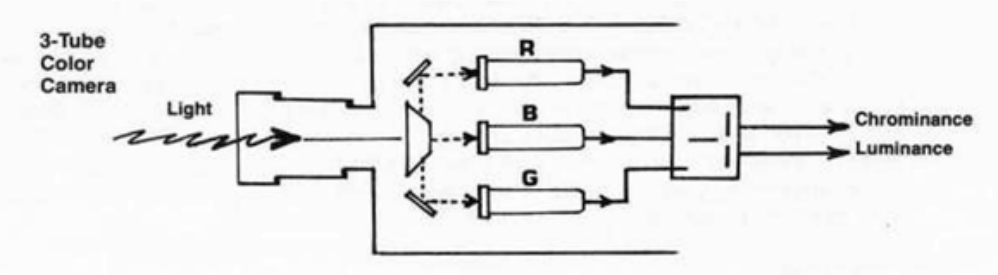

Figure 3.13 3-Tube color camera work principle [Bensinger (1981)]

The Hanlon video polarimeter was used for aerial recording of the polarization patterns of cephalopods moving in an aquarium. This camera is better suited than previously described polarimeters (Cronin et al. in 1994 and Wolff et al. in 1995) for recording the polarization patterns of moving animals, because it provides true instantaneous measurements.

In 2005, Miyazaki et al. [Miyazaki et al. (2005)] developed a device controllable from the computer to measure the Stokes parameters and represented it by using a material called PLZT. PLZT is transparent ceramics (made from (Pb, La)(Zr Ti)O_3), and has a birefringent properties depending on the voltage. Miyazaki configuration consists of the camera with neural density (ND) filter and PLZT in front of it (see Figure 3.14). Image acquisition is done by setting a linear polarizer in front of the camera, and obtain three images by setting three different electric voltages applied to the PLZT (here PLZT acts as a quarter waveplate). Next step to is change the polarizer into the ND filter, and obtain one image with no electric voltage to the PLZT unit. From these four images, the calculation of Stokes parameters of the light can be done. Visualization of the results can be seen in the Figure 3.14.

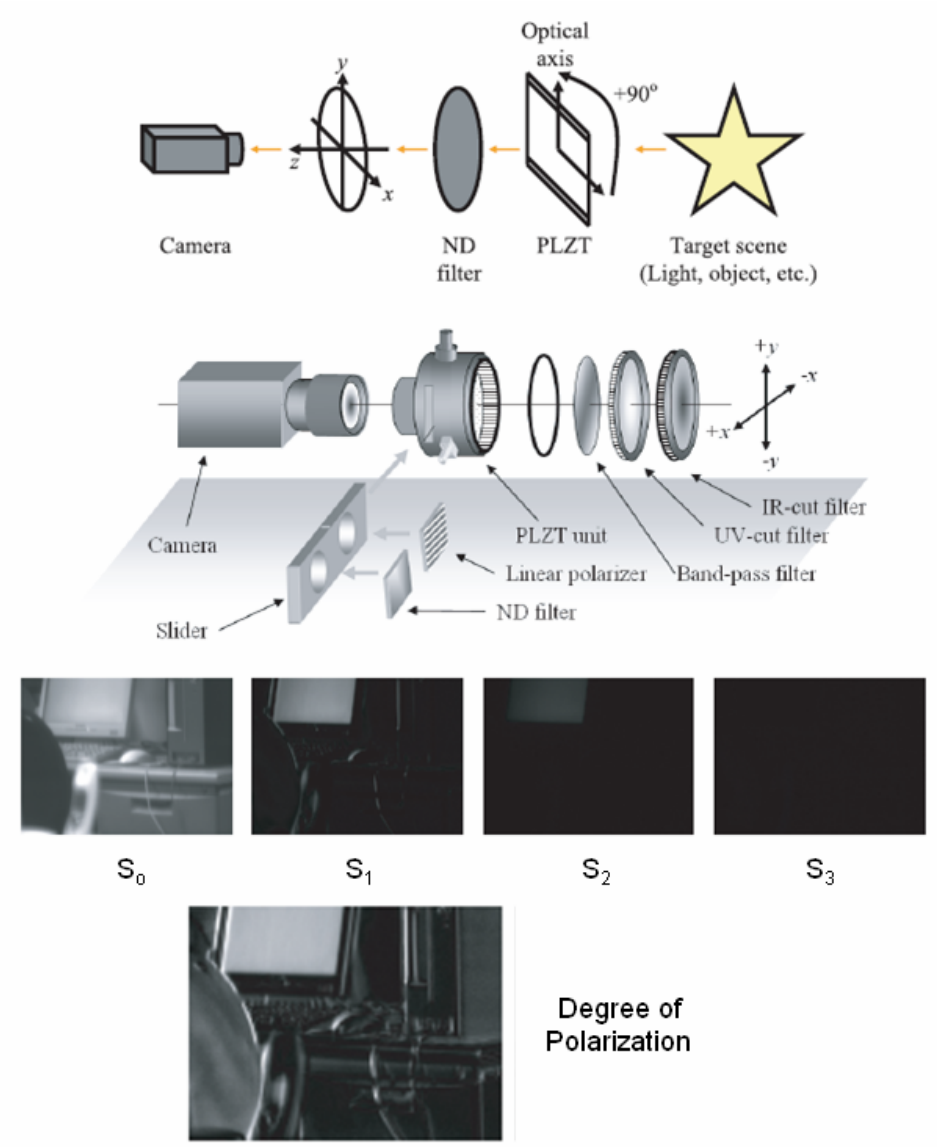

Figure 3.14 PLZT Camera configuration and stokes vector and Degree of Polarization as result [Miyazaki et al. (2005)]

(McGuire, 2006) [McGuire and Matusik (2006)] using passive polarization technique for blue screen matting to separates foreground and background elements of video for special effects shots. The camera design and comparison result of the polarization technique and blue-screen technique.can be seen at Figure 3.15.

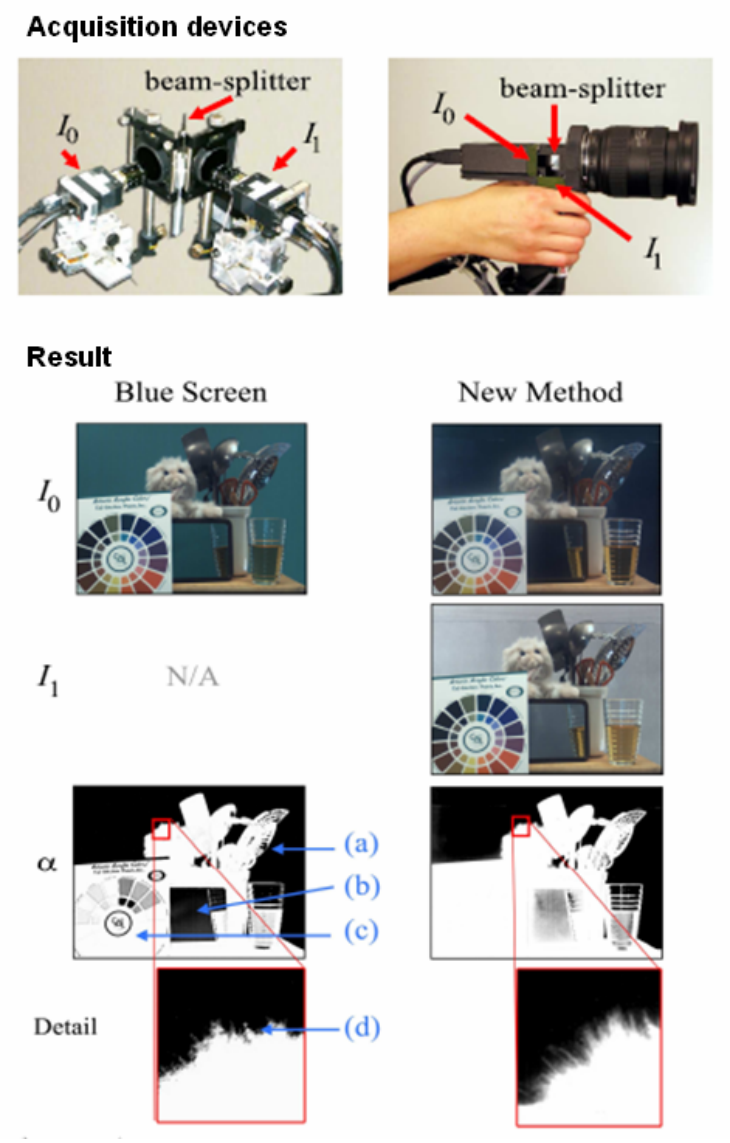

Figure 3.15 Prototype camera that splits on polarization (left side) and hand-held form factor with the beam-splitter behind of the lens (Right), I_0 and I_1 is two different intensity images captured by Polarization camera (90° difference) [McGuire and Matusik (2006)]

In the remote sensing area, Xingfa Gu in 2010 [Gu et al. (2010)] designed the DPC (Directional Polarimetric Camera). This instrument is a CCD camera that covers the spectral range of 400–900nm with three polarized spectral bands (490, 665, and 865nm) and work in spatial resolution (4x4m^2 at 4000m). The application of this camera is for monitoring aerosol emission and absorption sources in cities.

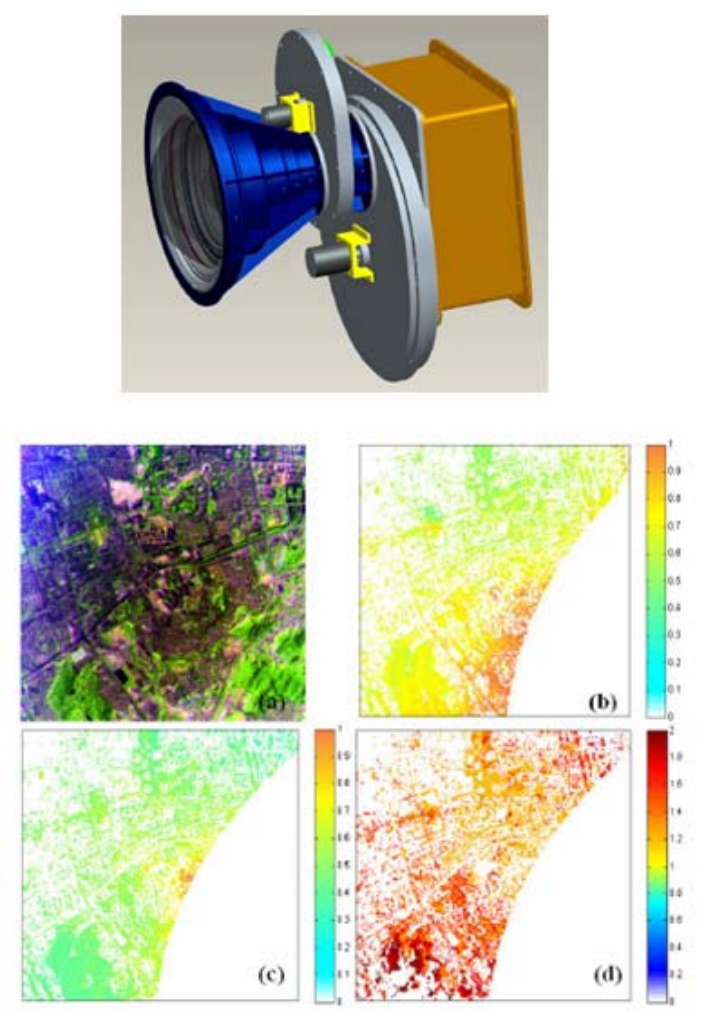

Figure 3.16 The Directional Polarization Camera for remote sensing application and the result [Gu et al. (2010)]

As seen at Figure 3.16, the imaging results of DPC measurement in the Pearl River Delta. (a) True-color map (b) Aerosol optical depth (AOD) at 0.665 μm. (c) AOD at 0.865 μm. (d) Angstrom exponent over vegetated surface in the region. Xingfa Gu claim, the result from their DPC measurement above is nearby ground-based Sun photometer measurements.

In 2003, Ramella et al [Ramella-Roman et al. (2003)] built a real-time hand-held polarized-light system as a device to guide clinical excision and to facilitate clinical mapping of skin cancer margins. The system consisted of two 8-bit CCD cameras (Camera 1 and Camera 2) mounted on two sides of a polarizing beam splitter. A

polarized light source was mounted on the camera assembly and illuminated the patient's skin. Light was polarized parallel to the source-patient-camera plane. The light, reflected from the patient, was collected with an objective lens mounted on the beam splitter and divided into a horizontal (H) and vertical (V) component. The H component was collected by Camera 1, and the V component was collected by Camera 2. A new image was generated based on the polarization ratio (H - V)/(H + V) and displayed. This image was sensitive to the superficial skin layer and some early clinical examples are presented.

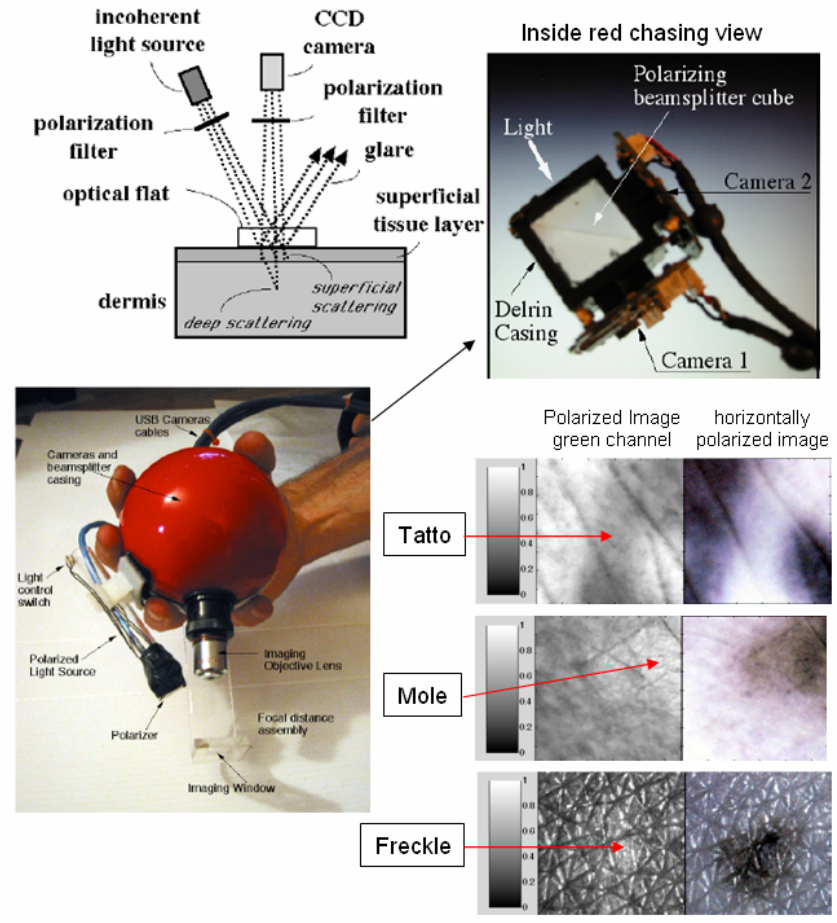

Figure 3.17 Setup, main component and result from Ramella handheld camera [Ramella-Roman et al. (2003)]

3.2.2.2 Commercial polarization camera

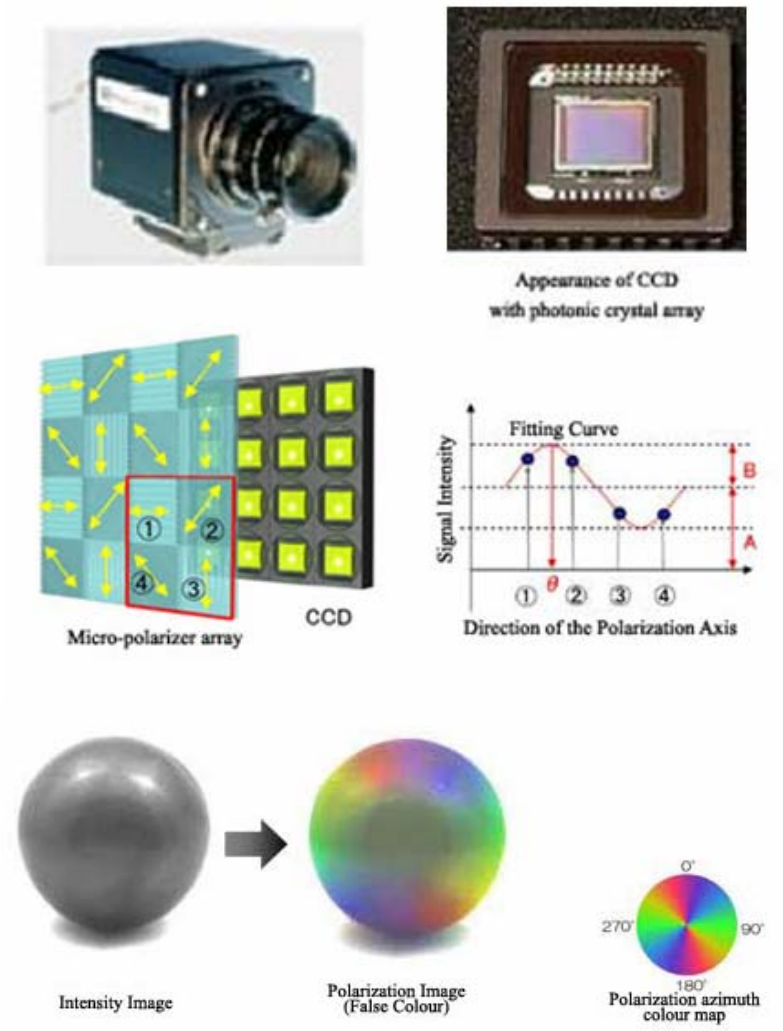

Figure 3.18 Photonic Lattice PI-100 polarization camera, consist of micro polarizer array in-front CCD sensor to compute a polarization state and the visualizing a image captured by camera [Photonic (2009)]

The polarization imaging camera from photonic Lattice (PI-100) [Photonic (2009)], CCD camera with resolution 1380x1024 pixel, 8 bit monochrome, can be used to record the brightness and polarization of light simultaneously. This camera is equipped by a polarizer array with elements in the same size as the pixels of the CCD assembled in front of the CCD (see Figure 3.18). Each pixel will detect a particular polarization by

calculating the intensity of each four neighbouring pixels that are connected to a unit cell (1,2,3,4).

Polarization camera from Fluxdata (type FD-1665P) [Fluxdata (2009)], uses a 3-ways beam splitter. This camera consists of two coating surfaces; the first coating surface reflects 30% and transmits 70% of the light. Then, the other coating surface provides a 50% reflectance and transmittance respectively. These combinations are splitting the incoming light into three components with equal spectral and spatial content (see Figure 3.19). The orientation of filters commonly at 0°, 45°, and 90° or three equal angular spacing in the range 380-1000nm can be customized according to the need. This camera also can be configured with either color or monochrome sensors for each channel.

Figure 3.19 Schematic view of 3-CCD Polarization Camera Flux Data and example images captured from that camera [Fluxdata (2009)]

Similar technology from Fluxdata can be found in product from Equinox Sensor [Equinox (2010)]. The polarization camera cans measures 3 out of the 4 Stokes parameters: intensity, degree of linear partial polarization, and orientation of the linearly polarized light. The system consists of three channels with 1024x1024 resolution, and 12-

bit dynamic range and can use real-time polarimetric video capability. The technology is based-on an optical beamsplitter that enables modular multispectral or polarimetric configurations. Figure 3.20 shows example of images captured by this camera.

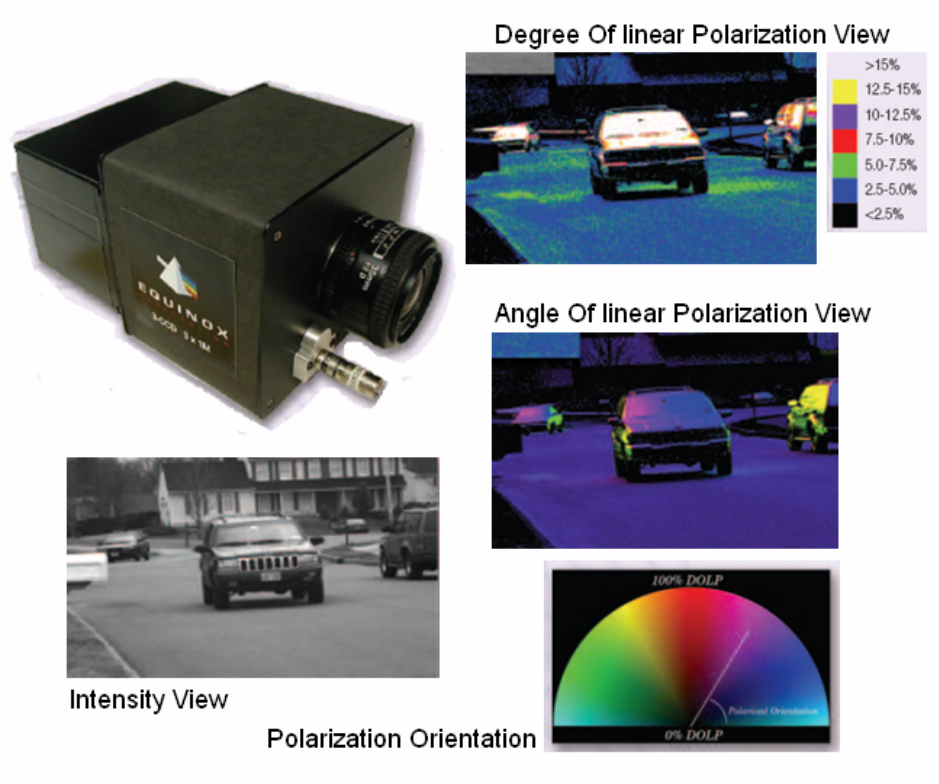

Figure 3.20 Equinox 3CCD Multispectral/Polarimetric Camera with example images capturing and processing in that camera [Equinox (2010)]

Polarization camera from Bossa nova Technology SALSA [Bossanovatech (2010a)] and SAMBA [Bossanovatech (2010b)]. SALSA is a linear Stokes polarization digital camera that has the polarization analysis capability for each pixel in the image and can operates in passive imaging (with un-polarized light source) and active imaging.

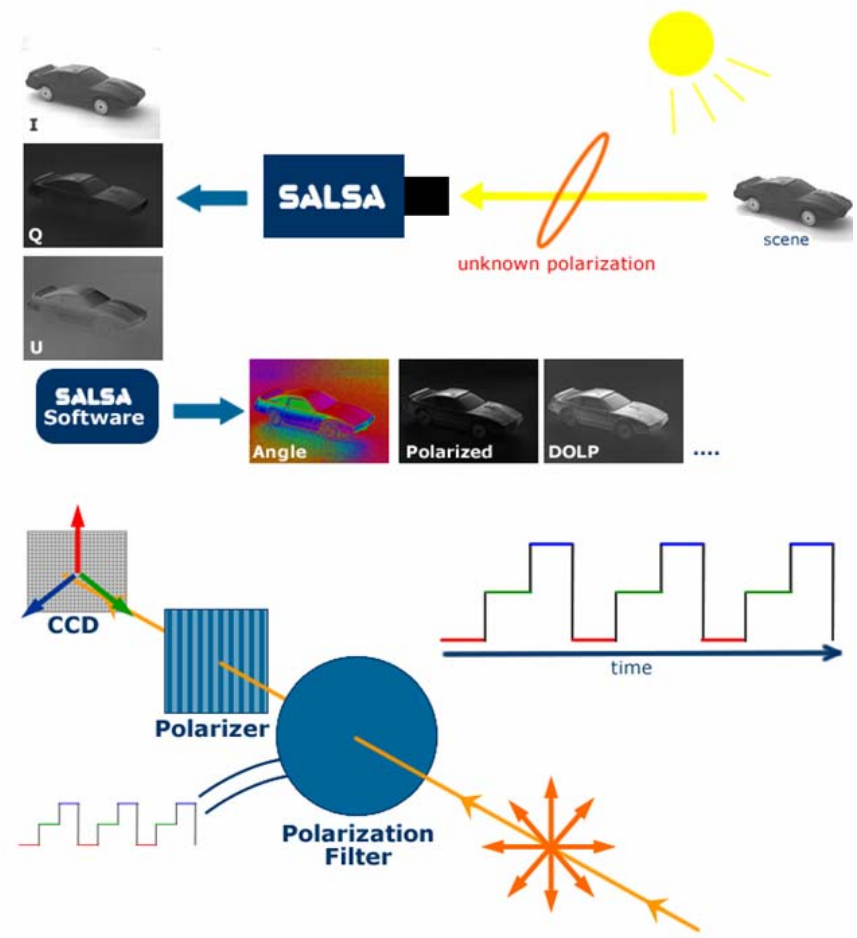

Figure 3.21 SALSA Camera work principle [Bossanovatech (2010a)]

SALSA camera capturing 3 raw images sequentially at video rate (in units of time) and represents it in the stokes vector I, Q, U or S_0, S_1, S_2. Then, the software calculates the state of linear polarization of light and allows visualizing many polarization parameters including degree of Linear Polarization, Angle of Polarization, Polarized and un-polarized light, in real time (see Figure 3.21). SALSA can also work in the near infrared (750 nm - 830 nm).

SAMBA is a digital camera based-on polarization-difference and mainly used in the scene with a light illumination from controlled light source with a known polarization state (active imaging configuration). SAMBA camera acquires the crossed (C) and parallel (P) polarization state for each pixel of the image at video rate from the incident light that is scattered by the object. Then, SAMBA measures the depolarization of the

polarized illumination for each pixel of the image (see Figure 3.22). Using two polarization images, P and C, various parameters for each pixel of the image can be computed based-on Table 3-1 below.

Table 3-1 Polarization Differential imaging principle in SAMBA Camera

Image Source	**Formula**
Specularity (S)	S=P-C
Diffuse (D)	D=2C
Intensity (I)	I=S+D or I=P+C
Degree of Polarization (DOP)	DOP=S/I or DOP=(P-C)/(P+C)

Bossa Nova technology claimed that SAMBA has a fast polarization analysis up to 10 KHz

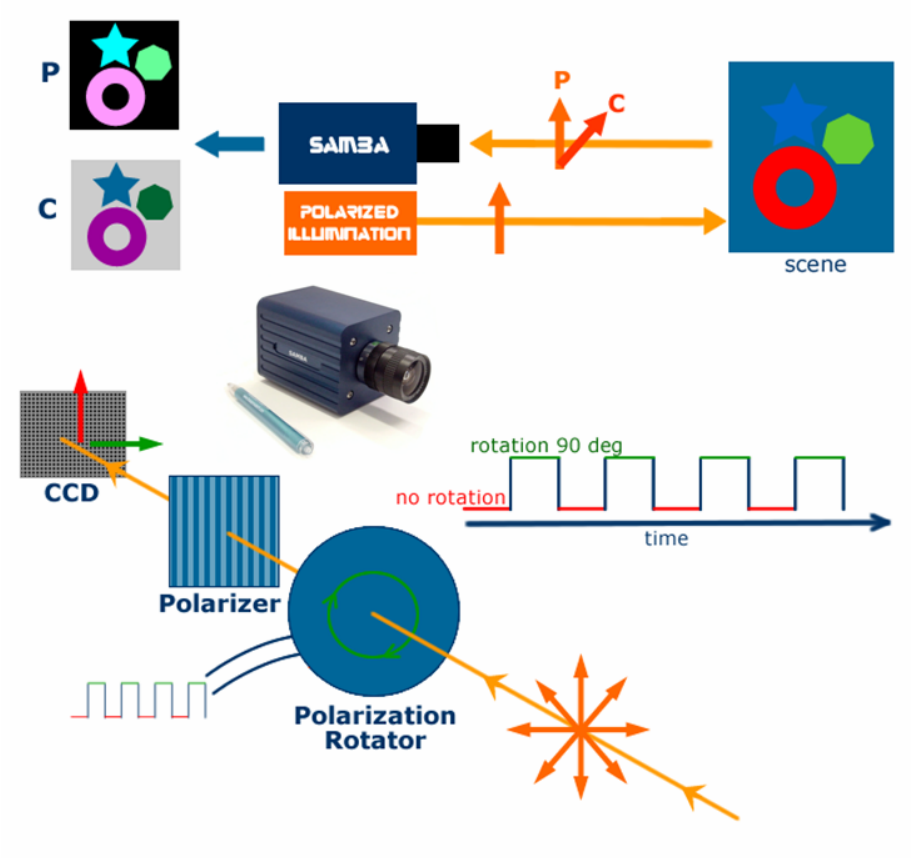

Figure 3.22 SAMBA Camera work principle [Bossanovatech (2010b)].

SALSA and SAMBA have been quite widely used for various purposes in the field of computer vision [Vedel et al. (2010)], one of which is to detect the mud [Rankin and Matthies (2008)].

3.2.3 *Polarization sensor*

The requirement a compact design and speed of generating polarization images shifting the research focus from imaging devices level to microscopic polarization filter. Polarization measuring instruments do not involve an imaging device again, but relying on array of photosensitive chip which are sensitive to polarization.

In 1995, Wolff and Andreou [Wolff and Andreou (1995)] started to develop a prototype of a polarization-sensitive chip with three photosensitive scanlines. Each scanlines is coated with one of 0°, 45° or 90° orientations of linearly polarizer material and consisting of 28 pixels. This is the first prototype of one-dimensional polarization-sensitive chip.

In 1996, Kalayjian et al. [Kalayjian et al. (1996)] also designed an one-dimensional polarization contrast retina that can be used as polarimetric scanning sensor for real-time in automated vision tasks. The sensor called retina to mimic polarization sensor of animal consists of the linear polarizer filters on the focal plane, on-chip analog circuit and subthreshold circuit to compute polarization contrast. The linear polarizer composed of two parallel linear arrays of 29 photodiodes utilized as sensing elements, with the transmission axis perpendicular each other (see Figure 3.23 top right). Then, an on-chip analog circuit compared the output signals from two diode rows to compute the polarization contrast.

Kalayjian et al shown that CMOS fabrication techniques can be used in the processing of linearly polarizing film in high resolution and two-dimensional partial polarization retina.

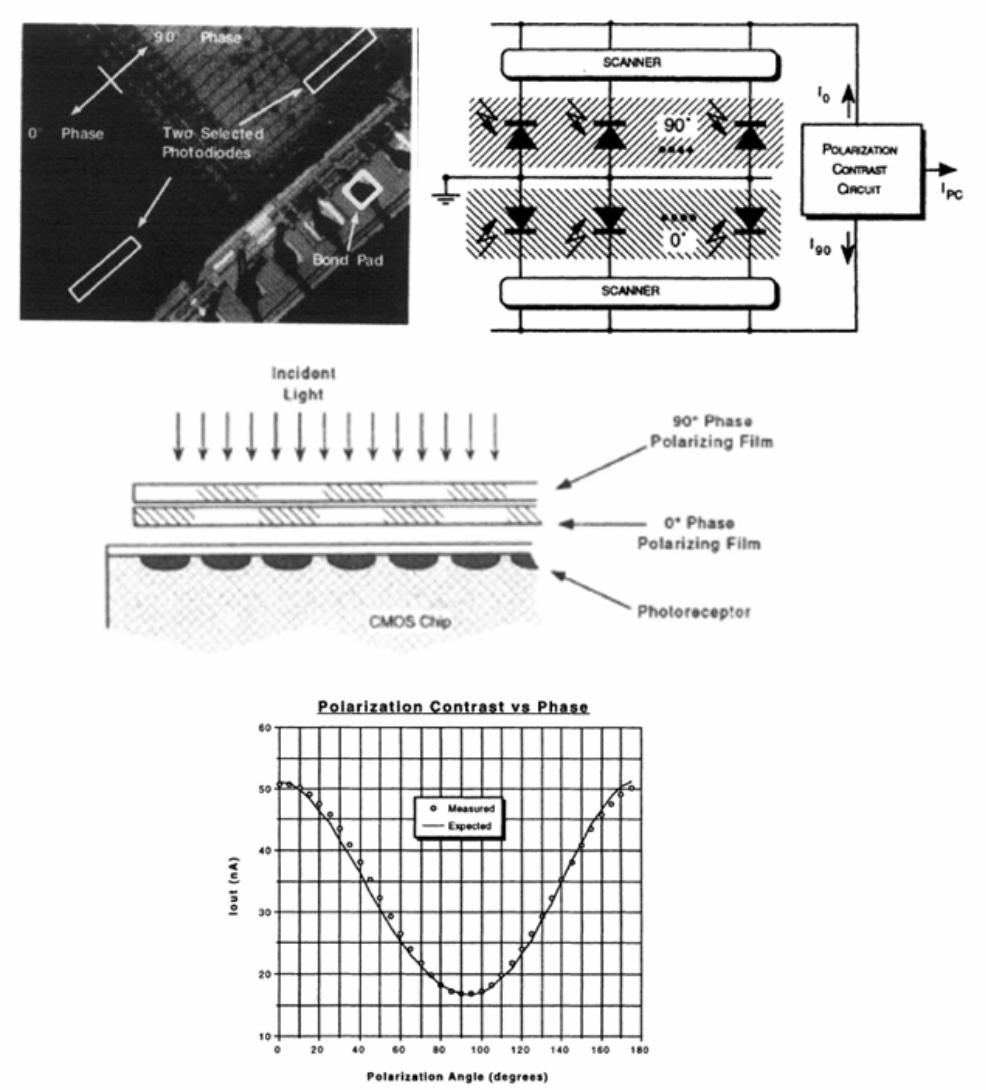

Figure 3.23 Sensor retina in photo micrograph (top left), schematic sensor (top right), schematic diagram focal plane linear polarizer (second row) and respons angle of polarization to rotating linear polarizer of sensor, o is measured and *line* is expected (bottom) [Kalayjian et al. (1997)]

In 1999, Kalayjian et al [Kalayjian and Andreou (1999)] proposed a polarization contrast retina with a CMOS sensor that uses a birefrigent crystal micropolarizer mounted on the focal plane to sense two orthogonal directions of linear polarization. A similar visual modality has been seen in underwater animal Octopus.

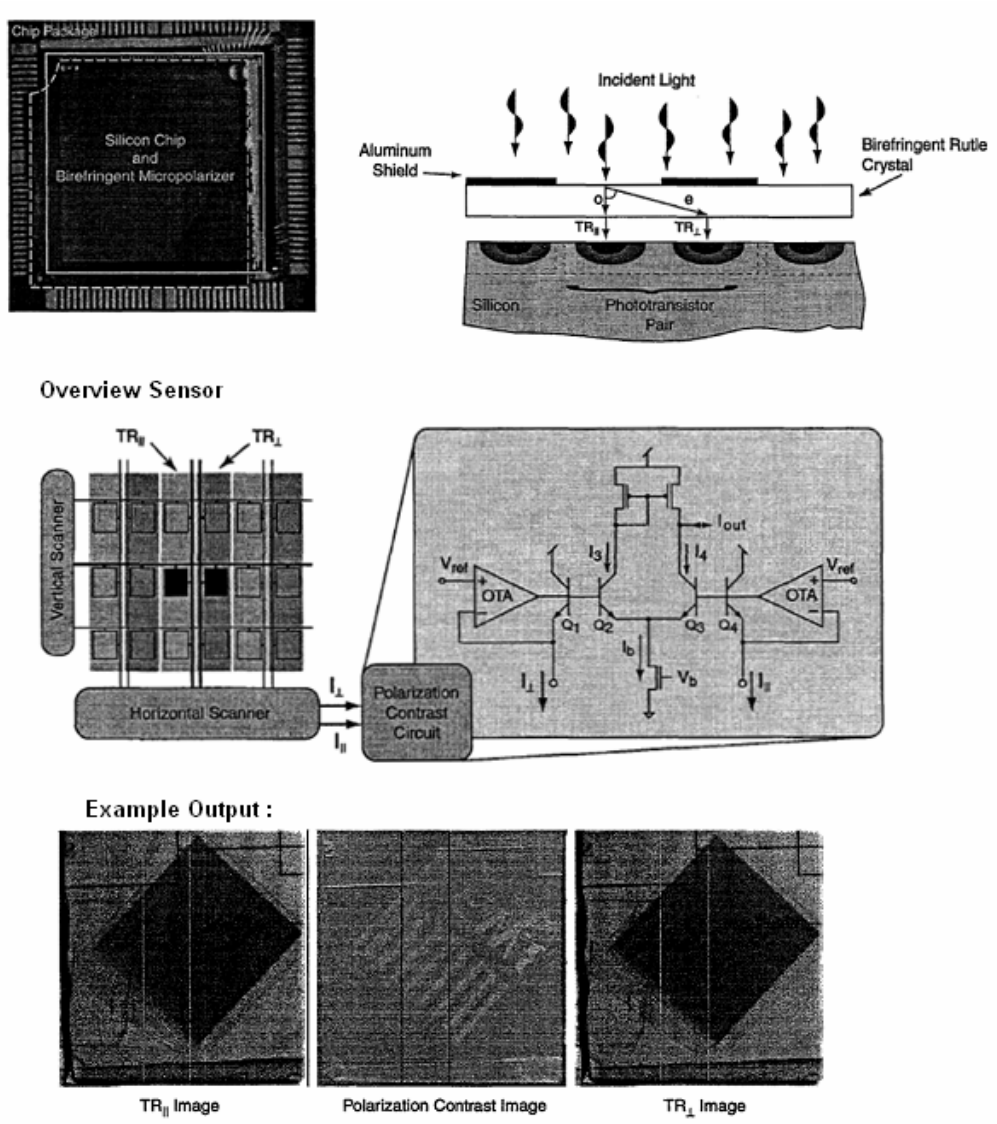

Figure 3.24 The focal-plane mounted birefringent crystal separates incident light into orthogonally polarized rays (top right), schematic cross-sectional diagram of the imager (second row) and visualized result (bottom) [Kalayjian and Andreou (1999)].

The sensor operates as follows; the *rutile birefringent crystal* is cut so that the angle of optical axis the crystal is at a 45° to the surface normal. The birefringent crystal will separate incident light into two orthogonally polarized components. One component, called the ordinary ray ($TR_{\|}$), passes un-refracted through the crystal into a photo detector part. The other ray, known as the extraordinary ray ($TR_{\perp}$), is refracted by roughly 6° from the surface normal. Finally, in this series of their research about polarization sensor,

a number of integrated sensory devices that have been engineered for polarization imaging have been discussed at research review of Andreou in 2002 [Andreou and Kalayjian (2002)].

In 2009, Gruev [Gruev et al. (2009)] divided polarization imaging sensors into two categories.

1. The polarization sensors is composed of standard CMOS or CCD imaging sensors coupled with electrically or mechanically controlled polarization filters and a processing unit. Included in this category are [Cronin et al. (1994)], [Fluxdata (2009)], [Hanlon et al. (1999)], [Gu et al. (2010)], [McGuire and Matusik (2006)], [Miyazaki et al. (2005)], [Ramella-Roman et al. (2003)] and [Wolff et al. (1997)]. The image acquisition sampling using two orthogonal polarization filters and the polarization contrast information is computed by a processing unit. One of the shortcomings of these systems is the high power consumption and the reduction of the frame rate.
2. The polarization sensors includes image acquisition (imaging), processing and micro polarization filters on the same substrate. The image acquisition sampling is achieved with spatially distributed polarization orthogonal filters over the neighbourhood of two pixels. The processing of the polarimetric information has been implemented within each pixel, leading to large photo pixels with limited fill factor. Included in this category are [Kalayjian et al. (1997)], [Kalayjian et al. (1996)], [Kalayjian and Andreou (1999)], [Photonic (2009)].

Gruev also developed a sensor capable of extracting complete polarization information in real time and in high resolution. The Gruev sensor is composed of an array of photo pixels, noise suppression and analog computation circuitry at the focal plane. The polymer micropolarizer array is attached separately on the sensor with the similar pattern with the Bayer pattern in color imaging. It shown in Figure 3.25 (bottom left).

As seen Figure 3.25 (top left), during image acquisition, the neighborhood of 2 by 2 pixels is addressed and accessed simultaneously. Inside the pixels' neighborhood, one pixel will records the 0° and projected polarized image (I(0°,0)), another pixel will records the 45° and projected polarized image (I(45°,0)), then the last two pixels record

the unfiltered intensity image (I_t). The polarization parameters are estimated by reading out all four pixels in parallel and scaling them individually at the special register outside the imaging array, using programmable analog scaling circuitry to obtain the first three Stokes parameter.

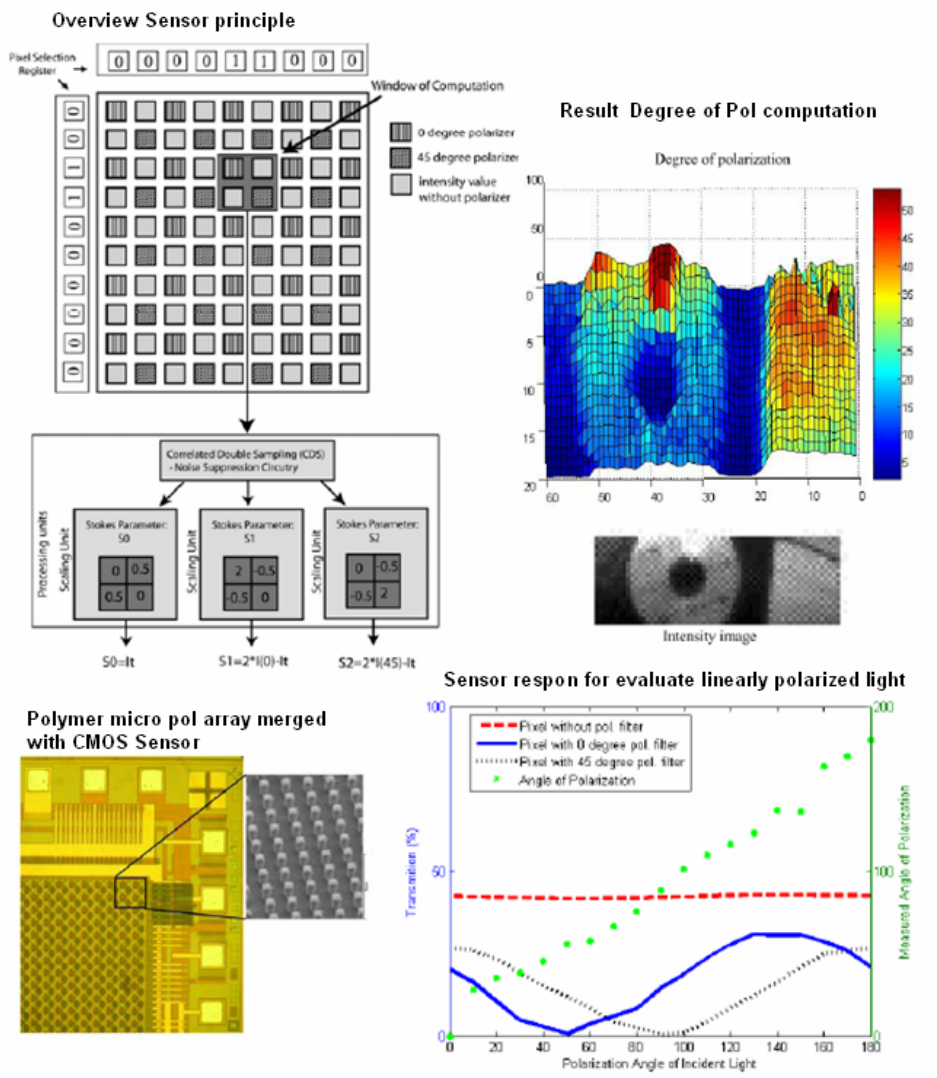

Figure 3.25 Gruev Integrated Polarization Sensor [Gruev et al. (2009)]

The linearly polarized light is used as a performance test to verify the polarization imaging sensor. The degree of polarization of the incident light is changed between 0 and 180° in increments of 10° while the intensity remains constant. The response of three neighboring pixels is presented in Figure 3.25 (bottom right) and Gruev claimed that their system can provide a good response to sense polarization information.

At this point, Polarization of light has been used in a wide area of computer vision applications. Later in this writing, the discussion will focus on the application of polarization to improve the quality of the image, for analysis and object recognition, for underwater vision applications, for navigation, and for medical imaging. The discussion will also deal with inter application that is a combination of polarization vision imaging system with wide-angle cameras and finally, the combination of polarization imaging with stereo vision as the main topic of this thesis.

3.3 Application of Polarization Imaging

Application of polarization Imaging in the computer vision field which can be used for automation in the field of robotics is to increase the visibility of the image, to the object of analysis, and most importantly, to aid navigation. In this section will be found several research results as it has been indicated above, plus two important research results, which is the utilization of Polarization imaging in underwater and medical research.

3.3.1 *Polarization for Enhancing Images*

Usability a polarization of light to enhance the image quality is very important in computer vision field. The following discussion will describe the research related to the polarization of light to improve the quality of the images, such as eliminating reflections ability and increasing contrast. It possible because they can manage the desired status of the incoming light into the sensor or remove an un-necessary light status.

3.3.1.1 Reduce Unwanted Light Effect

Nishiwaki in 2006 [Nishiwaki et al. (2006)] used polarization imaging to remove halation effect in the plant. Most parts of plants have a *cuticular* layer that causes halation effects; the specular reflected light on the surface of plants that is responsible for high intensity areas in the image, and then reduces image quality. To acquire high quality crop images, the imaging acquisition system is composed of a tractor-mounted with a frame box (1m x 1m x 1m) covered by a polarizing film (1m x 1m), two CCD cameras, one

camera with polarization filter fitted in front of the lens and a PC as processing unit. All four sides of the frame box were covered with black curtains so that only polarized sunlight could enter (see Figure 3.26 first row).

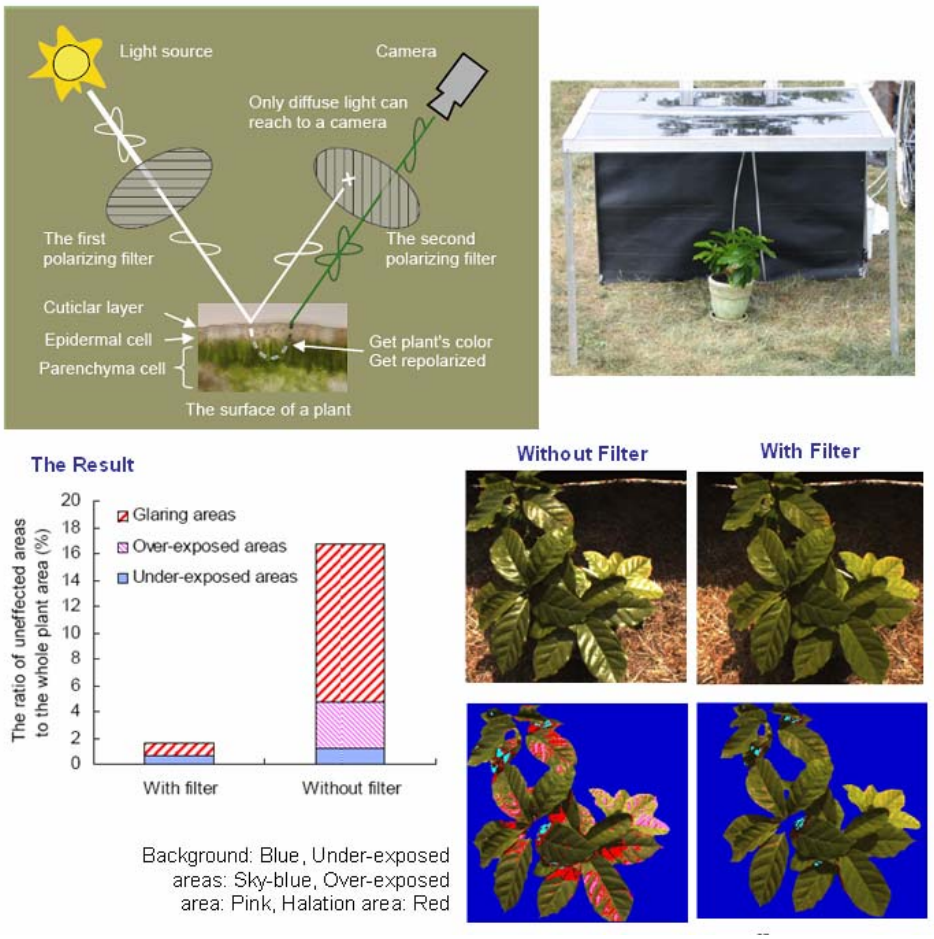

Figure 3.26 Reduce Halation image acquisition and the result [Nishiwaki et al. (2006)]

The polarizing filter at the top frame box allows only horizontally polarized light to reach the plant surface. The second polarizing filter, which passes only the vertically polarized light, is set in front of a camera. This is provide to filter out a polarized horizontally from specular reflected light and passes only a polarized light from the diffuse reflection. The experiments are done using images of coffee plants that were acquired under varying sunlight conditions. It was observed from the results, the polarization filtering technique was capable not only to reduce 97% of halation on the surfaces of leaves but also help in visualizing high accuracy color representation of the leaves (see Figure 3.26 second row).

3.3.1.2 Improve the quality of the image

Schechner, in 2001 [Schechner et al. (2001)] and 2003 [Schechner et al. (2003)] used polarization to improve the quality of the image taken in hazy weather. The approach is to model the image acquisition process with taking into account polarization effects of atmospheric scattering in haze and use the model to recover the dehazed scene. The model also obtains the information about scene structure and atmospheric properties.

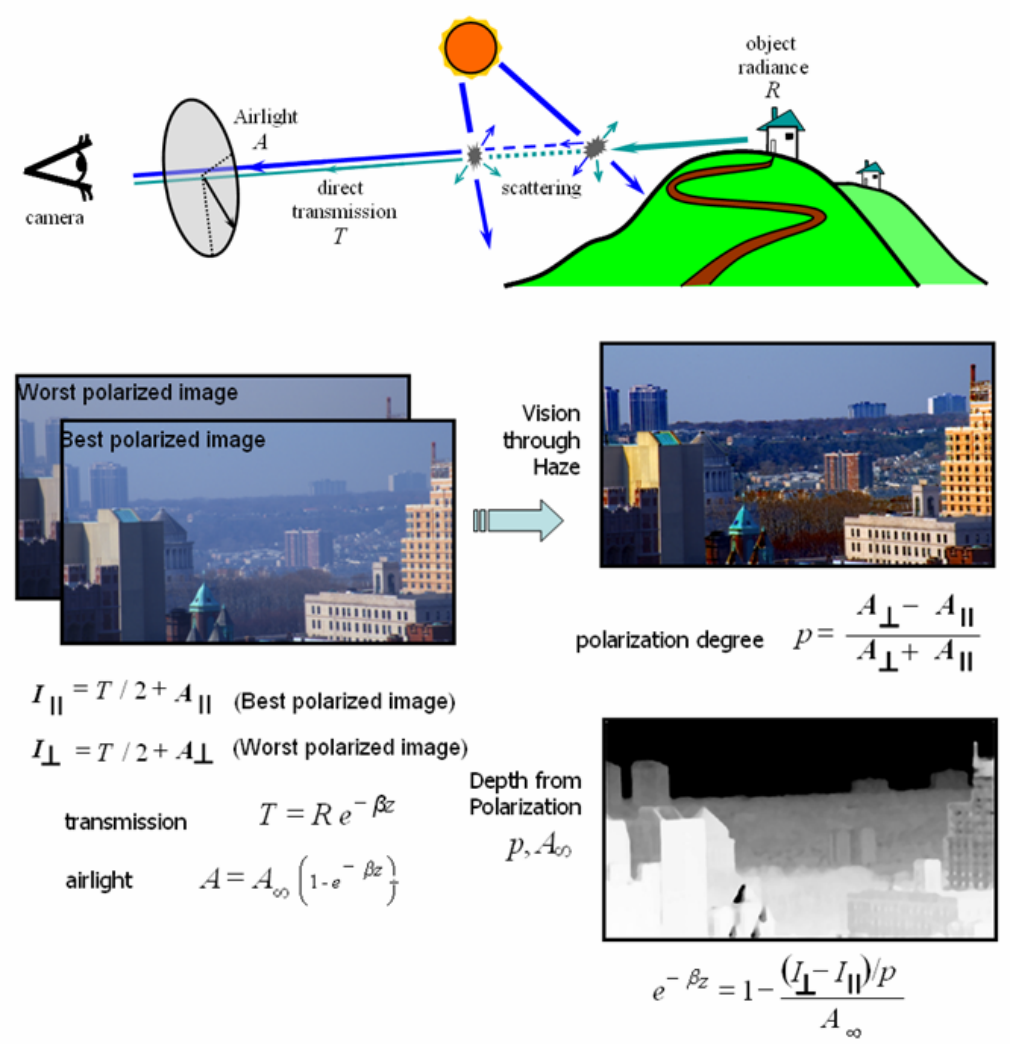

Figure 3.27 Dehaze using polarization technique [Schechner et al. (2001)]

As seen Figure 3.27, Schechner method is based-on polarization sum (PS) and difference (PD) to compute a partial polarization of airlight. Hence its stability will dependent to stability of degree of polarization, for instance, this method may be less

effective under an overcast sky and even may fail in very dense haze or foggy. Two images captured as input, images of the perpendicular and parallel polarization components. The parallel polarized images have the best image contrast, but comparing it with the perpendicular polarization images, it is only slightly better than the contrast in the image of the worst polarization state. The raw images were acquired instantly, without waiting for changes in the visibility.

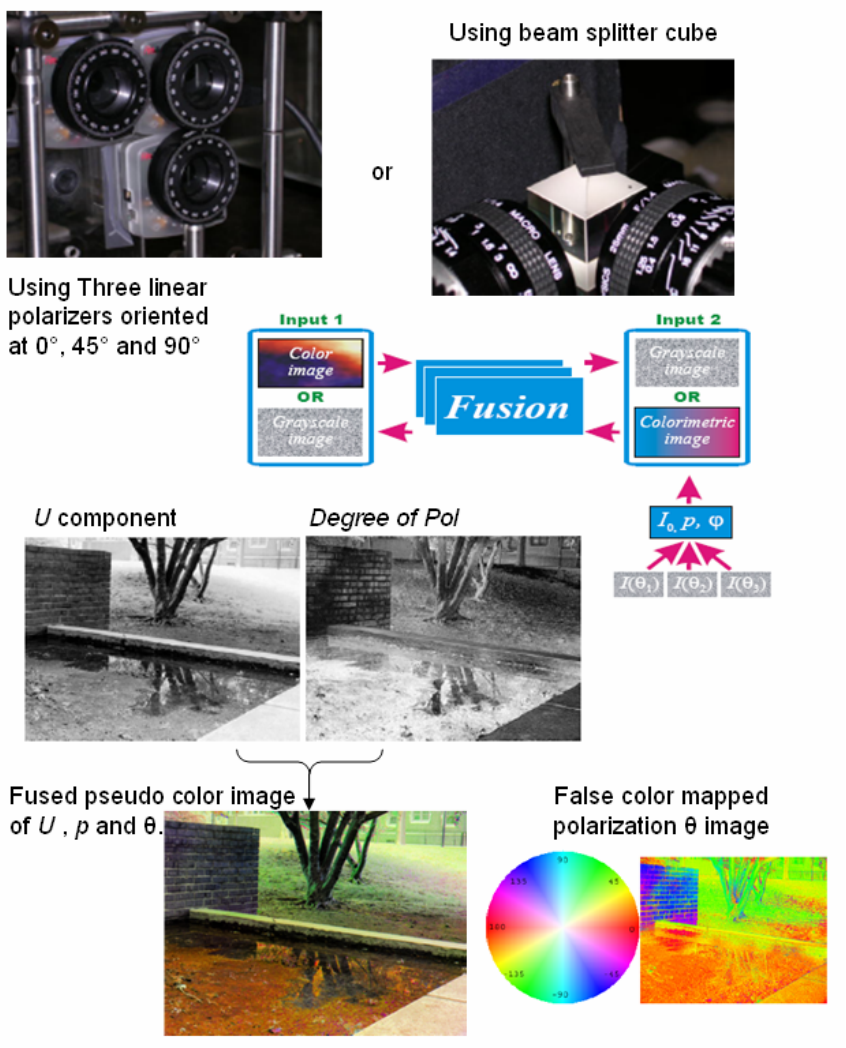

Figure 3.28 Improve target detection using polarization technique [Lin et al. (2004)]

In 2004, Lin [Lin et al. (2004)] presents a polarization based optical techniques to improve target detection in the visual surveillance system. The visual surveillance system relies on visible light to convey information about the environment. The sun light as the major natural light source, appear to be un-polarized, that light actually will enters a

surveillance camera, often has biased pattern of polarization distribution due to scattering and reflection by the environment. These biased can carry the important information about the environment. Lin designed a proper optical setup and polarization analysis used to help resolve ambiguities in conventional visual surveillance techniques. As seen Figure 3.28, Lin using polarization sum (PS) and Polarization difference (PD) image intensities to recover total intensity (U), Degree of polarization (A) and angle of polarization (θ).

3.3.2 *Polarization for Object Analysis*

One of the advantage polarization light analysis is the ability to recognize objects based-on the situation of the light that interacts with the object. With proper imaging setup, the light condition can be analyzed and the object can be segmented, classified, reconstructed or even identified. In this section, we will see area of research where people carry out research to estimate the shape of the object by the use polarization information.

3.3.2.1 Shape Estimation and Reconstruction

The famous photometric method for shape estimation is shape from shading, but this method has drawbacks on detecting the specular and highly reflective objects, and in by definition is not adapted to transparent object. The polarization method can overcome that problem.

In 1987, Kosikawa and Shirai [Koshikawa and Shirai (1987)] proposed a polarization-based determination of shape, to determine a surface normal of specular polyhedrons object. The degree of polarization is computed from circularly polarized light sources and Mueller calculus. Then, on the other hand Wolff [Wolff (1990b)] estimates the surface orientation using polarization data from two views.

Since [Wolff and Boult (1991)] presented a polarization reflectance model known as the Fresnel reflectance model using Fresnel reflection coefficient, many researchers have been taking advantages of this model for many applications. Below is a summary of their contribution.

[Saito et al. (1999b)] implemented a method to estimate surface orientation of transparents object using polarization highlight. However, because these methods do not

consider internal reflections of object, Saito could not reach a satisfying accuracy for estimating the shape of transparent objects. The degree of polarization provided two candidates of surface normal, and the author did not solve this ambiguity, moreover the refraction index of object has to be known and ideal lighting condition are needed.

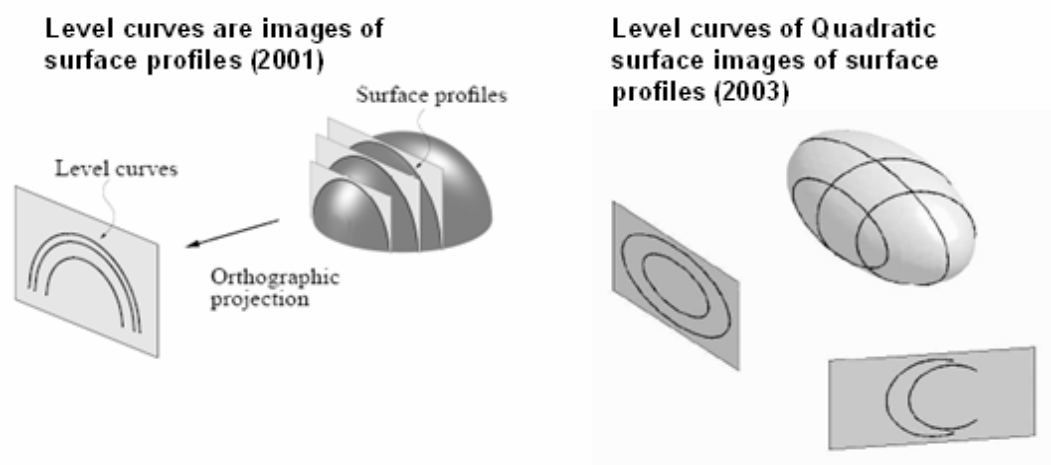

Figure 3.29 Rahmann's Analysis of surface profiles to estimate a shape from polarization [Rahmann and Canterakis (2001)], [Rahmann (2003)]

In 1999, Rahmann [Rahmann (1999)] presented a method to estimate the orientation of a flat object and the position of the light source by polarization analysis. Furthermore, in 2000 [Rahmann (2000)] presents a framework for geometric interpretation of a single polarization image from the specular reflecting object. Rahmann addressed the potential of recovering the shape of specular surfaces from polarization, by creating analysis of surface profiles qualitative and based-on it, performed a quantitative surface shape analysis (see Figure 3.29 about illustration of surface profiles by Rahmann). [Rahmann and Canterakis (2001)] estimated the shape of specular objects from multiple views. [Rahmann (2003)] also proved that the quadratic shape of specular objects can be estimated from two views. In this series of research, they take into account the specular and diffuse reflection types and use only the azimuth angles to establish correspondence. The advantages of shape reconstruction with this method are the results with a less noisy reconstruction but at the cost of discarding large amounts of information.

[Drbohlav and Sara (2001)] combined the photometric stereo and the polarization analysis to estimate shape of the objects with diffuse reflection. Photometric stereo determines local surface orientations from object viewed in a fixed position, but with illumination from at least three non-collinear directions. The combination of these methods can eliminate the disadvantages the polarization method to reconstruct the objects with diffuse reflection.

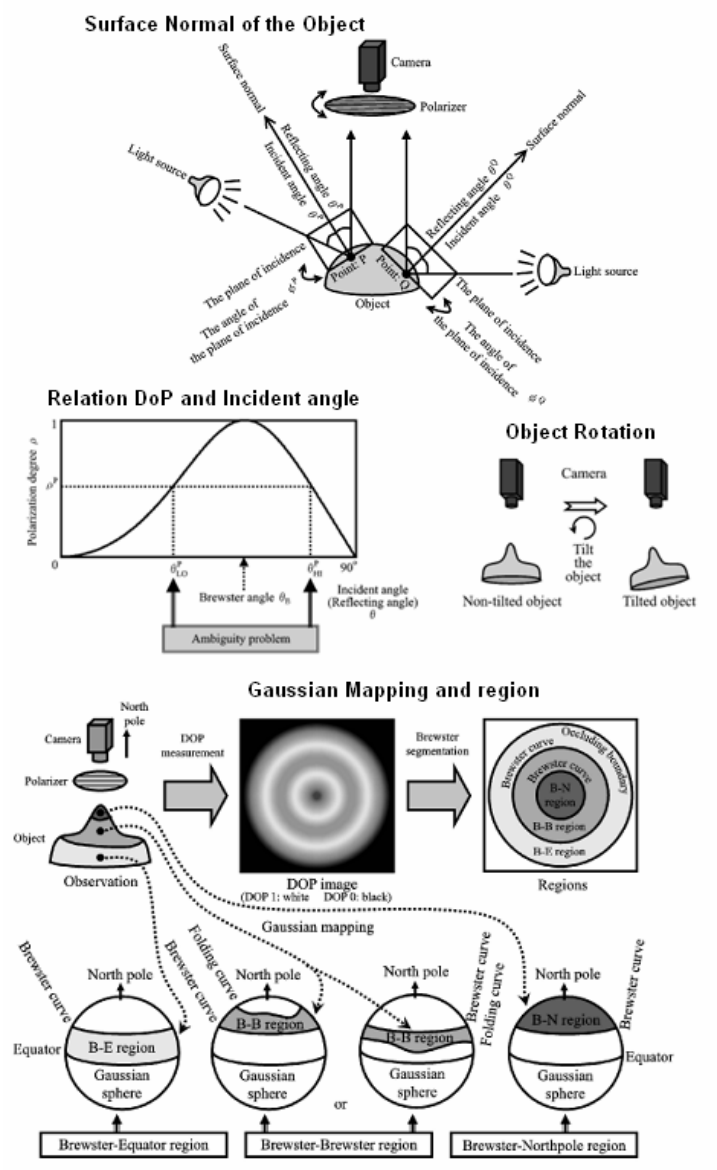

Figure 3.30 Transparent Surfaces Modeling from a Pair of Polarization Images [Miyazaki et al. (2004)]

[Miyazaki et al. (2003)] estimated the 3D surface shape and reflectance of specular objects using only a single view with multiple light sources. The ability to use only a single view has the advantage that less specific measurement conditions are needed. However, Miyazaki et al only partially solve the azimuth angle ambiguity and with restrictive assumptions about the shape histogram of object.

[Miyazaki et al. (2004)] resolved two ambiguity of the reconstruction of transparent objects by using a polarization analysis. This method obtains two sets of data of polarization from two different views. The object was observed twice from the same camera by rotated the object at a small angle and illuminated with several external light source from all directions, producing specular reflection over the whole object surface. By comparing the degree of polarization at the corresponding point of each set of polarization data, the unique surface orientation can determined (see Figure 3.30).

In 2005, Morel et al. [Morel et al. (2005)] proposed a shape reconstruction of very smooth metallic surfaces using a Fresnel reflectance model with complex index of refraction. This method is extended to metallic surfaces, because degree of polarization from fresnel reflection method can not be directly applied to metallic surfaces since their refractive indexes are complex. The complex index written in the attenuation index form. The difference between the true degree of polarization and its approximation grows slightly only for great values of the angle θ. In a later publication Morel et al. (2006) [Morel et al. (2006)], the ambiguity about the determination of the azimuth angle ϕ from the angle of polarization φ is resolved by varying the illumination with an active lighting system. The ring of LEDs is split into four parts that can be independently electrically controlled (see Figure 3.31 top right).

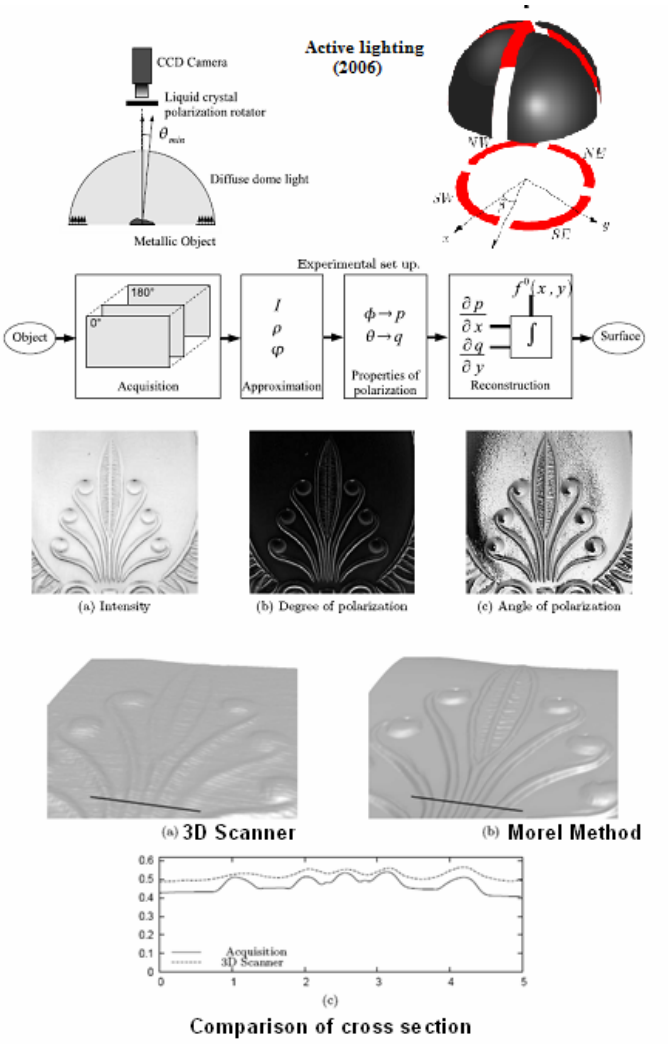

Figure 3.31 Shape reconstruction for smooth metallic Object ; experimental object and result compared with 3D Scanner [Morel et al. (2005)], plus addition active light to resolve ambiguity problem [Morel et al. (2006)]

In the same years, D'Angelo [d'Angelo and Wohler (2005)] presented an image-based method based on the simultaneous evaluation of reflectance and polarization information, for 3D surface reconstruction of metal object. Interesting part of D'Angelo method is using computation of means from a series images acquired by a linear polarization filter under different orientations to obtain corresponding properties of the surface material. Acquisition has be done with capturing five images through a linear polarization filter with orientation angle 0°, 45°, 90°, 135° and 180°. Then, both reflectance and polarization features are integrated into a unified framework. The

evaluation of this method using synthetically generated surface, working in a single view and a single light source (see Figure 3.32).

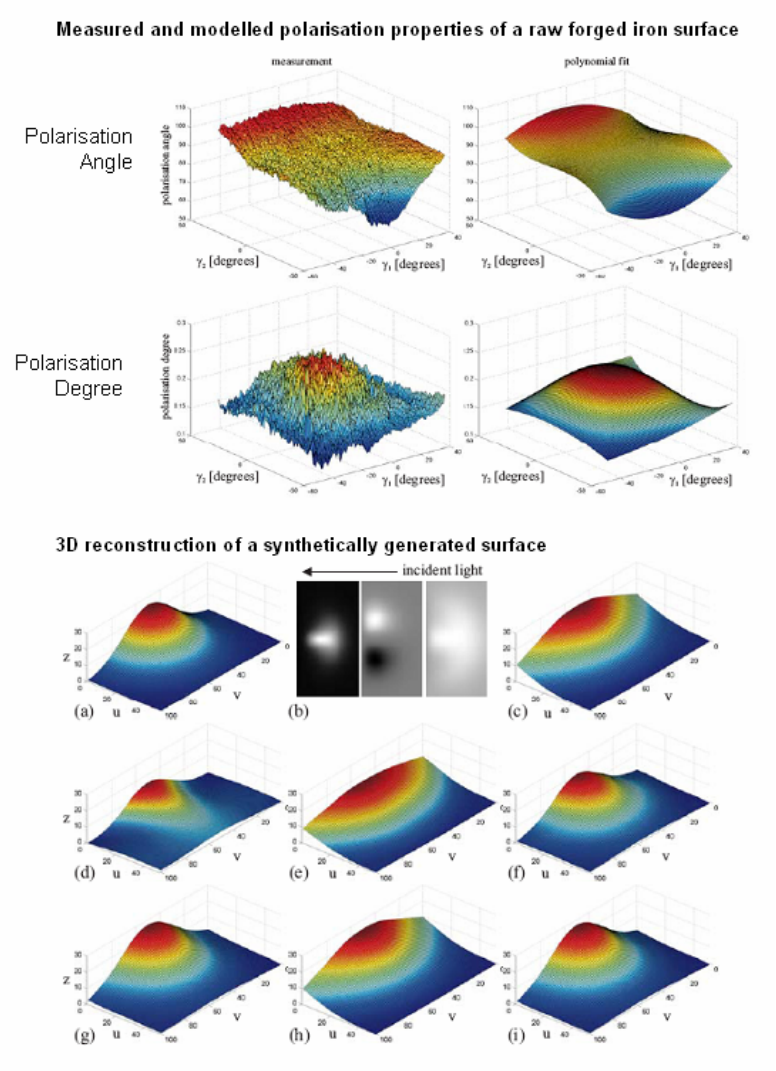

Figure 3.32 3D reconstructions Result of D'Angelo Method [d'Angelo and Wohler (2005)]

As seen Figure 3.32, the result of reflectance & polarization based shape reconstruction of a synthetically generated surface. (a) The ground truth. (b) Reflectance image, angle of polarization image, polarization degree image (left to right). Then 3D reconstruction result is obtained based on: (c) reflectance model, (d) angle of polarization, (e) polarization degree, (f) angle and degree of polarization, (g) reflectance

model and angle of polarization, (h) reflectance model and polarization degree, (i) Fusing reflectance, angle and degree of polarization.

In 2007, Atkinson [Atkinson and Hancock (2007)] combined a polarization and shading information system for 3D reconstruction from two views of smooth non metallic surfaces. The polarized images acquired using a linear polarizer installed in front CCD camera, and the images with diffuse reflection processes to estimate of surface normals using Fresnel theory. The main idea of Atkinson is to combine shading information to enhance the estimate of surface normal by measuring statistics on pixel brightness depending on the surface orientation. Atkinson extracted a surface patches from each view, then aligned them by minimising an energy based on the surface normal estimates and local topographic properties. The stereo correspondence composed from the optimum alignment parameters of different patch pairs can give an unambiguous field of surface normals, which can be incorporated to recover the surface depth. Atkinson method can be expressed as complements of existing correspondences stereo algorithms since it does not require any salient surface features.

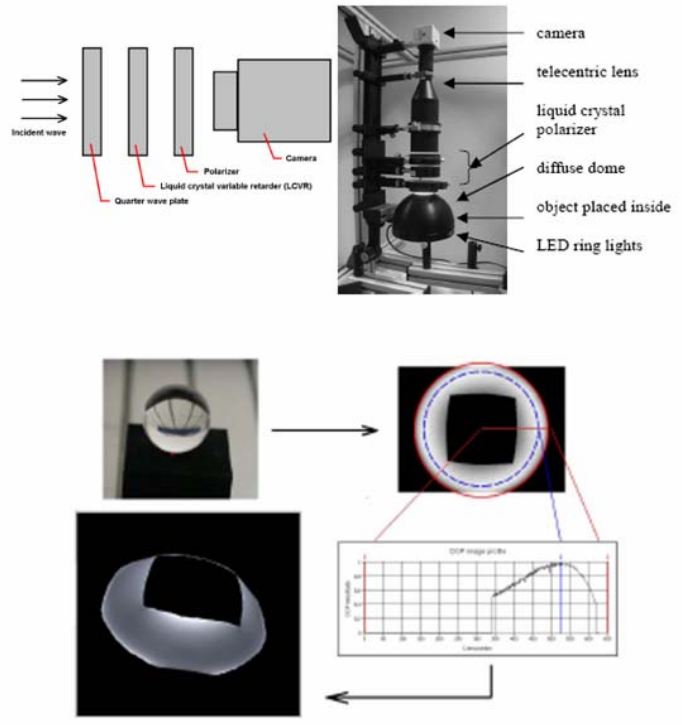

Figure 3.33 Optical design, experiment and result Shape from Polarization to reconstruct transparent object [Ferraton et al. (2008)]

In 2008, Ferraton [Ferraton et al. (2008)] proposed a method using multispectral measurements that can solve the ambiguities of 3D measurement by Polarization Imaging during the measurement process. The proposed system consists of a CCD camera, a diffuse dome light with three wavelengths and a polarization rotator with most parts are electrically controlled (see Figure 3.33), and three-dimensional surfaces are automatically computed in a few seconds.

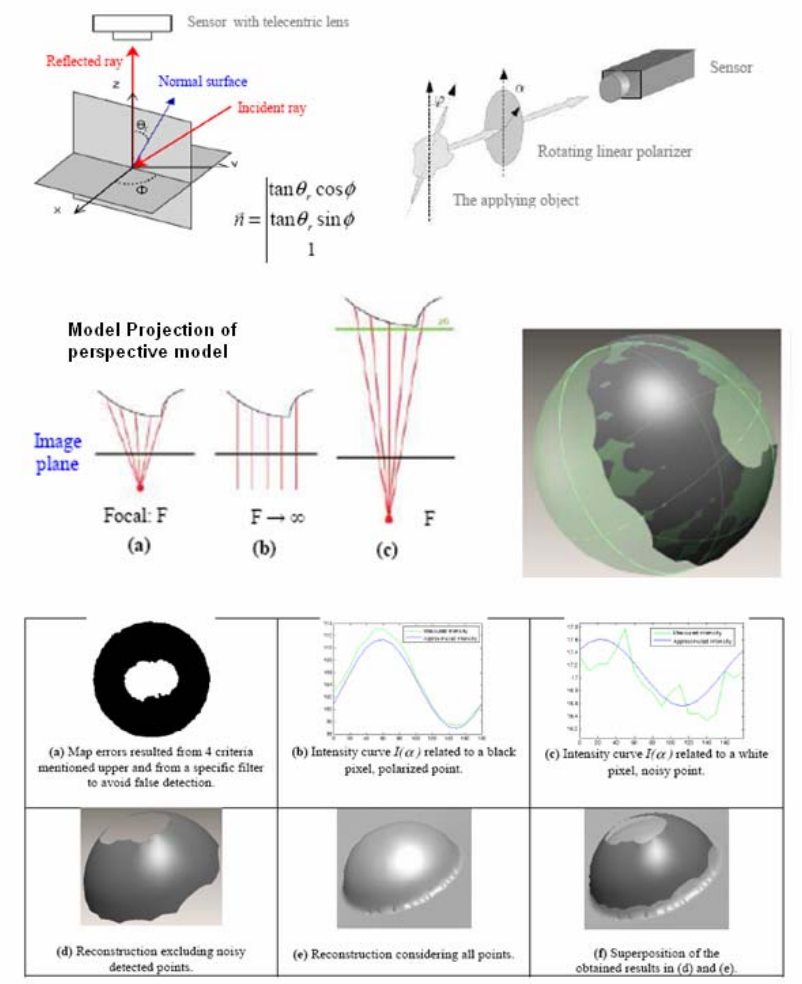

Figure 3.34 Practical setup with the use of rotating polarizer to compute metal object reconstruction, model projection of perspective model (Model projection related to perspective model (a); Model projection related to orthographic model (b); Model projection related to relaxed perspective model that we have suggested (c)) and reconstruction result [Rantoson et al. (2009)]

Recently, Rantoson in 2009 [Rantoson et al. (2009)] developed a non contact 3D measurement system using a polarimetric imaging method for metal or transparent objects, working in far infrared range. In this investigation, Rantoson has adapted a pinhole model corresponding to non-telecentric lenses in perspective model polarization reconstruction method. Then, she also proposed a mathematical approach that could be estimated from data analysis of Stokes parameter to reduce reconstruction error. Rantoson claimed, these methods are applicable to any linear system resolution and independent from the nature of the selected model.

Polarization imaging systems can nowadays found in numerous applications such as pattern recognition (Sadjadi in 1996 [Sadjadi and Chun (1996)]), image segmentation (Ainouz in 2006 [Ainouz et al. (2006)] and 2008 [Ainouz et al. (2008)], Ahmad in in 2007 [Ahmad and Takakura (2007)], Rankin in 2008 [Rankin and Matthies (2008)]), water hazard detection (Bin Xie in 2007 [Xie et al. (2007)]), robots navigation (Lambrinos in 2000 [Lambrinos et al. (2000)], Usher in 2001 [Usher et al. (2001)], Rankin in 2008 [Rankin and Matthies (2008)]), underwater imagery (Karpel in 2004 [Karpel and Schechner (2004)], Schechner in 2005 [Schechner and Karpel (2005)]), medical imaging application (Jacques in 2002 [Jacques et al. (2002)], Demos in 2005 [Demos et al. (2005)], Xuan [Xuan et al. (2007)] and Zhou [Zhou et al. (2007)] in 2007)

3.4 Conclusion

This chapter has described a review about polarization imaging research. The discussion begins from bio inspiring of visual ability of robotics or automatic machine vision, implementation of polarization imaging concept into imaging system and finally about research to integrate a polarization imaging in a sensor system.

The facts that recent discover in both land and marine animals, showing their capabilities to sense the polarization encourages human to integrate these aspects in machine vision or robotics application.

This section outlines step by step discovery of methods, algorithms and imaging systems, ranging from the basic configuration, the global method that can be used for various applications, the discovery of polarization camera, and finally polarization

sensor. It was shown that polarization camera available in the market (and also polarization sensor).

This chapter also gives several examples of the application of polarization imaging as a solution in a variety of vision problems such as application for enhancing visual visibility (for reduce unwanted light effect or to improve the quality of images), or application for object analysis (for object or shape estimation, recognition and reconstruction, or for segmentation and object classification).

We conclude this chapter with a summary of the above literature. The polarization imaging methods have proven to be of great use in many application of machine vision automation. These thesis will address some of a questions raised by the above literature, one of them is about combining a polarization imaging system and a stereo vision system. As described in one section, it is an open challenge to be explore, and chapter 4 will describe and largely concerned with the underlying techniques used in stereo vision to be ready implemented with polarization imaging.

Chapter 4

Polarization Imaging Using Stereo Vision

This chapter presents the polarization imaging system we designed. It consists of:

1. *An introduction, which describes the proposed system, starting with an overview of stereoscopic polarization imaging systems, a brief description of a stereo vision system and details of the acquisition principle.*
2. *The Calibration, discusses about stereo geometry and polarization calibration technique for our system.*
3. *A discussion of stereo matching and its evaluation for polarized images.*
4. *The Extraction of Polarization component and stereo triangulation technique for 3D reconstruction.*

4.1 Introduction

Polarization imaging has been described in chapter 2 and the stereo vision is a well known technique for obtaining depth information from pairs of digital images. One of the main focuses of research in stereo vision area is to get accurate stereo correspondences. In this chapter, we explore the advantages of combining stereo vision information with polarization information in order to obtain reliable 3D information. The research still relies on "traditional" stereo techniques that depend on salient features points for finding correspondences between the two images of the same scene under different viewpoints. Based on this, we propose a novel method for extract polarization information with compact setup imaging system and low cost polarized camera.

4.1.1 *Description of the Stereoscopic Polarization Imaging System*

To achieve the main objectives described above, classical stereo setup need to be adapted so as to acquire stereo information (for 3D reconstruction) as well as polarization information.

Conventional imaging sensors (for example CCD and CMOS) are only sensitive to the energy of the incoming light but not to its polarization state. These extra information can be obtained by mounting a rotating linear polarizing filter in front of a camera and capturing multiple images with different angles α (respect to the transmission axis) of the linear polarizer (details about technique are given in chapter 2).

Our imaging system setup consists of two cameras (AVT Guppy F-080B FireWire monochrome) mounted on a fixed baseline, with two liquid crystal cells placed in front of the respective lenses.

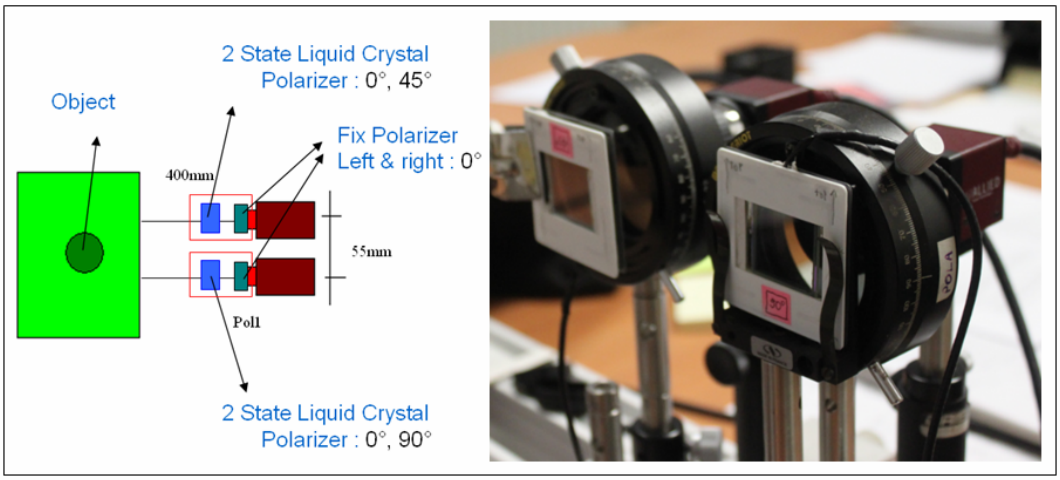

Figure 4.1 Imaging system setup of proposed system

Two Guppy F-080B monochrome FireWire cameras are arranged in stereo as shown in the Figure 4.1. At full resolution, these cameras have a frame rate up to 30 per second which corresponds to the maximum human-vision capture frequency. They also have a smart feature that can be programmed through a processing unit called a programmable LUT (look-up table). In addition, other parameters can be adjusted (gain, exposure, and shutter) so as to optimize their performances. In front of both cameras, the twisted nematic Liquid Crystal linear Polarization rotator system from ARCoptix System

are carefully installed. The system consists of a fixed polarizer, which sets an angle of polarization horizontally (0°) and a liquid crystal cell parallel to the axis of the fixed polarizer. The twisted nematic Liquid Crystal on the left camera can rotate the orientation of a linear polarization by a fix amount of 0° and 90°, whereas the one in front of the right can achieve rotation of 0° and 45°.

Briefly, in this acquisition setup, two pairs of images are taken with different polarization filter settings. The first acquisition produces two images with polarizers of the two cameras both oriented at 0°. The second acquisition is realized with the polarizer oriented for the left camera and the right camera at 90° and 45° respectively. The time required to capture the sequence of two pairs of these images depends on the speed of liquid crystal polarizers used in this setup (in the LC ARcoptix product, the switching speed ranges from 25ms, 70ms to 150ms).

This setup is then thoroughly calibrated (geometric calibration and polarization calibration) through procedures which are explained in the next sections.

4.1.2 *Brief Description of a Stereo Vision*

The goal of stereo vision is to obtain the depth information from two images taken from two different viewpoints. This information can be obtained by measuring the disparity between two images taken by two calibrated cameras. The primary problem to be solved in computational stereo is how to obtain the disparity thus how to find the correspondences of features between two images. Once the correspondences between the two images are known, the depth information of the objects in the scene can be easily obtained.

In general, there are three important steps to be solved in computational stereo: calibration, finding correspondences or matching, and reconstruction [Brown et al. (2003)]. Calibration is the first step to determine the camera internal parameters such as focal length, optical center, and lens distortion. Calibration is also used to get the relative position of each camera (external parameters). Correspondence step consists in associating two points from the two images (left and right) which are the projections of the same real point. Reconstruction is the conversion into a 3D map of the objects scene

based on the knowledge of the geometry of the stereo system and of the disparity map. Disparity is the difference between the same objects in two different stereo images.

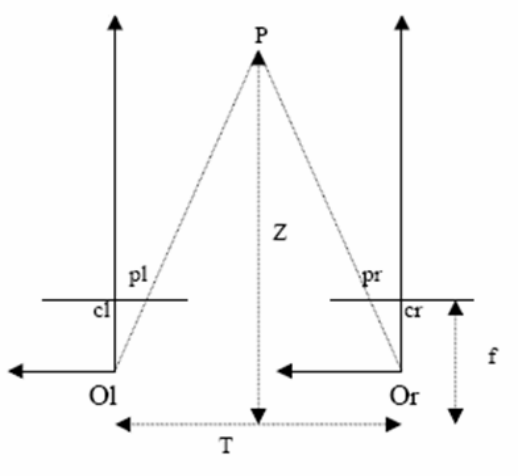

Figure 4.2 Simple stereo System Setup

In Figure 4.2, T is the baseline, Ol and Or are the optical centers, Z is the distance between P and the baseline, and f is the focal length. Calibration provides the intrinsic parameters to characterize the transformation mapping from an image point in camera coordinates to pixel coordinates in each camera, and the extrinsic parameters to describe the relative position of the two cameras. By finding these values, it is possible to compute 3D information. Without any prior knowledge of these parameters there are different techniques to compute 3D information known as un-calibrated stereo [Brunet and Chao (2004)], [Xie (1997)].

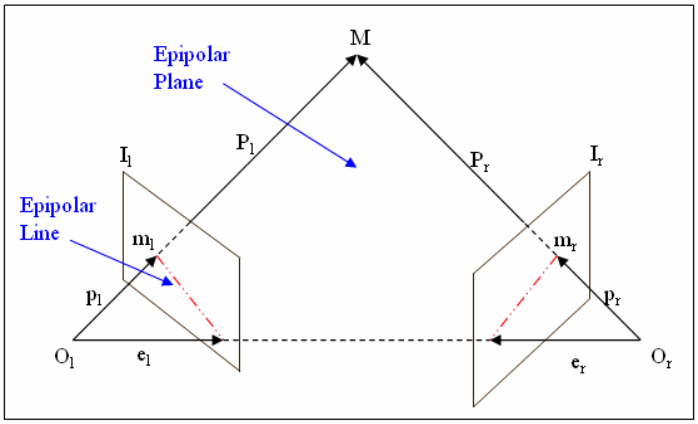

Figure 4.3 Epipolar Geometry Principle

In Figure 4.3, the triangle lies in the epipolar plane. The lower corners of the triangle (Ol & Or) are the optical centers. The intersections of the triangle's base with the planes are the epipoles. An epipole represents the image of the optical center of the opposite camera on the image plane. The red dotted lines are the epipolar lines.

The challenge in finding correspondences is the matching process which finds the corresponding features between the left and right images. The matching process can be viewed as a complex optimization problem in which image features are selected, extracted, and matched using a set of constraints that must be satisfied simultaneously.

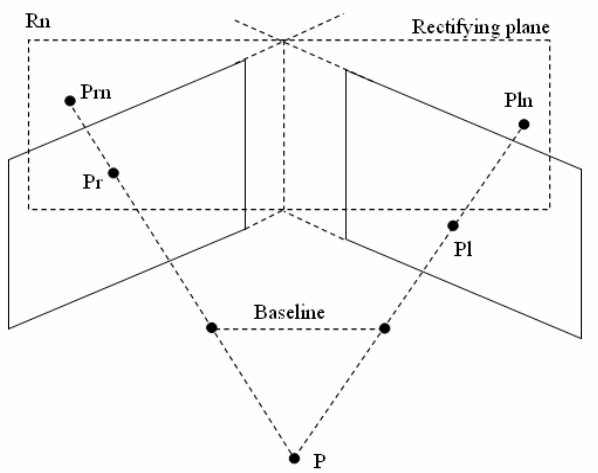

Figure 4.4 Rectifying Stereo Images Principle

The corresponding points between two images can be found by searching for the point correspondence along an epipolar line (epipolar constraints). In general, epipolar lines are not aligned with coordinate axis and are not parallel. Such searches are time consuming since we must compare pixels on skew lines in the image space. Therefore, one needs a method to rectify images [Fusiello et al. (2000)], [Loop and Zhang (1999)] to determine transformations of each image plane such that pairs of conjugate epipolar lines become collinear and parallel to one of the image axes (usually the horizontal one).

The work reported here, relies on calibrated stereo cameras, rectified images and the use of epipolar geometry to find point correspondences [Hartley and Zisserman (2000)]. Epipolar geometry enables the search for corresponding points on epipolar lines, and rectified images make the search easier and faster on horizontal lines.

4.1.3 *Acquisition Principle*

The acquisition process is directly related to the object or scene, the camera and the acquisition steps. This section will describe the definition of the object / scene, camera selection and image acquisition steps.

4.1.3.1 Object and Scene Definition

In general, the object or scenes in computer vision are recognized based on the properties of light interacting with it. Both in the stereo vision and Polarization imaging technique, the properties of light become a major point of concern. For instance, in the stereo matching conventional method, the reflection properties of the object is one of the constraints that can reduce the quality of the matching due for instance to specular reflections.

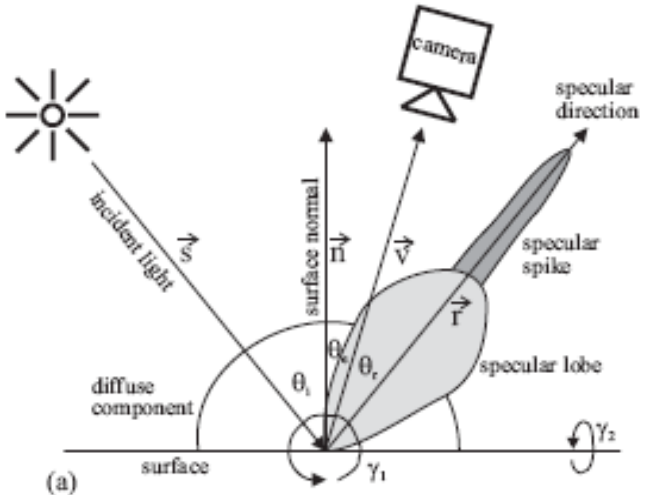

Figure 4.5 Light Reflection model [d'Angelo and Wohler (2005)]

According to De'angelo study in 2005 [d'Angelo and Wohler (2005)], the reflectance function of a typical rough metallic surface consists of three components:

- a *diffuse (Lambertian) component* is the function that is generated by multiple scattering internal processes,
- *Specular lobe* is the function that is caused by single reflection at the surface and distributed around the specular direction.

- *Specular spike* is the function that concentrated in a small region around the specular direction and represents mirror-like reflection, which is dominant in the case of smooth surfaces.

The imaging system is aimed at detecting objects related to the outdoor applications under a non uniform lighting.

Many matching algorithms will work if one assumes the case of Lambertian surfaces. Point matching algorithms rely on the assumptions that object reflects the light equally in all directions and that a certain point will have the same intensity regardless of the direction from which it is observed. However, this often does not occur. Also specular reflections can be reduced using a polarizer filter, showing in that case the advantage of associating polarization filters to a stereo system.

4.1.3.2 Camera Selection

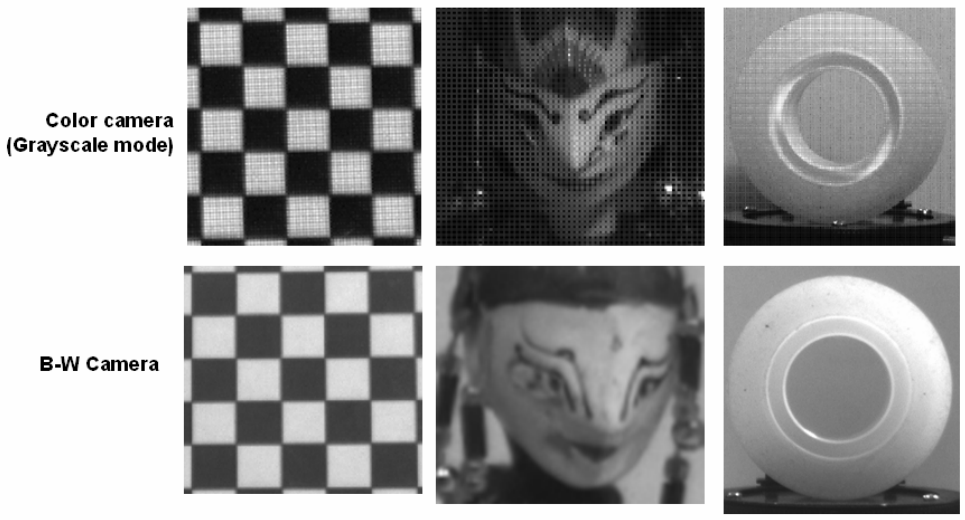

Figure 4.6 Picture Comparison captured by colour camera in greyscale mode with B-W camera, some artefacts appears as high noise due to color sensor.

In this study, we need a camera that has a good sensitivity and robust to noise. After some simple experiments, we considered to use a BW camera, because it offers a better sensitivity to the polarized images compared to a color camera and proves to be more robust to noise (see Figure 4.6).

4.1.3.3 Image Acquisition Step

Our cameras are cameras AVT Guppy F-080C with an IEEE 1394 (Firewire) producing easy control and flexibility. They were used under the Matlab environment through a DCAM driver created by Carnegie Mellon University (CMU) [Ulrich (2008)]. The process of acquiring the polarisation images is presented on Figure 4.7 ; each camera alternates an acquisition at 0° and then either at 45° or 90°.

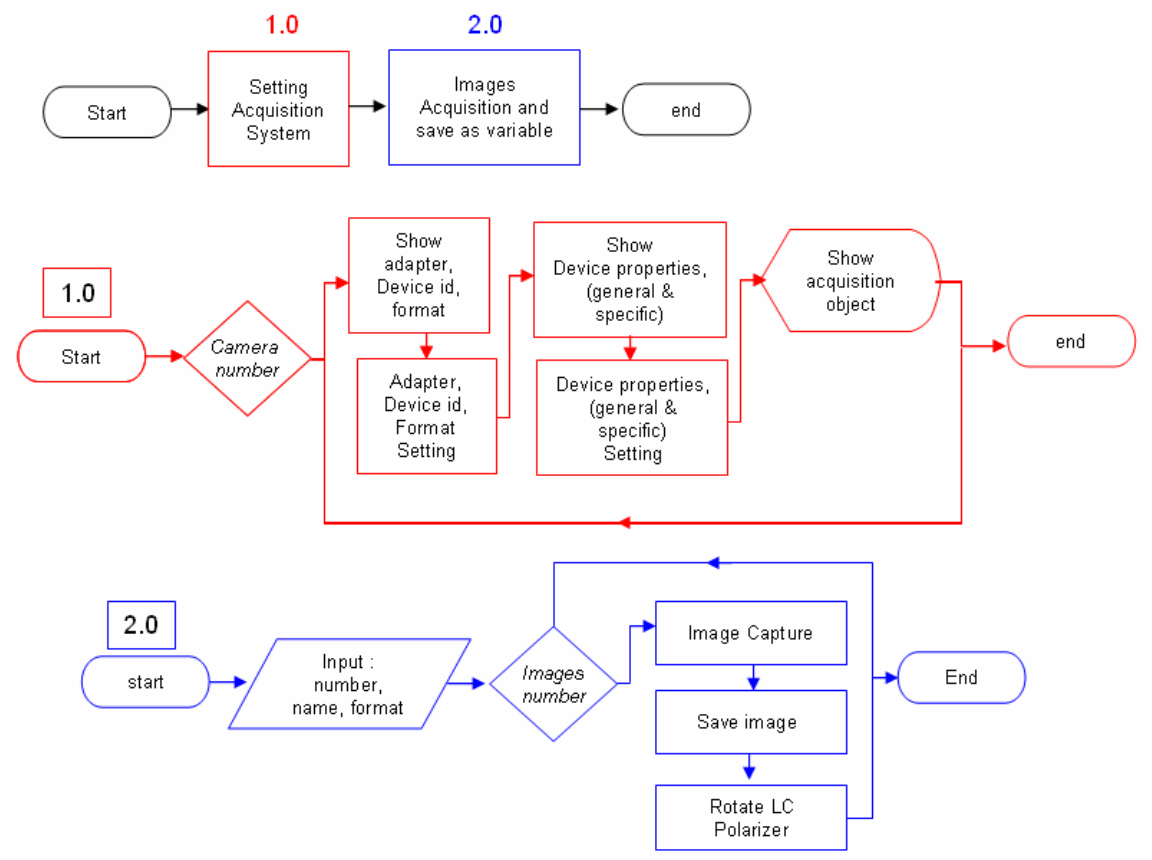

Figure 4.7 Flowchart Image Acquisition Step

4.2 Calibration

Calibration is an important part of computer vision applications and this section will be elaborated on the various calibration steps on stereo vision and Polarization imaging.

4.2.1 *Stereo Camera Calibration*

The goal of the geometric calibration is to estimate the internal and external camera parameters. The relationship between 3D coordinates points of the observed scene and their projection in the 2D coordinates point of image, are directly derived from the calibration pattern. The typical method for the calibration step leads the camera to observe a test pattern (see Figure 4.8), which can consist of spots, lines or squares (or indeed any easily identifiable repeating pattern).

This calibration step is the starting point for many computer vision applications, such as stereovision, structure from motion, robot navigation and object recognition and location (i.e dimensional control of parts and 3D reconstruction).

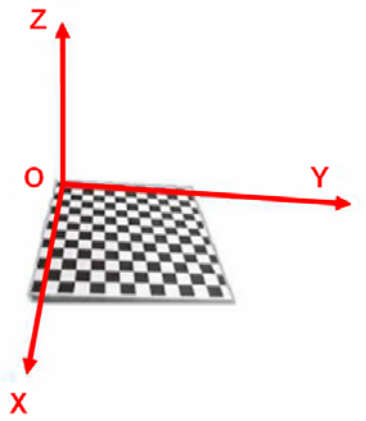

Figure 4.8 Calibration Pattern

4.2.1.1 Perspective Camera Model

We use the perspective camera model as base of calibration. A point M in the 3D scene, described by coordinates (X_s, Y_s, Z_s), has a direct link to the image plane I and projected at a retina point m in image coordinates (u, v) in pixels. O_c is the origin of 3D camera reference frame and the distance between O_c and I is called the *focal length* and the line through O_c and perpendicular to I is the optical axis (see Figure 4.9).

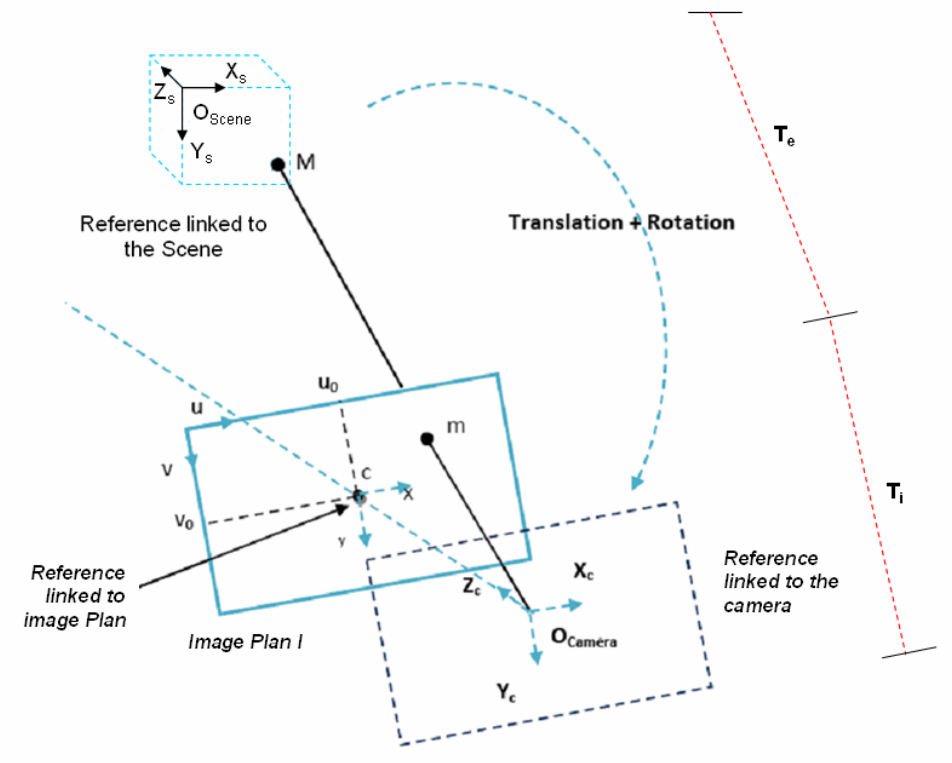

Figure 4.9 The perspective camera model

The principle of a camera model is to project a three dimensional point M from the camera reference frame into the two dimensional point in image plane I, where the point of $M(X_c, Y_c, Z_c)$ in image plane I becomes $m(x, y)$. In order to transform a world point of 3D into a image 2D point of the image requires the knowledge of the intrinsic and extrinsic camera parameters. This modelling consists of three different coordinate systems ; the world scene reference frame (x_s, y_s, z_s), the image frame (u, v) and the camera frame (x_c, y_c, z_c) with the optical centre as origin. The translation (t_x, t_y, t_z) and rotation (r) will convert a 3D point given in homogeneous world scene coordinates into the camera frame which is expressed by the extrinsic parameters T_e (See equation (4.1)).

$$\begin{pmatrix} x_c \\ y_c \\ z_c \end{pmatrix} = T_e \begin{pmatrix} x_s \\ y_s \\ z_s \\ 1 \end{pmatrix}, \quad T_e = \begin{pmatrix} r_{11} & r_{12} & r_{13} & t_x \\ r_{21} & r_{22} & r_{23} & t_y \\ r_{31} & r_{32} & r_{33} & t_z \end{pmatrix} \tag{4.1}$$

Afterwards, a 3D point of the camera frame (x_c, y_c, z_c) is projected to image plane on a point m(x, y) according to the following equation:

$$\frac{x}{f}=\frac{X_c}{Z_c} \text{ in the (X,Z) plane } \rightarrow x=f\frac{X_c}{Z_c}$$
$$\frac{y}{f}=\frac{Y_c}{Z_c} \text{ in the (Y,Z) plane } \rightarrow y=f\frac{Y_c}{Z_c} \quad (4.2)$$

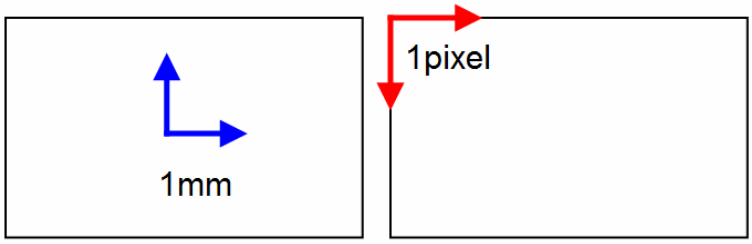

Figure 4.10 Image Coordinates and pixel Coordinates

Another important transformation is called affine transformation that describes the conversion of images coordinates (x,y) in metric units to discrete coordinates (u,v) in pixels unit (see Figure 4.10). A point will transform to the image plane using intrinsic parameters, such as the focal length f of camera, the centre of the image plane called principle point (u_0, v_0), and the pixel size (k_0, k_1) along the x and y directions respectively in mm or $\alpha = f / k_0$ and $\beta = f / k_1$ respectively, in the following equation:

$$\begin{pmatrix} u \\ v \\ s \end{pmatrix} = T_i \begin{pmatrix} x \\ y \\ z \end{pmatrix}, \; T_i = \begin{pmatrix} \alpha & 0 & u_0 \\ 0 & \beta & v_0 \\ 0 & 0 & 1 \end{pmatrix} \quad (4.3)$$

The knowledge of these intrinsic and extrinsic camera parameters are needed for the rectification of images and ensures the epipolar constraint. In summary, a point $M(X_s,Y_s,Z_s)$ expressed in world coordinates system is projected onto a two dimensional image plane using the following equation:

$$\begin{pmatrix} u \\ v \\ s \end{pmatrix} = T_i T_e \begin{pmatrix} x_s \\ y_s \\ z_s \\ 1 \end{pmatrix} \text{ or } m = PM, \quad (4.4)$$

where the perspective transformation P is:

$$P = \begin{pmatrix} \alpha & 0 & u_0 & 0 \\ 0 & \beta & v_0 & 0 \\ 0 & 0 & 1 & 0 \end{pmatrix} \cdot \begin{pmatrix} r_{11} & r_{12} & r_{13} & t_x \\ r_{21} & r_{22} & r_{23} & t_y \\ r_{31} & r_{32} & r_{33} & t_z \\ 0 & 0 & 0 & 1 \end{pmatrix} \tag{4.5}$$

The process of extracting or estimating this transformation matrix P is called *Camera Calibration*.

4.2.1.2 Tsai Camera Model

The Tsai camera model is an extension of the pinhole perspective projection model. Tsai used this camera model to develop a calibration based on the knowledge of the position of some points in the world (using non planar calibration grid) and the correspondent projections on the image. The improvement from the classical perspective camera model relies on the fact that Tsai's algorithm also includes the radial lens distortion coefficient (see Figure 4.11).

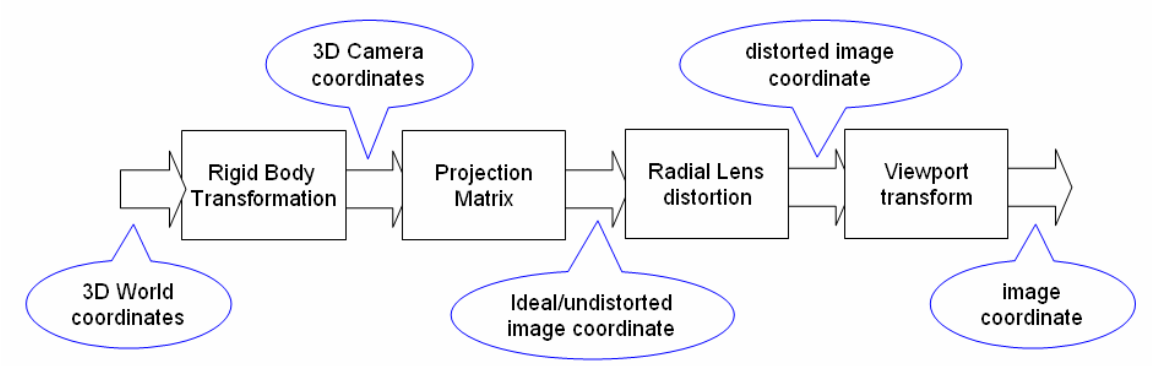

Figure 4.11 Four steps in transformation of Tsai Calibration Model

We used the Matlab Bouguet Toolbox [Bouguet (2008)] to calibrate our system. This toolbox is based on the Tsai's camera model and uses checkerboard as calibration pattern as used by Zhang method [Zhang and Kambhamettu (2002)].

4.2.2 *Polarization calibration*

In polarization imaging system, one must be sure that polarization information from the scene are completely captured by the imaging system setup. The polarization angle is estimated by placing another linear polarizing filter in front our polarizing filter

setup (Mpol1) and capturing several frames for different orientations α of the polarizer (see Figure 4.12).

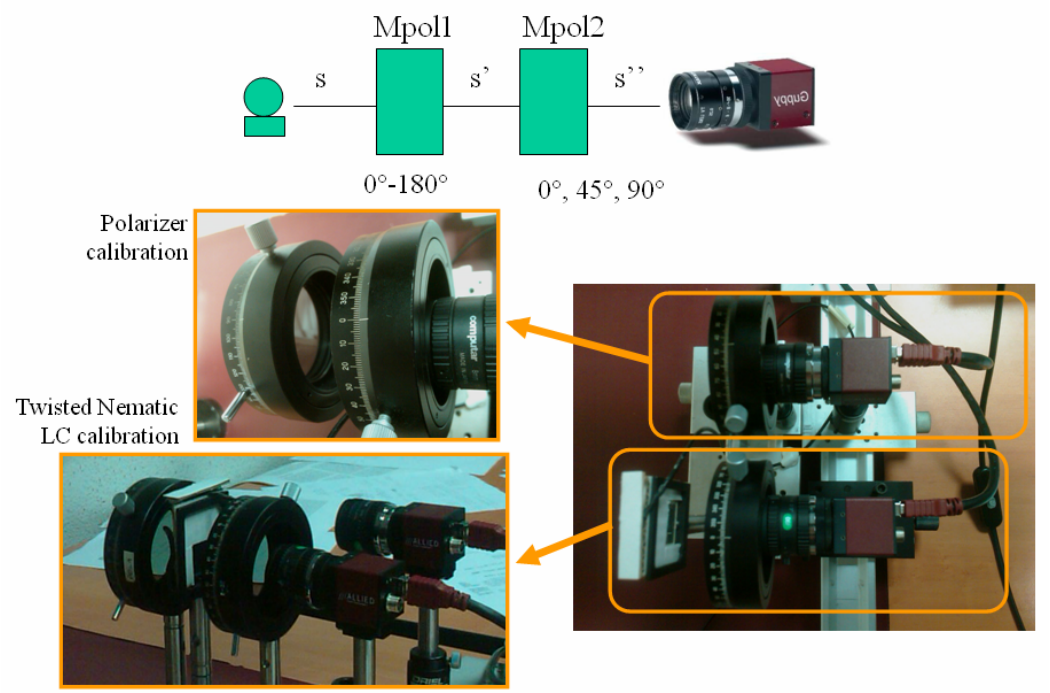

Figure 4.12 Polarization Calibration system setup. Mpol1&Mpol2 is a linear polarizer and analyzer respectively, s, s',s'' is incident light polarization state.

The polarization calibration procedure is:

1. Capturing images, with condition :
    - Left camera with Mpol2 : 0° and 90° for each Mpol1 orientation : 0°-180°
    - Right camera with Mpol2 : 0° and 45° for each Mpol1 orientation: 0°-180°
2. Select two random region of interest in the images (pix1o and pix2o) to compute the mean observed intensity in that area.
3. Measure a stokes vector, to compute predicted intensity :
    - Use Mueller Matrix theory
        - $s' = Mpol1.s$
        - $s'' = Mpol2.s' = Mpol2.Mpol1.s \rightarrow Ip = a\ s0 + b\ s1 + c\ s2$
    - Use Least Square method to get Stokes parameters *s0, s1* and *s2 :*

- For α =0°-180° compute $Ip(\alpha) = \frac{1}{2}(s0 + \cos 2\alpha.s1 + \sin 2\alpha.s2)$ → Matrix *M*.
- $y=M.x$ and $x=(M^tM)^{-1}M^t.y$ → $H=(M^tM)^{-1}M^t$
- Then the stokes parameter is :
  1. $s0 = s0+H(1,\alpha)*Ip(\alpha)$
  2. $s1 = s1+H(2,\alpha)*Ip(\alpha)$
  3. $s2 = s2+H(3,\alpha)*Ip(\alpha)$

- Get predicted intensity :
  - $Ip = a\ s0 + b\ s1 + c\ s2$
  - Select two region of interest in the predicted images (pix1p and pix2p) and compute the mean.

4. Verify mean result from step 3 with the mean of observed Intensity.

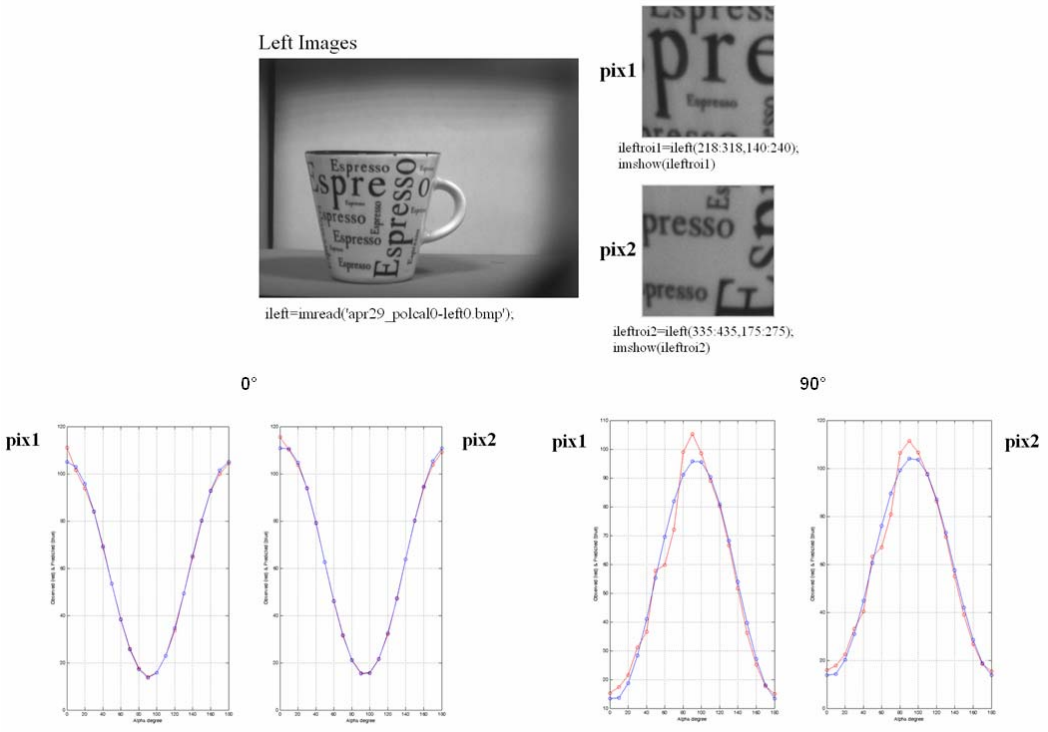

Figure 4.13 Polarization Calibration of LC in the Left Camera Result for polarizer in 0° and 90° and for region pix1 and pix2. The observed mean intensity in red line and predicted mean intensity in blue line.

The result of polarization calibration can be seen in Figure 4.13 and Figure 4.14.

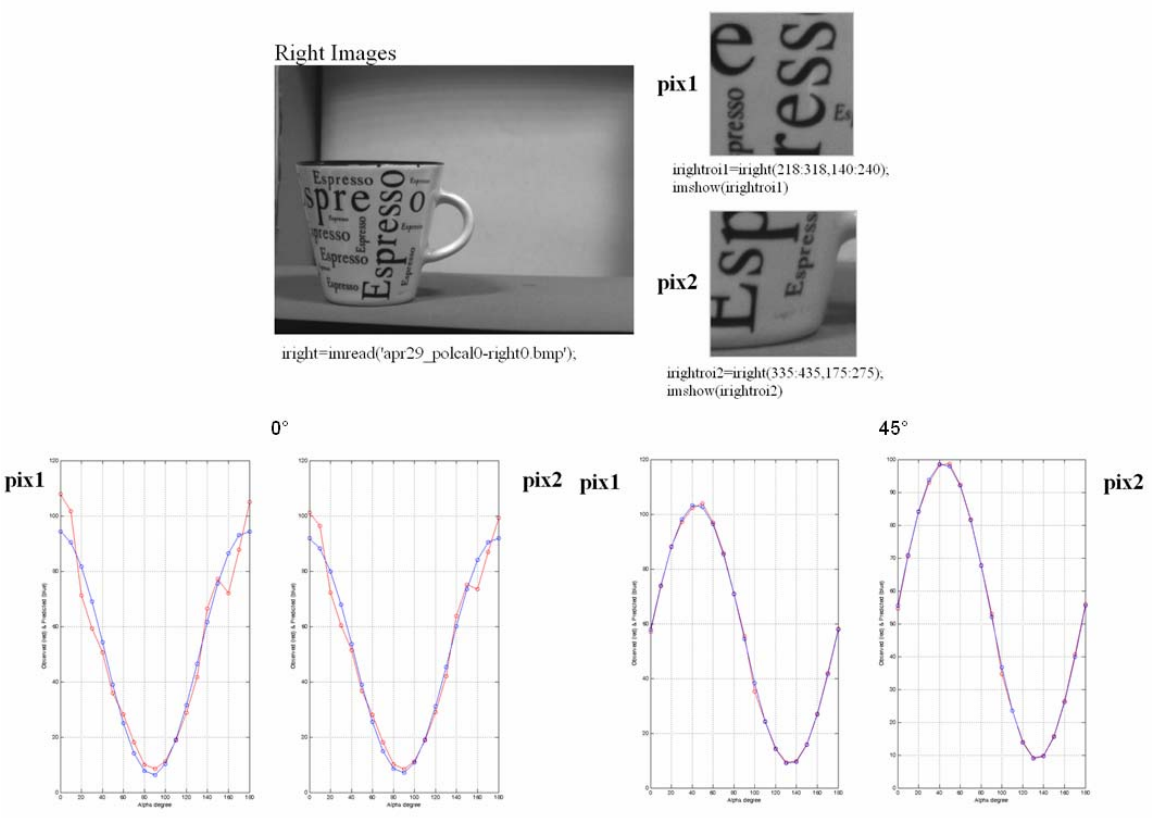

Figure 4.14 Polarization Calibration of LC in the Left Camera Result for polarizers in 0° and 45° and for region pix1 and pix2. The observed mean intensity in red line and predicted mean intensity in blue line.

Table 4-1 Average Error Calibration of LC Polarizer

No	***Calibration Scenes***	***Mean Error of Pix1 and pix2***
1	left 0°	0,7
2	left 90°	3,6
3	right 0°	4,9
4	right 45°	0,5

Ideally, the difference between the predicted intensity and the measured intensity should be zero. But a slight difference in the range of one to five grey levels can be tolerated on a scaled of 256 grey levels (the mean error of polarization calibration result can be seen at Table 4-1).

4.3 Stereo Matching and evaluation Problem

The goal of stereo vision is to obtain 3D information from two images taken from different viewpoints. The depth information can be achieved by measuring the disparity between two images taken by two calibrated cameras. Disparity is the difference of the position in both vertical and horizontal directions of the correspondent points in the stereo pictures, and it can represent at the *disparity map*. However, the difficult problem in obtaining the disparity is to find the correspondence of features between two images. Once the correspondences between the two images are known, the depth information of the objects in the scene can be obtained easily.

One of the key step in stereo vision is to find the corresponding features between the left and right images (or also called matching process). Many techniques have been applied to reduce the search space in order to solve matching ambiguity in the correspondence problem. One of the most effective approaches is to apply constraints to restrict possible feature matches. The matching process is a complex optimization problem where the processes to select, extract and match image features perform using a set of constraints that must be satisfied simultaneously. Another problem to solve is that extracted image features and the stereo system usable constraints are variable depending on the application.

Briefly, the matching problem can be formulated as : *"For a point m_L (projection of M) in left image , find the point m_R of right image which corresponds to the same physical point M of the observed scene"*

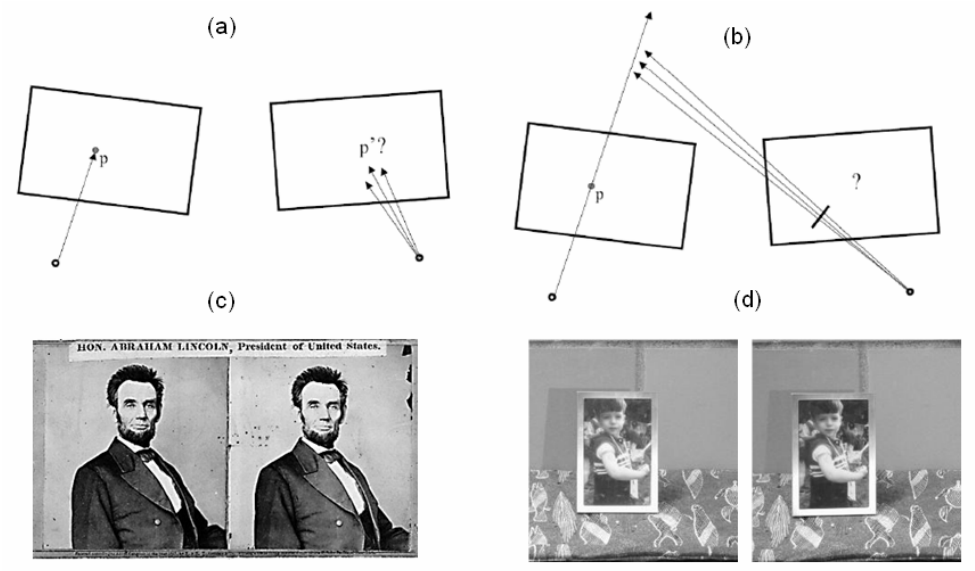

Figure 4.15 The Stereo Matching Problem, (a) How to select possibilities of correspondence point between two images, (b) occlusion problem, (c) textureless surfaces, (d) non lambertian or specularities problem (image (c) and (d) courtesy of University of North Carolina, US)

Ideally, all matching algorithms must deal with at least the following problems :

- Problem associated with light situation on the object, such as specular reflections caused by the reflectance properties of the object, radiometric distortion caused by differences in camera parameters (e.g gain, bias, and gamma factor).
- Problem associated with pattern condition such as a noise which is introduced by the image acquisition and digitization process, the regions which do not contain enough information for matching (e.g. a featureless wall), and repetitive patterns which can potentially result in invalid matches.
- Problem of Perspective distortion that occurs due to a change in the shape of object when they are viewed from a different point of view.
- Problem of occlusions caused by portions of a scene being visible in only one image.

In this study, the problem was constrained with the assumptions that there exists a sharp intensity difference between the two polarized images.

4.3.1 *Feature Detector*

Feature extraction is the first step to solve a matching problem. It allows to highlight information of interest from the images to represent a target. The features to be extracted can be grouped into three main classes [Cavallaro and Maggio (2011)], namely:

- Low-level (e.g. colour, gradient, motion)
- Mid-level (e.g. edges, interest point ; corners, regions)
- High-level (objects)

The matching problem of images with a variety of illumination conditions is a clearly combinatorial problem. So, the best features that have to be chosen is a feature in the mid level class such as edges, chains of contour points or regions. In addition, with respect to high speed processing, to solve this matching problem, a usage of specific constraints to reduce the complexity of the matching process is needed. For that reason, the epipolar geometry can be used as a constraint. From many feature extraction algorithms, two algorithms sufficiently reliable in this field are tested in these Polarization stereo imaging system prototype, there are the Harris Corner detector and the Scale Invariant Feature Transform (SIFT) descriptor.

The use of polarizer filter in front of the camera makes images appearances darker than the usual intensity image. It depends on the settings of the polarizer angle direction. Intensity difference between the two image pairs will be greater if each stereo image has a high difference of polarizer angle setup. For that reason, our setup required a feature detector that is capable to handle these constraints. We conducted two evaluations detector features Harris corner detector and SIFT to be used with polarized images.

4.3.1.1 Harris Corner Detector

The Harris corner detector is an extension of the Moravec detector. The corner is defined as a position of interest point in the image that is characterised by large intensity variations in multiple directions ([Moravec (1977)]). The Moravec detector does not need high computational demand, but has a drawback to respond an anisotropic interest score. As a consequence, the output of the detector is not rotation invariant, and has a problem in affecting the repeatability of the interest-point detection under target rotations.

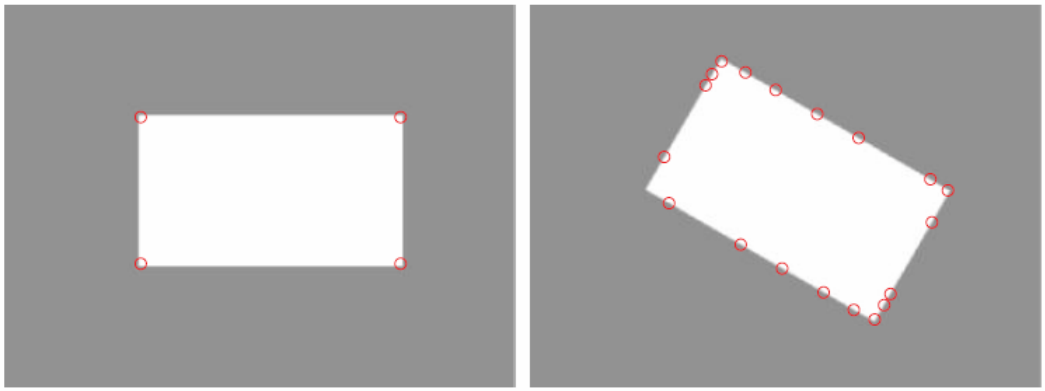

Figure 4.16 The response of the Moravec cornerness score for rotation of target is anisotropic, the number and location of the detected interest points may vary with the orientation of the target. (Cavallaro, 2011) [Cavallaro and Maggio (2011)]

The Harris Corner Detector (Harris, 1988) [Harris and Stephens (1988)] improves the rotation invariance with respect to the Moravec detector. This method based on the use of the auto-correlation matrix and the relation of its eigenvalues. The procedure is as follows:

1. Compute the derivatives of the intensity image in the x and y directions for every pixel. In this way we obtain $I_x = \frac{\partial I}{\partial x}$ *and* $I_y = \frac{\partial I}{\partial y}$ for every point of the image. Then, make a computation of : I_x^2, I_y^2 *and* I_x, I_y.
2. Next, the squared image derivatives should be smoothed by convolving them with a Gaussian filter g.,

$$\langle I_x^2 \rangle = g \otimes I_x^2 \tag{4.6}$$

where $\otimes$ is the convolution operator. Consider all small shifts by Taylor's expansion, then:

$$
\begin{aligned}
E(u,v) &= \sum_{x,y} w(x,y)\left[I(x+u,y+v)-I(x,y)\right]^2 \\
&= \sum_{x,y} w(x,y)\left[I_x u + I_y v) + O(u,v)\right]^2 \\
E(u,v) &= Au^2 + 2Cuv + Bv^2 \\
\rightarrow A &= \sum_{x,y} w(x,y) I_x^2(x,y) \\
\rightarrow B &= \sum_{x,y} w(x,y) I_y^2(x,y) \\
\rightarrow C &= \sum_{x,y} w(x,y) I_x(x,y) I_y(x,y)
\end{aligned}
\tag{4.7}
$$

Equivalently, for small shifts [u,v] we have a bilinear approximation:

$$E(u,v) \cong \begin{bmatrix} u, v \end{bmatrix} \quad M \quad \begin{bmatrix} u \\ v \end{bmatrix} \tag{4.8}$$

and the autocorrelation matrix 2x2 M can be defined for every pixel:

$$M = \sum_{x,y} w(x,y) \begin{bmatrix} I_x^2 & I_x I_y \\ I_x I_y & I_y^2 \end{bmatrix} = \begin{pmatrix} \sum_w \langle I_x^2 \rangle & \sum_w \langle I_x I_y \rangle \\ \sum_w \langle I_x I_y \rangle & \sum_w \langle I_y^2 \rangle \end{pmatrix} \tag{4.9}$$

Where W is a 3×3 neighbourhood around the point.

3. M can be used to derive a measure of "cornerness" for every pixel. Depending of the rank of M, the pixel belongs to an homogeneous region (rank M = 0), an edge (significant gradient in 1 direction, that is, rank M = 1), or a corner (significant gradients in both directions, thus, rank M = 2).
4. Harris and Stephens proposed the use of the determinant and the trace of M to detect corners:

$$R = \det(M) - k.tr(M)^2 \tag{4.10}$$

Where: k is a constant (with a value of 0.04-0.06)

det (·) is the determinant and tr is the trace (sum of the diagonal elements).

4.3.1.2 Scale Invariant Feature Transform (SIFT)

The SIFT algorithm was developed by David G. Lowe at 2004 [Lowe (2004)]. This algorithm performs image features extraction by calculating a local image feature

vector that is invariant to image scaling, translation, rotation, and partially invariant to changes in illumination and affine transformations. SIFT consists of four major stages: scale-space extrema detection, keypoint localization, orientation assignment and keypoint descriptor.

Scale-space extrema detection: The first stage of computation searches over all scales and image locations. It is implemented efficiently by using a difference-of-Gaussian function to identify potential interest points that are invariant to scale and orientation. If $G(x, y, \sigma)$ is a Gaussian function, $L(x, y, \sigma)$ a scale space function, then Difference of Gaussians (DOG):

$$\begin{aligned} D(x, y, \sigma) &= \left(G(x, y, k\sigma) - G(x, y, \sigma)\right) * I(x, y) \\ &= L(x, y, k\sigma) - L(x, y, \sigma) \end{aligned} \tag{4.11}$$

where the x and y are related to the blur radius r by $r^2 = x^2 + y^2$ and σ is the scale. $I(x, y)$ is the gray scale image, and * is the convolution operation in x and y. A factor k is multiplied by σ where $k = 2^{1/s}$ and s is an algorithm parameter such that $s+3$ is the number of images in an octave. An example of DOG implementation can be seen in Figure 4.17.

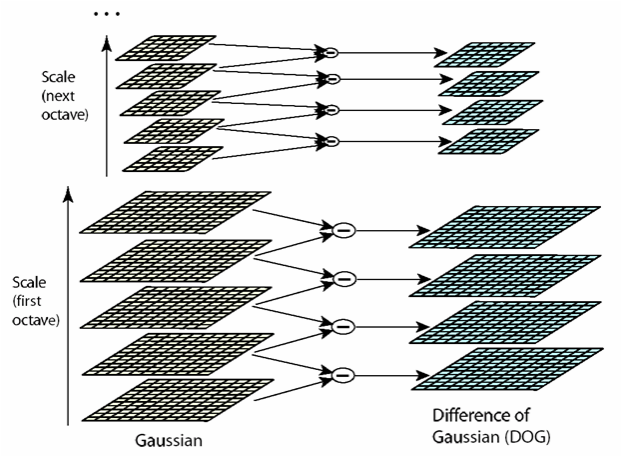

Figure 4.17 SIFT Difference of Gaussians computation

The next step is to detect the local maxima and minima of $D(x, y, \sigma)$, each sample point is compared to its eight neighbours in the current image and nine

neighbours in the scale above and below (see Figure 4.18). X is selected if it is larger or smaller than all 26 neighbours in 3x3 regions.

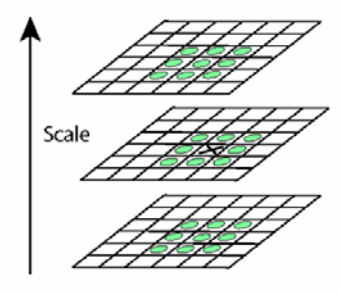

Figure 4.18 Maximum Minimum Difference of Gaussians computation

Keypoint localization: At each candidate location, a detailed model is fit to determine location and scale. Keypoints are selected based on measures of their stability. Some keypoints are unstable (points with low contrast, point along an edge). This step refines the location of the detected extrema and a remove low contrast points.

- Fit keypoint at $\underline{x}$ to nearby data using quadratic approximation:

$$D(\underline{x}) = D + \frac{\partial D^T}{\partial \underline{x}} \underline{x} + \frac{1}{2} \underline{x}^T \frac{\partial^2 D^T}{\partial \underline{x}^2} \underline{x} \tag{4.12}$$

- Calculate the local maxima of the fitted function:

$$\hat{\underline{x}} = -\frac{\partial^2 D}{\partial \underline{x}^2}^{-1} \frac{\partial D}{\partial \underline{x}} \tag{4.13}$$

- A location refinement is performed if $\hat{\underline{x}} > 0.5$ in any dimension. The weak keypoints are removed if $D(\hat{\underline{x}}) < 0.03$ (discard a local minima) for pixel values in the [0,1] range. Then eliminate edge responses by computing the 2x2 Hessian matrix:

$$H = \begin{bmatrix} D_{xx} & D_{xy} \\ D_{xy} & D_{yy} \end{bmatrix} \tag{4.14}$$

If the ratio of principal curvatures are less then:

$$\frac{\lambda_{\max}}{\lambda_{\min}} < r \Leftrightarrow \frac{Tr(H)^2}{Det(H)} < \frac{(r+1)^2}{r} \tag{4.15}$$

For r = 3, the keypoint is also pruned. Where $\lambda_{max}, \lambda_{min}$ are the eigenvalues of the Hessian matrix.

Orientation assignment: One or more orientations are assigned to each keypoint location based on local image gradient directions. All future operations are performed on image data that has been transformed relative to the assigned orientation, scale, and location for each feature, thereby providing invariance to these transformations.

The first step is to create a weighted (magnitude + Gaussian) histogram of local gradient directions computed at selected scale, for each image sample, $L(x, y, \sigma)$ at the closest scale, the gradient magnitude and the orientation are respectively:

$$m(x,y) = \sqrt{\left(L(x+1,y) - L(x-1,y)\right)^2 + \left(L(x,y+1) - L(x,y-1)\right)^2} \tag{4.16}$$

and

$$\theta(x,y) = \tan^{-1} \frac{L(x,y+1) - L(x,y-1)}{L(x+1,y) - L(x-1,y)} \tag{4.17}$$

A smoothed histogram is built from the gradient orientations of the neighbours of a keypoint. The histogram represents the possible 360 degrees possible into 36 slots. Each point sampled from around the keypoint is weighted by its gradient magnitude and with a Gaussian-weighted circular window with σ equal to 1.5 times the scale of the keypoint [Lowe (2004)]. The highest peak in the histogram, and all other peaks within 80% of the highest peak, is set as the orientation of the keypoint.

Keypoint descriptor: The local image gradients are measured at the selected scale in the region around each keypoint. These are transformed into a representation that allows for significant levels of local shape distortion and change in illumination.

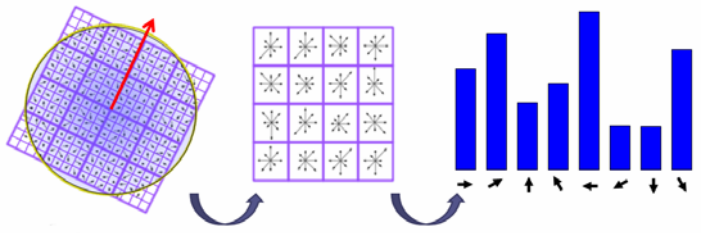

Figure 4.19 Keypoint descriptor Generation

After having assigned location, scale, and orientation to each keypoint, the next step is to impose a repeatable local 2D coordinate system and provide invariance to these parameters. The created samples are accumulated into orientation histograms over 4x4 subregions, as shown on the middle of Figure 4.19. The length of each arrow corresponds to the sum of the gradient magnitudes near that direction within the region. Figure 4.19 is a 4x4 descriptor computed from a 16x16 sample array. Using this method, a descriptor of 4x4x8=128 with dimensional feature vector elements is created. In the next step, the gradient orientation relative to keypoint's orientation is computed followed by the orientation histogram of each 4x4 pixel block. Due to the Gaussian weighted window, pixels closer to the center of the 16x16 patch contribute more to the orientation histograms.

Briefly, keypoint descriptors are generated by:

1. Computing gradients,
2. Computing relative gradient orientations,
3. Defining an accumulator variable for each of the 8 orientations in each of the 16 histograms (128 total), and finally
4. For each pixel, calculate the pixels contribution to each accumulator variable.

The SIFT algorithm is robust to detect a feature changes due to point of view illumination, noise, which can be found in images of the polarization of light ([Lowe (2004)]). The following section describes the tests performed in implementing the SIFT algorithm for polarized images.

4.3.1.3 Experiment with Harris Corner Detector and SIFT Detector

The following section discusses about the implementation of Harris Corner Detector and SIFT detector onto polarized images.

4.3.1.3.1 Imaging System Installation and Object Test

The imaging System is composed of the AVT Guppy F-080B CCD cameras assembled in stereo configuration with the intrinsic and extrinsic camera parameters

obtained from Bouguet calibration toolbox. In front of each camera are mounted a set of linear polarizer filters (see Figure 4.20).

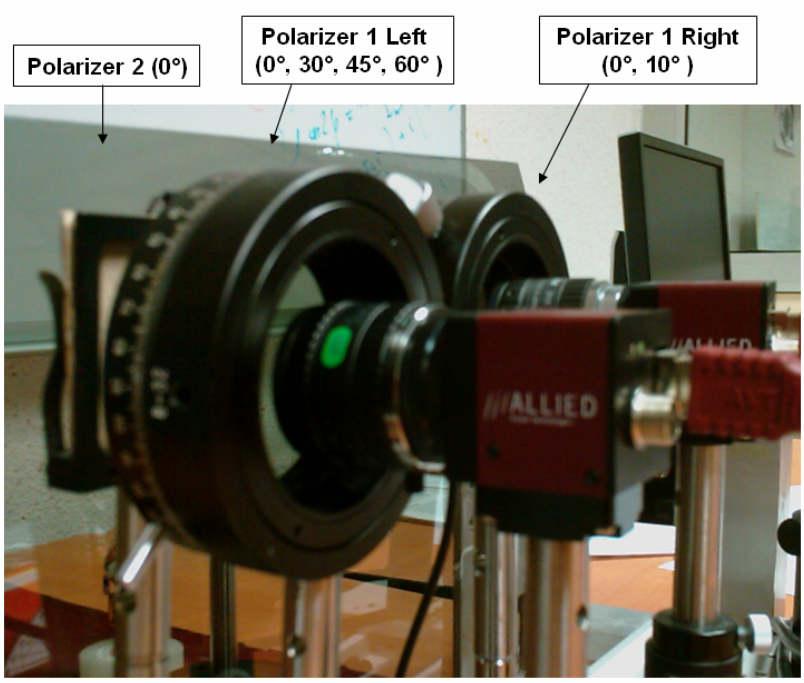

Figure 4.20 Setup Stereo and Polarizer for Harris Corner and SIFT Test

4.3.1.3.2 Harris Corner Detector Polarized Images Test Result

To see the ability of extracting features from stereo polarized images that have illumination changes, the experiment begins with artificial scenes with a basic shape to be extracted, then the subsequent scenes have extreme differences in illumination. In these tests we only measure the illumination value and do not use any image-processing technique to improve the quality of the image target, moreover, in these tests we also do not consider the accuracy of the correspondence features found between stereo images, this point being specifically addressed later on the matching score section. For the Harris corner computation, the parameter set k=0.04 and Sigma=2 are used. The first object test shows the robustness to rotation and scale can be seen in Figure 4.21.

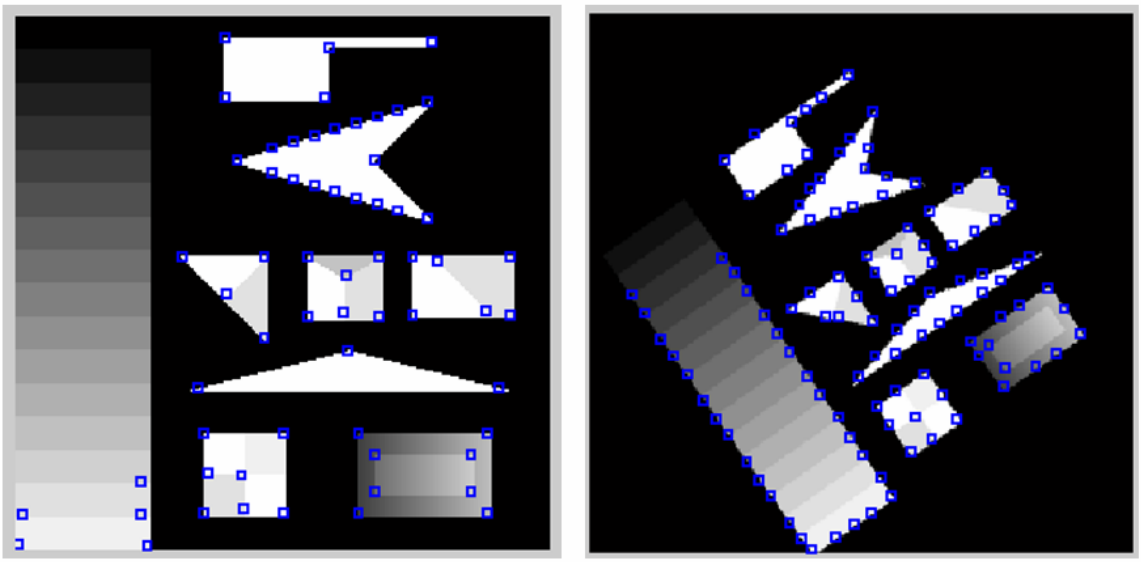

Figure 4.21 Rotate and Scale Test Result of Harris Corner Detector

The observations were made on a number of features found and the time required for the process. Detail results can be seen in the Table 4-2.

Table 4-2 The Results of Keypoints Extraction using Harris Corner Detector Algorithm

Code	**Image Test**		**Keypoint found**			
	Pol left	**Pol right**	**Img1 (left)**	**Time (s)**	**Img2 (right)**	**Time (s)**
TR&S	Rotate and scale test		62	0.3448	113	0.3313
0	90°	10°	3	0.8987	40	0.3981
1	0°	0°	31	0.8390	40	0.3669
2	30°	0°	8	1.0176	41	0.4700
3	60°	10°	8	0.8579	40	0.3618
4	45°	10°	8	0.9584	42	0.4157
5	30°	10°	8	0.9533	40	0.3815

Rotation and scale invariant test results show that Harris corner detector was able to detect the exact points that exist on the object corners but failed on the part where a high vertical gradient is present.

In real images with extreme illumination in 90° (Figure 4.22 – (0) left image), Harris corner detector failed to detect the corners in both images. It also occurs in the images at 30°, 45° and 60°, which are rather darker because of the effect of polarized filters, Harris could only detect a few features (see Figure 4.22 – (2), (3), (4) and (5) the left). Even in the best quality of polarizer images at 0° (Figure 1 left and right), Harris corner detector does not find many features.

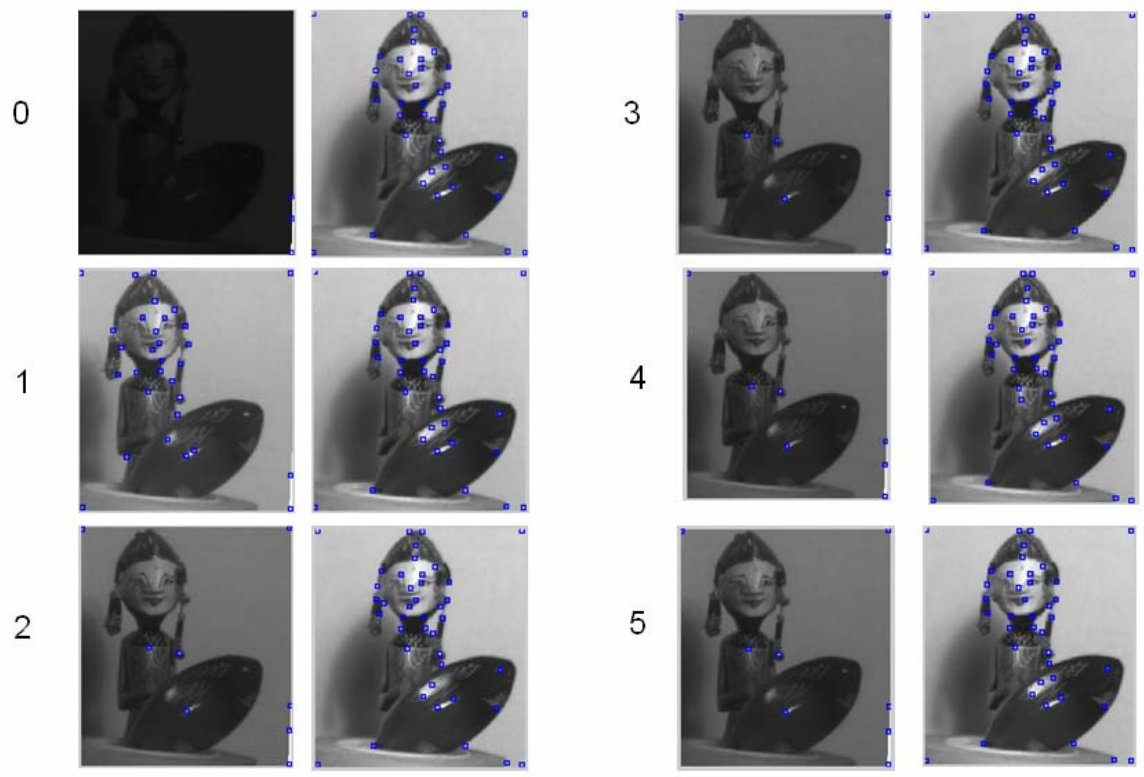

Figure 4.22 Variation of Illumination Test Result of Harris Corner Detector

4.3.1.3.3 SIFT Detector Polarized Images Test Result

SIFT algorithm was applied on the same set of images. The visual result of the first rotation and scale invariant test can be seen in Figure 4.23. SIFT is able to find a more keypoints including keypoints in the part of different gradients in the images. SIFT is also robust to rotation and scale.

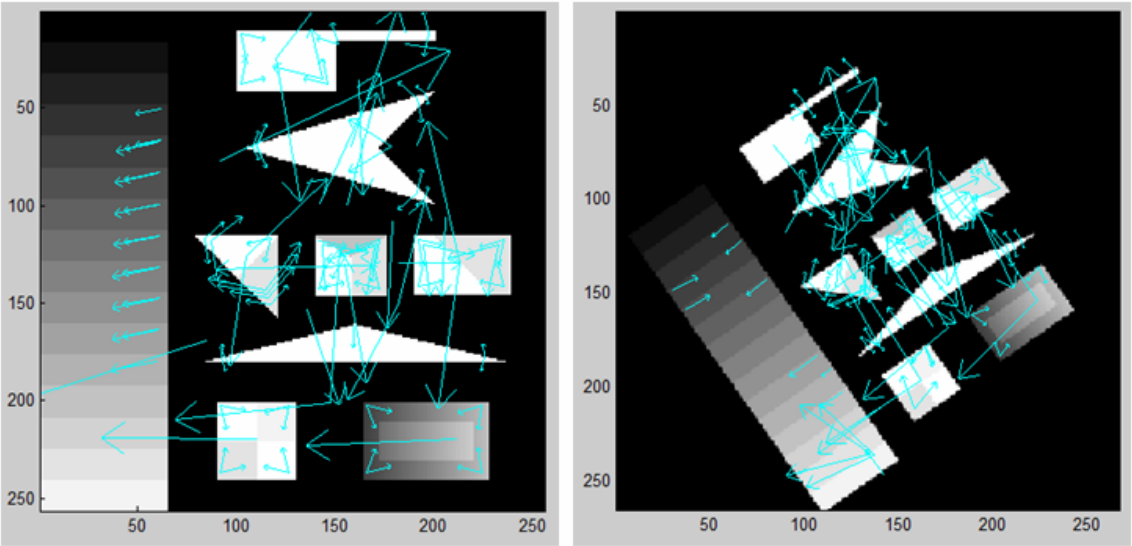

Figure 4.23 Rotate and Scale Test Result of SIFT Detector

The observations were made on a number of features found and the time required for the process, can be seen in the Table 4-3.

Table 4-3 The Results of keypoint extraction and stereo matching using SIFT algorithm

No	Image Test		Keypoint found				Keypoint Matching (Img1 & Img2)	
	Pol left	Pol right	Img1 (left)	Time (s)	Img2 (right)	Time (s)	Point found	Time (s)
TR&S	Rotate & scale test		132	0.6105	131	0.6956	43	1.0424
0	90°	10°	0	0.3319	152	0.6309	0	0
1	0°	0°	132	0.4758	152	0.6677	33	0.7815
2	30°	0°	87	0.4007	154	0.6531	24	0.8324
3	60°	10°	87	0.3649	165	0.5639	24	0.8562
4	45°	10°	87	0.4494	146	0.5400	23	0.7885
5	30°	10°	87	0.3950	152	0.5521	23	0.7499

In images with extreme illumination in 90° (Figure 4.24 – (0) left image) SIFT detector is not reliable, however on the images with polarizer angles set at 30°, 45° and

60°, which are rather dark because of the effect of polarized filters, SIFT detector could detect many features (see Figure 4.24 – (2), (3), (4) and (5) the left).

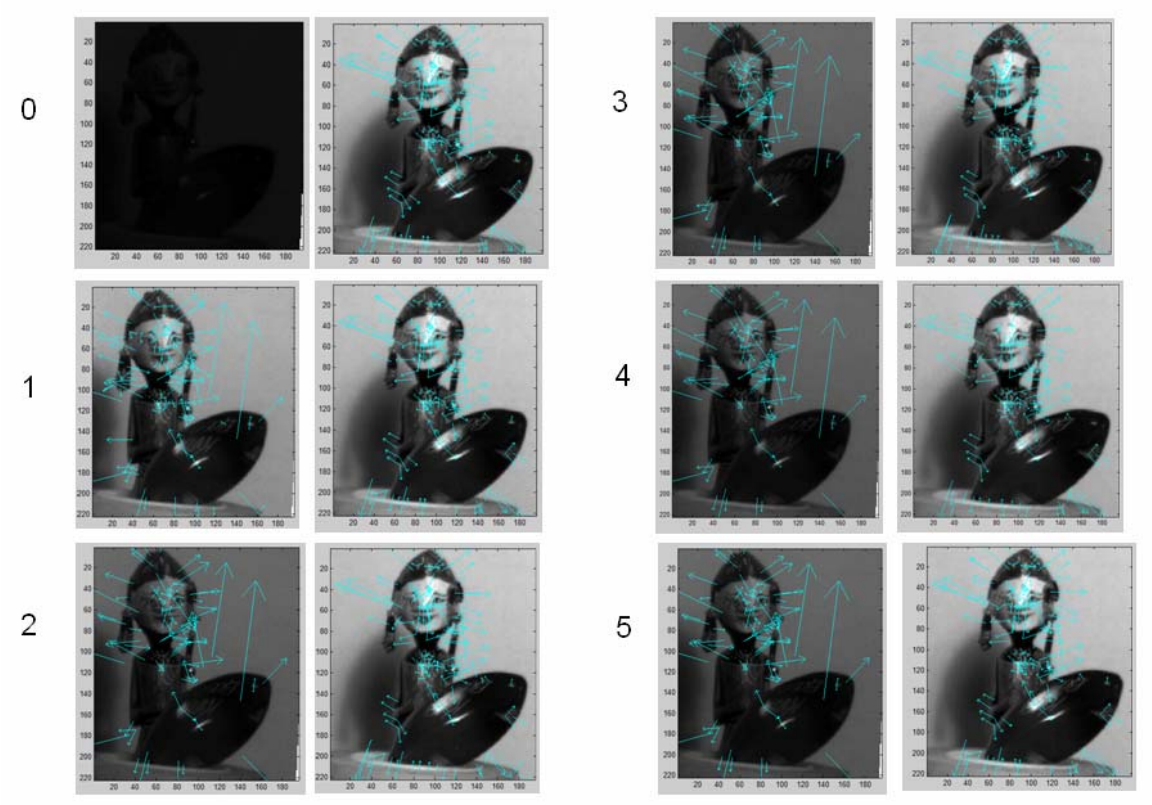

Figure 4.24 Variation of Illumination Test Result of SIFT Detector

In these experiments we also tried the stereo matching point function, which is contained in the SIFT algorithm. The match results obtained in Table 4-3, SIFT matching point function could only detect approximately 30 percent of the feature points. Therefore for polarized images, the SIFT matching point algorithm did not provide good result.

4.3.1.3.4 Conclusion

As expected, these primary results show that SIFT is more appropriated to work on polarized images than the Harris Corner detector, however the matching process still need to be selected.

4.3.2 *Stereo Matching Score Methods Applied to Polarized Images*

Discussion about matching problem in stereo vision is a subject that received a lot of attention from researchers. A large variety of algorithms have been developed. At least in recent decades, these researches result can be grouped and categorized, as done by [Banks et al. (1997)], [Lane and Thacker (1998)] and [Brown et al. (2003)].

4.3.2.1 Local Matching vs Global Matching Method

Brown, in 2003 [Brown et al. (2003)] divided stereo matching methods into two types, local and global methods. Local matching performs an evaluation of local characteristics on a small part of the image source and search for corresponding points with the same characteristics in the target image. Meanwhile, the global matching evaluates the global characteristics of the source image and then compares it with those of the target.

In local methods, matching is performed by looking for the most similar matches based on local image properties. Each matching element has a signature. The main focus of local methods lies in the definition of the appropriate windows that represent the signatures, and their similarity evaluated statistically over these signatures. Several algorithms included in the local method are grouped in three categories, block matching (by comparing small region of template, i.e. NCC, SSD, SAD, rank and census), gradient method (or optical flow, by formulating equation of motion and image brightness) and feature matching (by limiting the region search to specific reliable features).

In global methods, the matching is performed by defining the prior model of the world first and relies on iterative schemes that make disparity assignments, based on the minimization of a global cost function. This method usually consisting of two terms: one represents the world model with all its assumptions, and the other measures the consistency with the input images. According to Brown, several algorithms are included in the global methods, which are dynamic programming, intrinsic curve, graph cut, non linear diffusion, belief propagation and correspondence-less method.

4.3.2.2 Feature Based vs Area-based Method

Banks in 1997 [Banks et al. (1997)] provided a taxonomy of Image Matching method for Stereo Vision. It consists of 9 taxonomy of matching method, such as area based, transform based, feature based, hybrid, phase based, combining independent measurement, relaxation dynamic programming and Object space. But, related to this research, only area based and feature based will be discussed.

In area-based method, the matching elements are the region of individual pixels values. The advantages of these algorithms are their simplicity and their ease to be implemented. The methods focusing on finding pixel-to-pixel correspondences resulting in dense disparity maps but are very sensitive to noise. According to Banks, several algorithms are included in the area-based method, i.e. SAD, SSD, NCC and their derivative, adaptive windows method, etc. The rank and census method are categorized to be transform based method.

In the feature-based methods, the features are typically the regions that contain easily distinguishable elements in the input images. The matching element are characterised by the use of image features such as edges, corner, contour, etc. These methods are faster than the area-based methods since only subsets of pixels are used, the matching is more accurate and less sensitive to photometric distortion. However, these methods typically produce very sparse disparity maps.

In this work, we use local or area-based methods for the matching score because while extracting polarization information, observations were made on a pixel level basis.

4.3.2.3 Similarity Statistics

To process the polarized images using the local or area-based methods, the matching cost is evaluated based on similarity statistics between image neighbourhoods of the processed pixels. To improve similarity matching, three different metrics have to be taken into consideration [Brown et al. (2003)]:

- Intensity differences such as SSD (Sum of Squared Differences) and it can be normalized as well (Normalized-SSD), and SAD (Sum of Absolute Differences).

- Correlation based, such as NCC (Normalized Cross Correlation), this is a standard statistical method for determining similarity.
- Rank metrics such as rank transform and census transform [Zabih and Woodfill (1994)].

The correspondences are selected based on these statistics. The principle of selecting the matching is winner-takes-all (WTA) [Szeliski and Scharstein (2002)] principle, so, for each point in a reference image is (somehow) selected the best tentative pair (the winner) and the images matched by taking either left image as the reference (left-to-right matching).

4.3.2.3.1 Intensity Differences Based Matching

The intensity differences matching methods are based on the subtraction of pixel. The simplest statistics computation is directly to compare a pixel intensity values which is very sensitive to noise and various image distortions. A better and robust approach is to compute a similarity statistic is using a comparison window containing the property values (statistics) of image neighbourhood of the processed pixel.

4.3.2.3.1.1 Sum of Absolute Differences (SAD)

The Sum of Absolute Differences (SAD) is the similarity measures which is calculated by subtracting pixels within a square neighbourhood between the reference and the target image at a distance d.

$$\sum_{u,v}\left|\left(I_1(u,v)-I_2(u+d,v)\right)\right| \tag{4.18}$$

4.3.2.3.1.2 Sum of Squared Difference (SSD)

The Sum of Squared Differences (SSD), compute the square of the intensity differences within a window shifted with a distance d.

$$\sum_{u,v}\left(I_1(u,v)-I_2(u+d,v)\right)^2 \tag{4.19}$$

4.3.2.3.1.3 Normalized SSD

Polarization images are subject to large intensity variations which need to be compensated by a normalizing factor. For these reasons, we use to normalize the pixels in each window. Related to SSD matching, the normalized SSD equation is given by:

$$\sum_{u,v}\left(\frac{\left(I_1(u,v)-\bar{I}_1\right)}{\sqrt{\sum_{u,v}\left(I_1(u,v)-\bar{I}_1\right)^2}}-\frac{\left(I_2(u+d,v)-\bar{I}_2\right)}{\sqrt{\sum_{u,v}\left(I_2(u+d,v)-\bar{I}_2\right)^2}}\right) \tag{4.20}$$

4.3.2.3.2 Correlation Based Matching

A few techniques have been developed using the properties of the correlation. Cross-correlation is sensitive to variations in the intensity of the image such as illumination change. To avoid this effect, cross-correlation function should be first normalized. This technique is referred as normalized cross-correlation (NCC).

$$NCC=\frac{\sum_{u,v}\left(I_1(u,v)-\bar{I}_1\right).\left(I_2(u+d,v)-\bar{I}_2\right)}{\sqrt{\sum_{u,v}\left(I_1(u,v)-\bar{I}_1\right)^2.\left(I_2(u+d,v)-\bar{I}_2\right)^2}} \tag{4.21}$$

4.3.2.3.3 Rank Metrics

These transform have been designed to improve matching in order to eliminate sensitivity to radiometric gain and bias. This metric is applied locally (local nonparametric transforms) to regions in both images before matching. After the rank metrics are applied onto each image, block matching methods are performed (i.e., SSD, SAD) to find matches. Zabih and Woodfill [Zabih and Woodfill (1994)] propose these methods in two approaches; rank transform and census transform.

4.3.2.3.3.1 Rank Transform

Rank Transform is a form of non-parametric local transform (i.e. relies on the relative ordering of local intensity values, and not on the intensity values themselves)

used to rank the intensity values of the pixels within a square window. The centre pixel's intensity value is replaced by its rank amongst the neighbouring pixels. A pair of stereo images transformed using the rank transform would then be matched using one of the previously discussed metric, such as SAD or SSD.

$$\sum_{u,v}\left(I_1'(u,v)-I_2'(u+d,v)\right)$$
$$I_k'(u,v)=\sum_{m,n}I_k(m,n)<I_k(u,v) \tag{4.22}$$

4.3.2.3.3.2 Census Transform

The census transform maintain the spatial distribution of ranks by encoding them in a bit string.

$$\sum_{u,v} Hamming\left(I_1'(u,v),I_2'(u+d,v)\right)$$
$$I_k'(u,v)=Bitstring_{m,n}(I_k(m,n)<I_k(u,v)) \tag{4.23}$$

The first step describes the relationship between the pixel and its surrounding neighbourhood. Neighbour pixels with intensity smaller than the centre pixel result in zero in the census vector and one otherwise. The second step is computing a sum of Hamming distances.

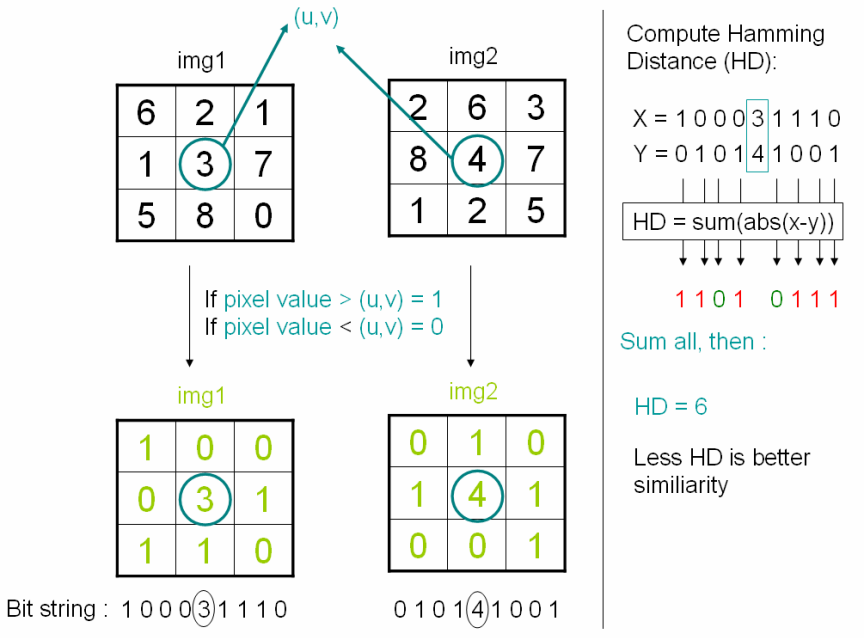

Figure 4.25 Census Transform Method Illustration

4.3.2.4 Searching Method

The success of local matching methods to discriminate the signature of a feature depends on the proper selection of the windows shape and size. The windows must be large enough to capture intensity variation for reliable matching and at the same time, must be small enough to avoid the projective distortions effects. Several work attempted to overcome this: Shiftable windows [Bobick and Intille (1999)], windows with adaptive size [Kanade and Okutomi (1994)], windows using image segmentation [Zhang and Kambhamettu (2002)] and windows modeled based on disparity [Boykov et al. (1997)] [Szeliski and Scharstein (2002)].

4.3.2.4.1 Determination of Searching Windows

In the Shiftable windows approach, the position of the windows shifts over the examined pixel, in order to cover more matching elements of the input images. These methods modify neither the shape nor the size of the windows. The selected signature in the target image tagging the pixel represents the window at the best matching position with the reference image (see Figure 4.26).

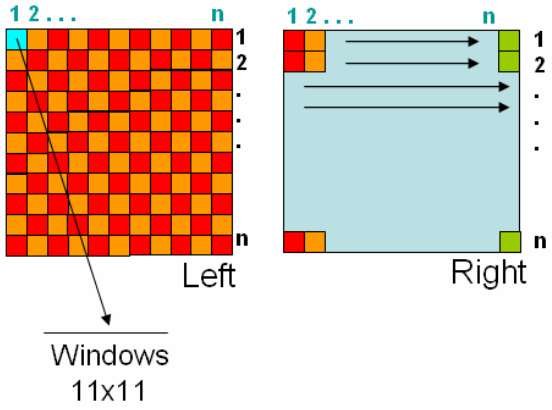

Figure 4.26 Searching windows Illustration

4.3.2.4.2 Image Rectification

Epipolar geometry establishes a mapping between points in the left image and lines in the right image. Rectification determines the transformation of each image plane

such that pairs of corresponding epipolar lines become collinear and parallel to the image and therefore the corresponding point on the both images are only shifted horizontally, which reduces the search space from 2-D to 1-D search along the epipolar line (see Figure 4.27).

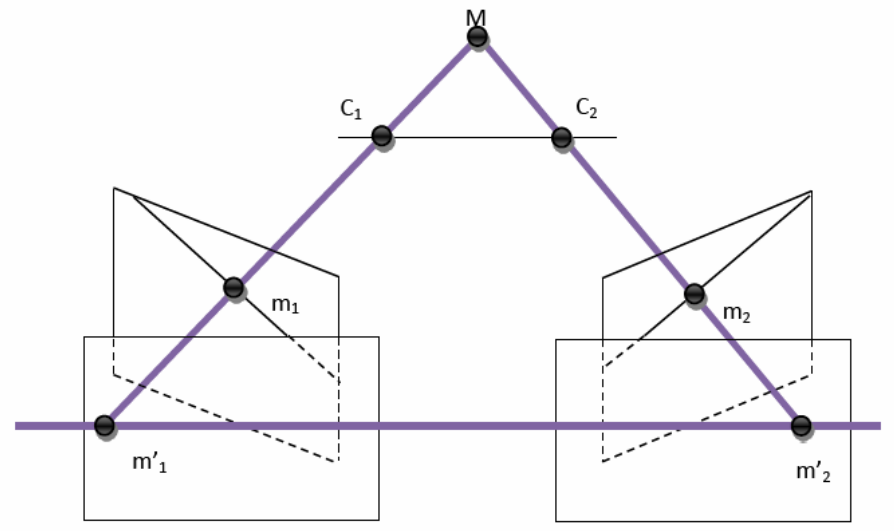

Figure 4.27 Rectifying Images Principle

We use the planar rectification introduced by Faugeras [Faugeras (1993)] and Zhang [Loop and Zhang (1999)] (Figure 4.28).

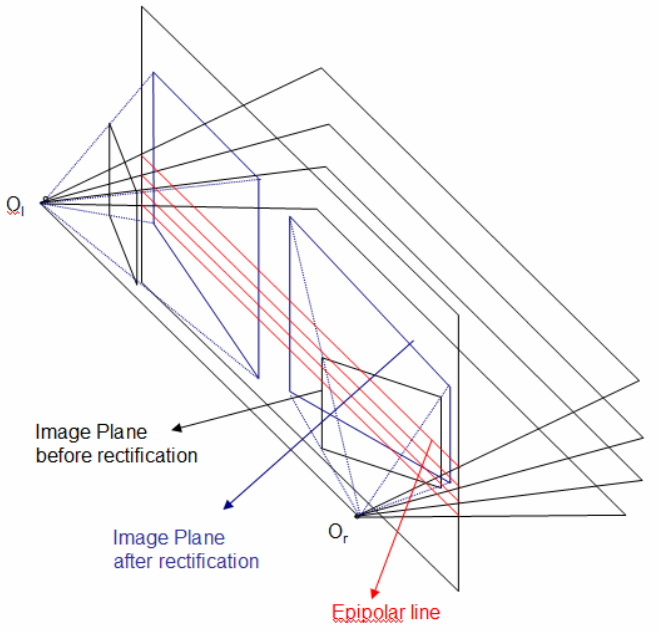

Figure 4.28 Planar Rectification

The Figure 4.29 illustrates the result of the rectification applied to stereo polarized images.

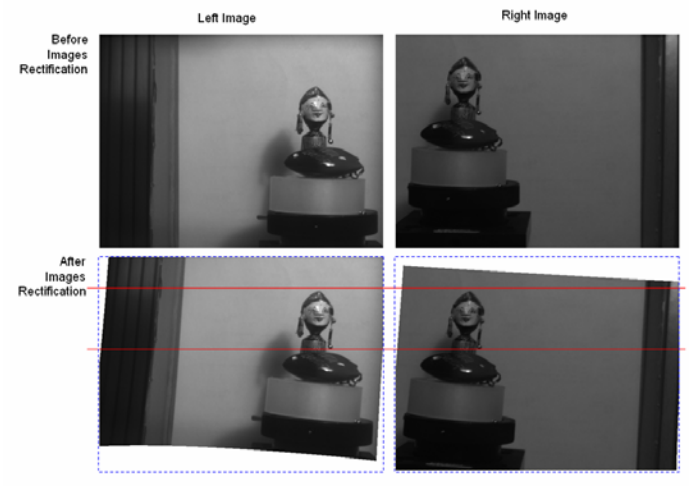

Figure 4.29 Two Stereo images taken before and after Rectification

4.3.2.4.3 Stereo Matching using Epipolar Geometry Constraints

In this research, the value of a matching metric is computed using a fixed template window in the reference image and shifting candidate window in the target image. The corresponding points between two images are found by searching for the point correspondence using shifting template window along an epipolar line.

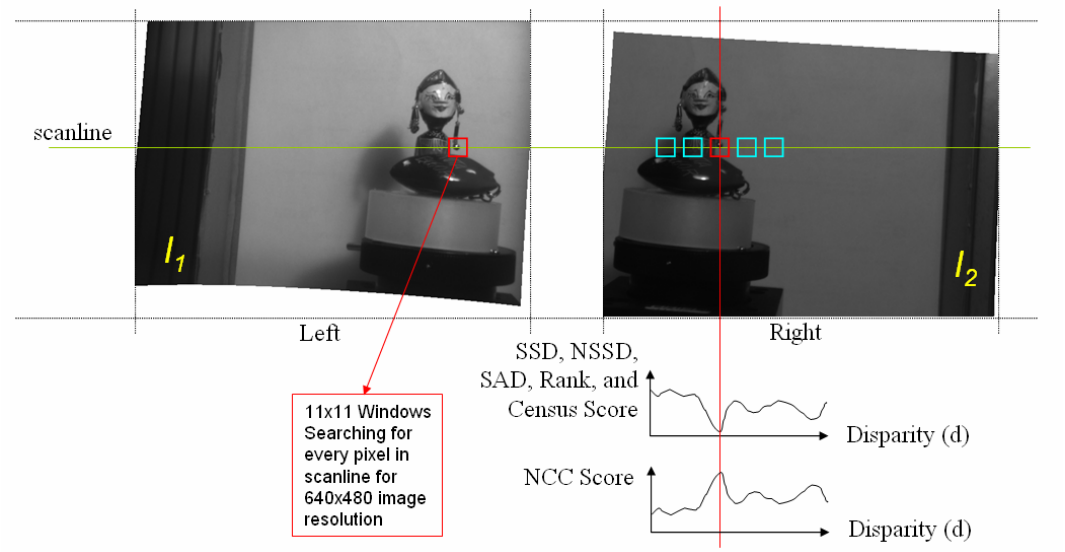

Figure 4.30 Score matching Provision for every pixel

4.3.2.5 Validation and Evaluation Measurement Stereo Matching Algorithm

Szeliski and Zabih [Szeliski and Zabih (1999)] proposed an experimental comparison of stereo matching algorithms using real images. They classified the validation and evaluation measurement of stereo matching in two groups, first based upon manual computation of dense ground truth and the second methodology uses the notation of prediction error.

Ground-truth is obtained from independent measurement. It is must be obtained by a method which is more accurate than the tested one (in this case is stereo vision), which is not always possible. In principle, the measurement of complicated scenes is still possible as long as their complexity does not prevent for obtaining an accurate ground truth model. In the computer vision literature, performance tests for stereo vision algorithms are usually performed with standard databases composed of static images, well-calibrated and acquired in uniform lighting. The web site of Scharstein and Szeliski [Scharstein and Szeliski (2008)] is a good reference for some stereo images and for comparing some stereovision algorithms.

A well-known method based on prediction error is RANSAC. This method can be use to reject inconsistent matches, called outlier, and only accept the inliers as a points that have correct matches in the input image.

4.3.2.5.1 Random Sampling Consensus (RANSAC)

In regression problem with samples contaminated with outliers, RANSAC (Random Sampling Consensus) [Fischler and Bolles (1981)], [Choi et al. (2009)] is a popular technique. The RANSAC considers the features that do not fit the current geometric model as outliers and eliminates them in an iterative manner and the geometric model is estimated again on the basis of newly identified inliers. RANSAC is applied to make sure that the points found in the second image are in the correct positions. Different from similar techniques that found in the previous researches such as Hough transform or M-estimator, RANSAC does not need high amounts in memory usage to keep parameter space alike Hough transform or use a complex optimization alike M-estimator. RANSAC is simple iteration of two steps: hypothesis generation and hypothesis verification. The

RANSAC algorithm is used here because of its applications in the computations of parameters for several models required for feature extraction and correspondence point in stereo vision in epipolar geometry.

In RANSAC algorithm, to deal with any sample of data that may have a number of outliers that do not correspond to the referred model, the classification of data into inliers and outliers is done with estimating the parameters of the model repeatedly with combinations of (n-x) elements and keeping track of how many points agree with each of these models (where a set of n data points, and number of outliers x). The *set of consensus* or accepted points with a model are those that are within a threshold of the model (calculated using a Euclidian distance).

RANSAC algorithm :

1. A sample of s data points from S, randomly select and initiate the model from this subset
2. Determine the set of data points Si, which are within a distance threshold t of the model. The set Si is the consensus set of the sample and defines the inliers of S.
3. If the size of Si is greater than some threshold T, re-estimate the model using all the points in Si and terminate.
4. If the size of Si is less than T, select a new subset and repeat the above.
5. After N trials the largest consensus set Si is selected and the model is re-estimated using all the points in the subset Si

Adapted from Hartley [Hartley and Zisserman (2000)]

This method involves certain minimum number selection of randomly sampled data elements. Then the parameters of the model are estimated using these elements. The number of elements accepted in a set of consensus is noted by counting how many points are within the threshold, it is called the support for estimated model step. The process of random selection, parameter estimates and support computation step is repeated several times and the model with the most support (have the largest consensus set) is selected. The Current model parameters then are estimated again, but with all the elements

obtained from the previous consensus that has been selected. This final model is the output of the RANSAC algorithm.

4.3.2.6 Choosing Local Matching method for Polarized Images

4.3.2.6.1 Imaging Installation and Object Test

Two units of AVT Guppy camera (F-080B monochrome camera) are installed to get stereo images on the baseline. In front of the stereo cameras, we setup an optical device such as a polarizer with different orientation values, the first polarizer (pol1right) is set at 45° for the right camera and, the liquid crystal (LC) polarizer (pol1left) is used to create automated image capture with different alpha values 0° and 90° for the left camera. We also install another polarizer rotator (pol2) to imply various polarization states at the entrance of the system (Table 4-4).

Table 4-4 Polarizer Setup for Local Matching Test Scenes

Images Scene	**Polarizer setting (degree)**		
	Pol1 Liquid Crystal left Cam	***Pol1 Right Cam***	***Pol2 All cam incoming***
1	0	45	0
	90	45	0
2	0	45	10
	90	45	10
3	0	45	20
	90	45	20
4	0	45	30
	90	45	30
5	0	45	45
	90	45	45

The processing was carried out only on polarized images with a linear polarisation, of 0°, 10°, 20°, 30°, 45°. Then, to obtain a good stereo matching results, coresponding points were calculated on the intensity image (I0+I90)/2 for the left, image and I45 image in the right image.

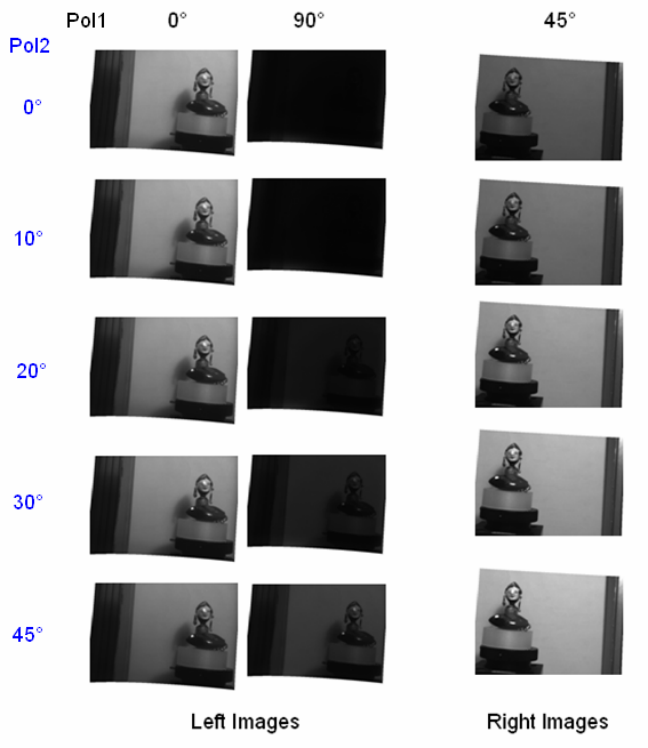

Figure 4.31 Polarized Image sources

The evaluation of the stereo matching algorithms is done by comparing the sum of the absolute differences between the matching results for each algorithm and the ground truth. For each image, we calculate the absolute differences in all image pairs then compare it with the ground truth extracted with the SIFT detector.

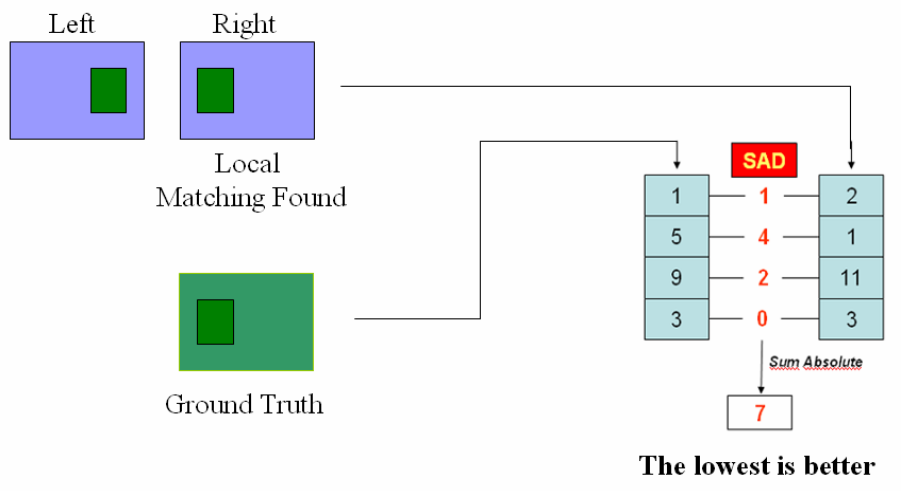

Figure 4.32 Evaluation of the matching Score Algorithm

4.3.2.6.2 Test Result

Table 4-5 below represents the results of the evaluation of the matching algorithm applied to images with a variety of polarized incident light scene.

Table 4-5 Mean of SAD Error Result for Six Matching Algorithm For Each Scenes Incident Light (0°,10°,20°,30°,45°) – Lowest is the best

Matching Cost	0°	10°	20°	30°	45°
NSSD	24.3995	23.7455	16.3755	17.419	18.998
SSD	46.3375	37.7695	27.75	31.7645	48.7465
SAD	41.7585	35.1755	25.6105	29.0845	44.004
Rank	24.1925	26.147	23.6615	22.965	23.234
Census	25.0885	26.1345	16.658	16.7345	19.132
NCC	27.5605	27.5655	22.463	21.024	21.5435

The comparison in graphical form can be seen in Figure 4.33.

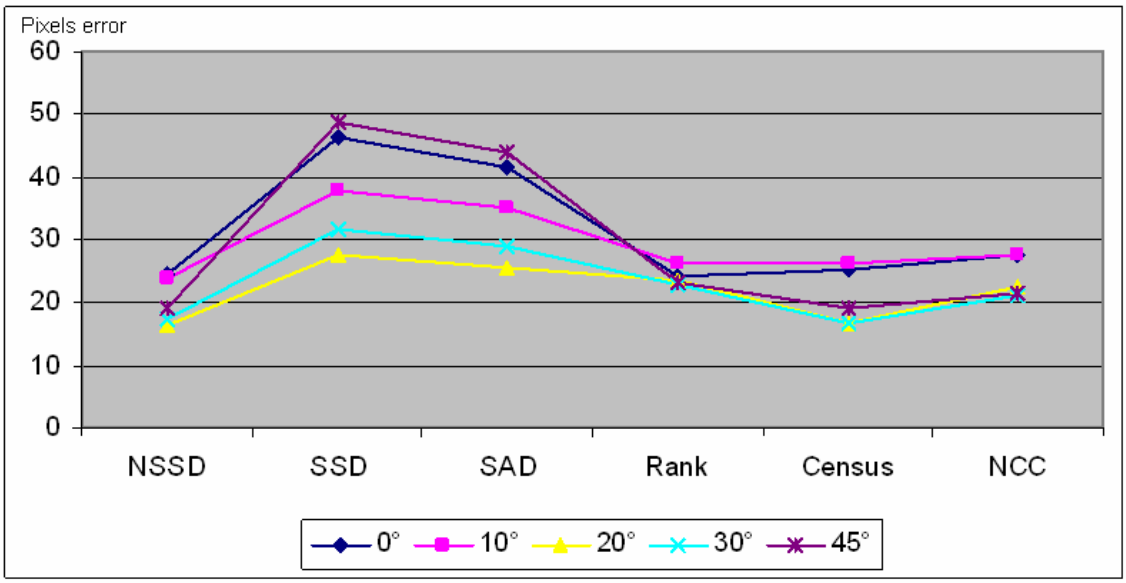

Figure 4.33 Graphics representation for Matching Result 6 Local Algorithm for 5 Incoming Polarized Light Conditions

There are interesting results that can be observed here, for the condition of pol2 with orientations at 20° and 30°, this imaging system has the ability to detect the smallest errors from others. This can be explained as follows, when light passes from pol2 with orientation 0° into pol1, then one of the polarizers in the left with orientation 90° block it, this situation also occurs for the light that passes through pol2 with orientation 45°. From six local matching methods then we find that the NSSD provides a smaller error than the other methods and was selected for the rest of this work.

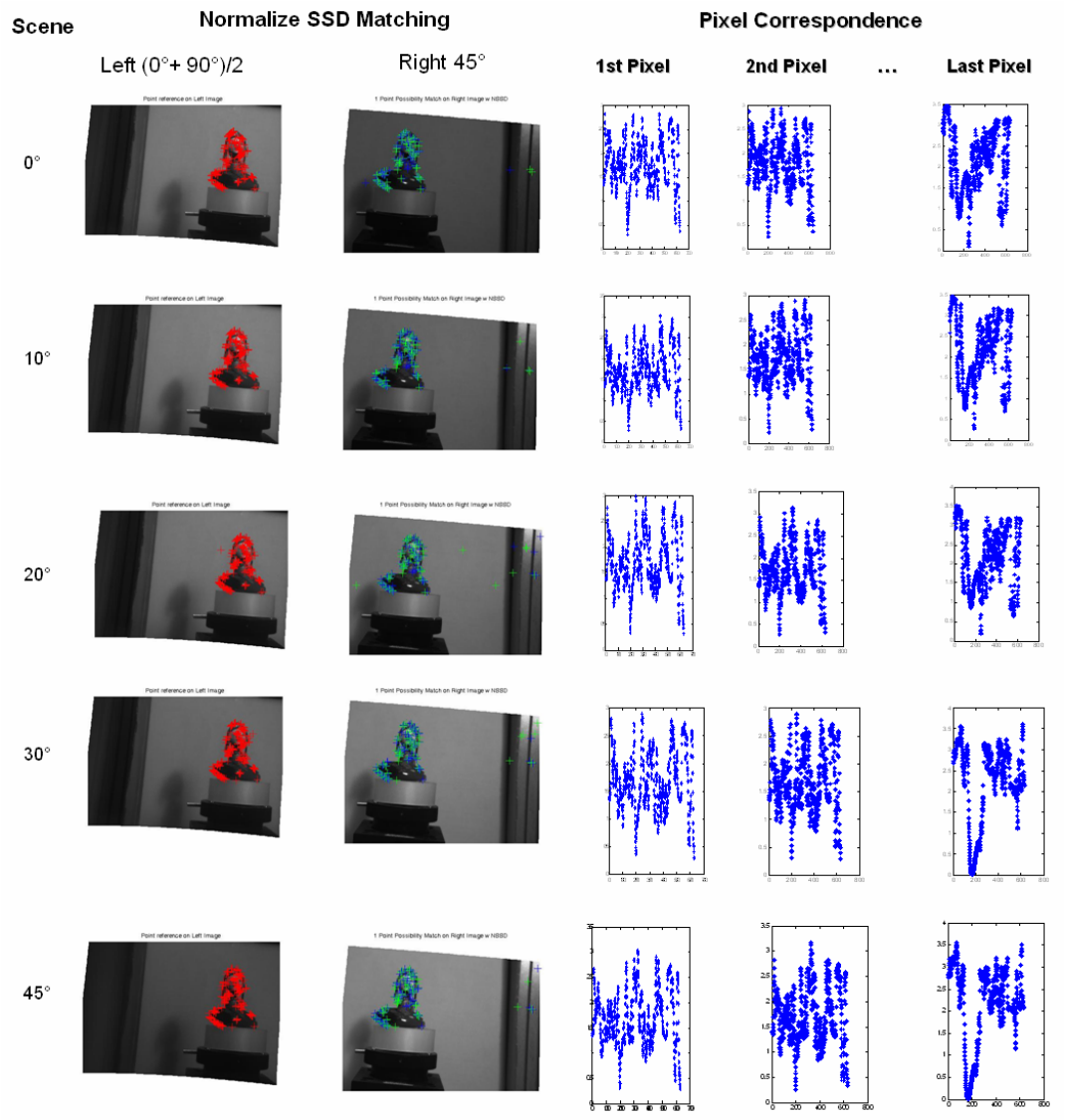

Figure 4.34 Detail Visualization Normalized SSD Matching Score for all Scenes, the pixels with low score is the best match.

4.4 Extract Polarization component

In this work, the polarization information are extracted from each pixel selected after the matching algorithm. The imaging setup is installed as presented in Figure 4.1, where the liquid crystal polarizer (LC) filter in the left camera has two states (0° and 90°) and so on in the right camera (at 0° and 45°). In front of the LC filter are installed other filters to generate a known polarized input image with certain angle of polarization at 0°, 10°, 20°, 30° and 45°. Image acquisitions are performed on each angle of the polarization for each state of liquid crystal for the right and the left camera. Acquisition performed in two sequences, in which the first acquisition is performed for left and right LC polarizer status at 0° and 0° respectively, and the second acquisition is for left and right LC polarizer status at 90° and 45° respectively.

The matching stereo step consists of three stages, namely feature detector, stereo matching and removal of the outliers. The feature descriptor SIFT [Lowe (2004)] is used as input for the matching process. Stereo correspondence points are found using local methods by looking the most similar matches based on local image properties in predefined neighbourhood window. Two sequences inputs from left image and right image are compared by local matching score algorithm Normalized SSD (Sum of Squared Differences). Regarding the matching results, this algorithm performs better for polarized images than the other local matching algorithms (NCC, SSD, SAD, census, rank) [Iqbal et al. (2010a)]. Once the point matches were computed, outliers were removed using RANSAC method [Fischler and Bolles (1981)]. This approach fits a fundamental matrix to a set of matched image points.

4.4.1 *The Technique of Polarization Component Extraction*

A basic but efficient technique to obtain the state of polarization of incident light is to capture three different intensity images through a set of polarization filters. If I0, I45 and I90 are a representation of the image intensity measurements taken at an angle of polarizer of 0°, 45° and 90°, the angle of polarization (φ), the degree of polarization (ρ) and the intensity (I_{tot}) can be obtained based on the basics equations of polarization imaging as described in chapter 2 equation (2.41).

From the three different direction of the polarizer (0°, 45° and 90°), the three equation can be obtained:

$$\begin{aligned} I_0 &= \frac{I_{tot}}{2}(1+\rho\cos 2\varphi) \\ I_{45} &= \frac{I_{tot}}{2}(1+\rho\sin 2\varphi) \\ I_{90} &= \frac{I_{tot}}{2}(1-\rho\cos 2\varphi) \end{aligned} \tag{4.24}$$

By combining these three equations, we can obtain:

$$I_{tot} = I_0 + I_{90} \tag{4.25}$$

$$\varphi = a\tan\left(\frac{1-\frac{2I_{45}}{I_{tot}}}{1-\frac{2I_{90}}{I_{tot}}}\right)/2 \tag{4.26}$$

$$\rho = \frac{1-\frac{2I_{45}}{I_{tot}}}{\sin\left(a\tan\left(\frac{1-\frac{2I_{45}}{I_{tot}}}{1-\frac{2I_{90}}{I_{tot}}}\right)\right)} \tag{4.27}$$

In our setup, the polarization state estimated is only performed at the pixels which were found by the matching algorithm described in the previous step. For two matching point, we obtain four values that can be written according equation (2.40):

$$\begin{cases} I_0^{left} = \frac{1}{2}(S_0 + S_1\cos 2\alpha_0^{left} + S_2\sin 2\alpha_0^{left}) \\ I_{90}^{left} = \frac{1}{2}(S_0 + S_1\cos 2\alpha_{90}^{left} + S_2\sin 2\alpha_{90}^{left}) \\ I_0^{right} = \frac{1}{2}(S_0 + S_1\cos 2\alpha_0^{right} + S_2\sin 2\alpha_0^{right}) \\ I_{45}^{right} = \frac{1}{2}(S_0 + S_1\cos 2\alpha_{45}^{right} + S_2\sin 2\alpha_{45}^{right}) \end{cases} \tag{4.28}$$

Where α_0^{left}, α_{90}^{left}, α_0^{right} and α_{45}^{right} are obtained according to the polarization calibration process described in 4.2.2. The Least Mean Square method can be applied for estimate S_0, S_1 and S_2.

$$\underbrace{\begin{pmatrix} 2I_0^{left} \\ 2I_{90}^{left} \\ 2I_0^{right} \\ 2I_{45}^{right} \end{pmatrix}}_{y} = \underbrace{\begin{pmatrix} 1 & \cos 2\alpha_0^{left} & \sin 2\alpha_0^{left} \\ 1 & \cos 2\alpha_{90}^{left} & \sin 2\alpha_{90}^{left} \\ 1 & \cos 2\alpha_0^{right} & \sin 2\alpha_0^{right} \\ 1 & \cos 2\alpha_{45}^{right} & \sin 2\alpha_{45}^{right} \end{pmatrix}}_{H} \underbrace{\begin{pmatrix} S_0 \\ S_1 \\ S_2 \end{pmatrix}}_{x} \tag{4.29}$$

x can be produced by:

$$x = (M^t M)^{-1} M^t y \tag{4.30}$$

I_{tot} is equal to S_0 and from the equation (2.24) and equation (2.26) we can derived ρ and φ from S_0, S_1 and S_2.

4.4.2 *Experimental Result*

In this section, a quantitative comparison between theoretical predictions with the real observation set has been performed. The first step is to validate that the angle of polarization found by the proposed system is the correct angle of polarization in nature. Secondly, choosing a "polarizer intensity" to accommodate stereo matching computation, for enhanced a matching result.

4.4.2.1 Validating Angle of Polarization Information

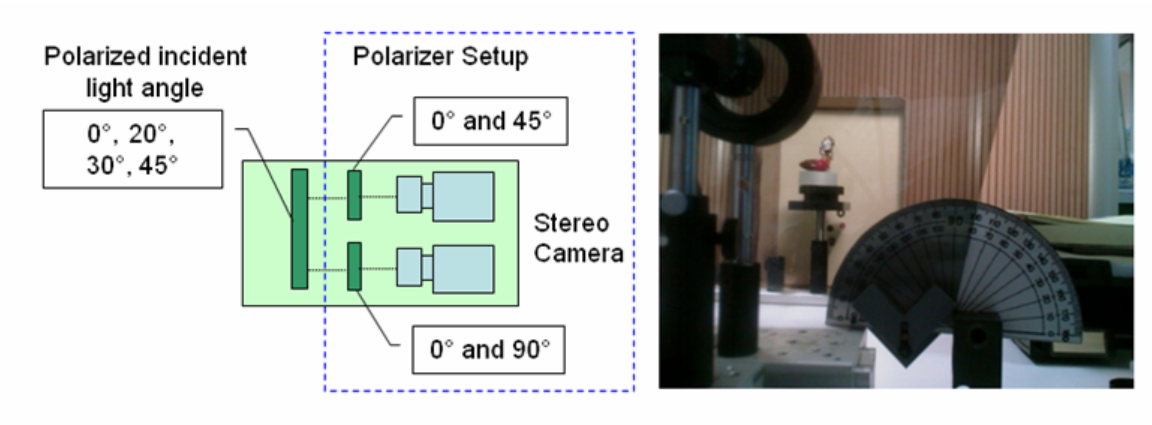

Figure 4.35 Validating Angle of Polarization Result

In this work, we use an Indonesian traditional puppet called "wayang" as the object. To ensure the calculation of the polarization state of the light is correct, we set the polarized incident light condition with a known angle. This step can be achieved by

inserting a polarizer in front of the setup system (see Figure 4.35). Four set conditions of incident light (0°, 20°, 30°, 45°) were used and compared with the angle of Polarization obtained with our method.

Table 4-6 Average Results of Polarization Information for each scenes Incident Light (0°,20°,30°,45°)

Incident Light angle	**Average result Angle of Pol**	**Absolute Differences of Angle of Pol ($\|d\|$)**
0°	2.16	2.16
20°	16.05	3.95
30°	26.62	3.38
45°	39.70	5.3
	$\sqrt{\sum \|d\|}$	3.85

Table 4-6 presents an average result from computation when extracting the angle of polarization with our system obtained from each pixel found by our matching algorithm, compared to the incident polarized light angle. This experiment shows that the calculated angles are not precise and that our system setup still requires improving in the quality of stereo matching result, in which has direct influence on increasing the quality of the polarization information result.

4.4.2.2 Choosing Polarizer Angle Combination To Enhance Stereo Matching Result

The aim of this part is to find the best combination of our imaging system that can improve the quality of the stereo matching result.

Table 4-7 Combination Polarization Intensity for Input Imaging System

Setup	**Left camera**	**Right Camera**
Data 1	I0	I0
Data 2	(I0+ I90) / 2	I0
Data 3	(I0+ I90) / 2	I45
Data 4	(I0+ I90) / 2	(I0+ I45) / 2

Table 4-7 shows the various combinations which were used and Figure 4.36 presents the 5 objects which were observed by our system.

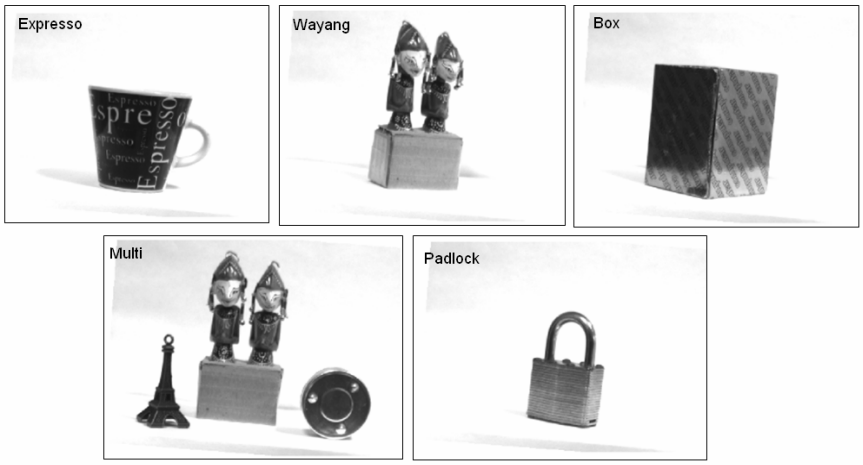

Figure 4.36 Test Object for Enhance Stereo Matching result

In Figure 4.37, for all class combination of polarization intensity (Data 1-4), our imaging setup gives a good results for the object with complex scene (multi). Good result is generated if we can increase the number of correct matching points. We found that for the two objects, the results obtained with the object with complex pattern such as "*wayang*" gave good results, however the object with simple pattern (not enough texture) such as padlock gave rather low result.

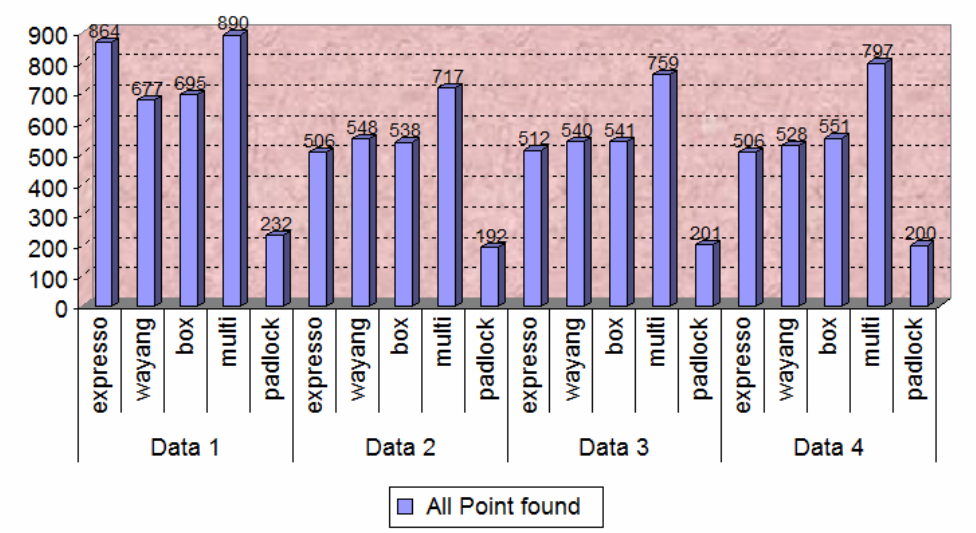

Figure 4.37 All point found in all scenes (0°, 20°, 30°, 45°) of incident light in various data class object.

The distribution of matching points as a function of the angle of polarization can be seen in Table 4-8. Column 0-15 denotes the number of matching points found near to their correct angle of polarization (0 meaning correct angle and 15 meaning at a position difference of 15 pixels from the correct angle). Similar results were obtained for the various combinations of incoming polarizations, with a point distribution close to the expected one. As expected, the class data 1 gives the best result, but it only can be use for incident polarizer angle other than 90°. Data 4 give less point found than Data 1, but can be use for all condition polarized incoming light.

Table 4-8 Distribution of matching points result, mean of Angle of polarization and square root of sum absolute differences of Angle of Polarization for ($\sqrt{\sum|d|}$) each scenes Incident Light (0°,20°,30°,45°) on Polarizer Class data 1 – data 4

Polarizer Class	Scenes	Mean of AoP	$\sqrt{\sum\|d\|}$	Point Found Distribution		
				0-15	16-30	31-45
data 1	0	0.3	2.8	550	61	1
	20	17.9		528	52	0
	30	25.6		505	120	1
	45	45.9		431	30	31
data 2	0	0.6	2.4	405	24	0
	20	18		445	44	0
	30	26.7		424	86	1
	45	44.9		419	41	37
data 3	0	0.7	2.8	438	39	1
	20	18		420	37	0
	30	25.6		409	100	1
	45	45.6		427	33	34
data 4	0	0.7	2.3	441	38	1
	20	19		426	31	0
	30	26.2		417	86	2
	45	45		439	36	44

4.4.2.3 Multiple Orientation Filter in One Scene

In nature, the light reflected from real objects would have many variations in orientations. Therefore, we carried out experiments to show how our setup has the ability to capture the variations of incident light and extract the polarization information with the

proper orientation and use it for further processing such as segmentation or object identification.

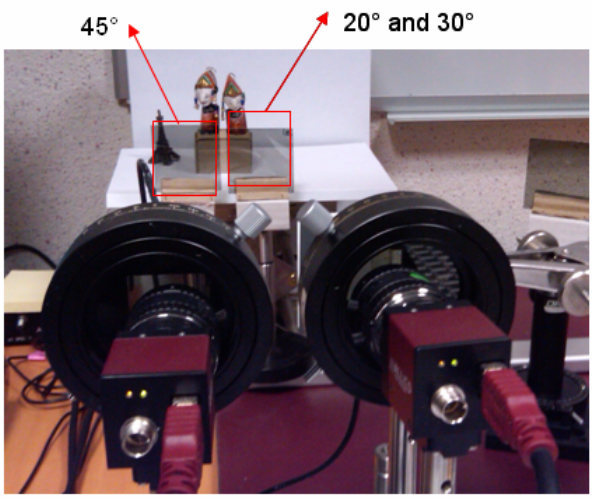

Figure 4.38 Multi Orientation Filter Setup

Experiments were realized by adding a polarizer sheet with a known angle of 20°, 30° and 45° between the scene and the imaging system. The first step is to capture images of a scene for which the reflection is different, we chose a combination of polarizers set at 20°, 30° and 45°. The next step is to analyze and visualize the results to see the accuracy of the polarization angle of that multi-orientation filters.

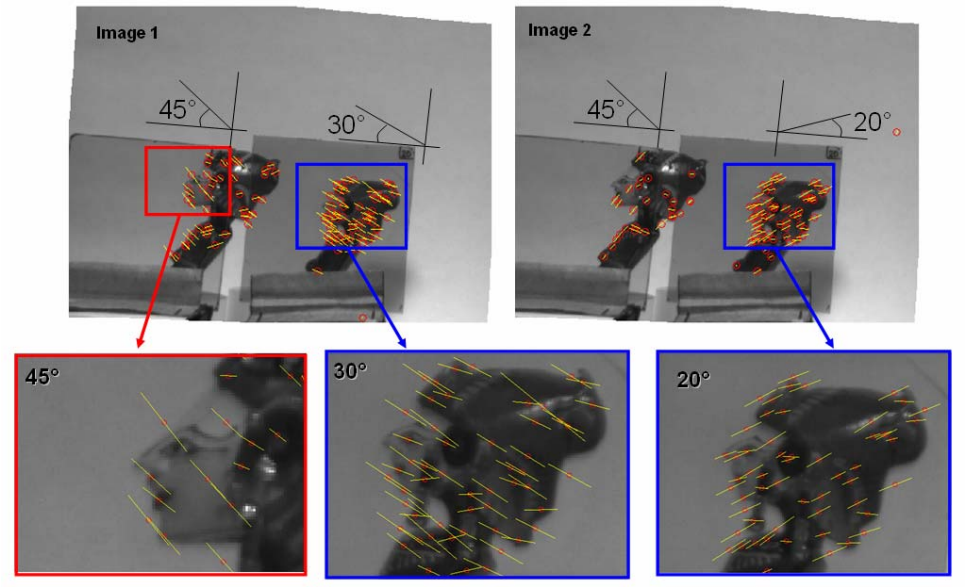

Figure 4.39 Angle of Polarization result with Multi Orientation Filter

Visually, the algorithm is able to extract the polarization state in accordance with the actual situation (see Figure 4.39 and Figure 4.40).

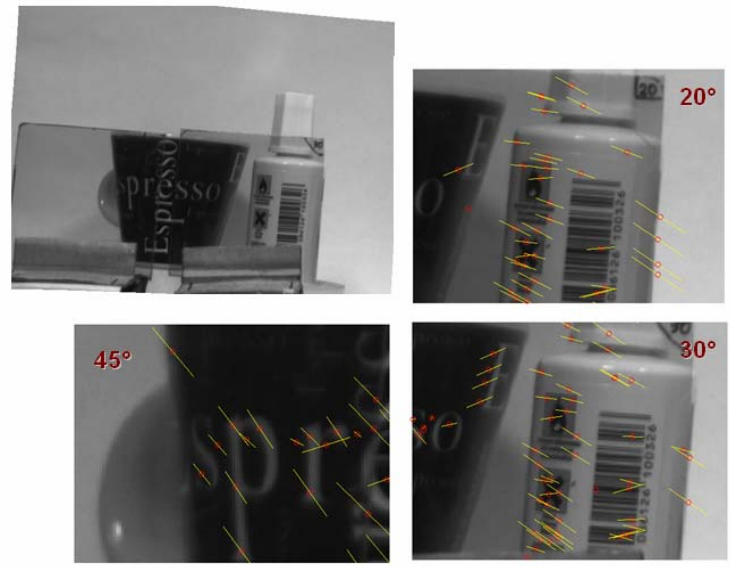

Figure 4.40 Angle of Polarization result with Multi Orientation Filter with other object

4.5 Triangulation and Recovery of 3D Coordinates

Unlike what was presented in the calibration part, this section, present the "reverse" problem which consists in computing the location of the 3D points from their projections ml and mr in the 2D image planes. The relative position and orientation (intrinsic and extrinsic camera parameters) of the two cameras are known from calibration, then 3D position of a point M (X,Y,Z), can be reconstructed from the perspective projection on the image planes of the cameras by the basic triangulation technique.

Triangulation works under the assumption that the world point M lies at the intersection of the two rays from C_L through m_L and from C_R through m_R, where points m_L and m_R (point in image plane left and right respectively) represent the same point M in the real world. So, an algorithm for matching these two points must be performed because the accuracy is highly dependent on the exact matching of two images point.

The reconstruction of the projection matrix is dependent on the calibration method that was used, in our study we are using the Tsai model, where the projection matrix *P* derived in 4 x 4 matrix, then the 3D projection point (X,Y,Z,1) becomes:

$$\begin{pmatrix} x_i \\ y_i \\ z_i \\ w_i \end{pmatrix} = \begin{bmatrix} \quad & P & \quad \end{bmatrix} \begin{pmatrix} X \\ Y \\ Z \\ 1 \end{pmatrix} \tag{4.31}$$

In Tsai model, the homogeneous image coordinates that have two additional scaling factors, z_i and w_i, then the pixel coordinate (x,y) is recovered by:

$$(x, y) = \left(\frac{x_i}{z_i}, \frac{y_i}{z_i} \right) \tag{4.32}$$

If we include equation (4.32), into equation (4.31), then:

$$\begin{pmatrix} x.z_i \\ y.z_i \\ z_i \\ w_i \end{pmatrix} = \begin{bmatrix} P_{11} & P_{12} & P_{13} & P_{14} \\ P_{21} & P_{22} & P_{23} & P_{24} \\ P_{31} & P_{32} & P_{33} & P_{34} \\ P_{41} & P_{42} & P_{43} & P_{44} \end{bmatrix} \begin{pmatrix} X \\ Y \\ Z \\ 1 \end{pmatrix} \tag{4.33}$$

This equation can be rearranged in the following equation:

$$\begin{pmatrix} -P_{14} \\ -P_{24} \\ -P_{34} \\ P_{44} \end{pmatrix} = \begin{bmatrix} P_{11} & P_{12} & P_{13} & -x & 0 \\ P_{21} & P_{22} & P_{23} & -y & 0 \\ P_{31} & P_{32} & P_{33} & -1 & 0 \\ P_{41} & P_{42} & P_{43} & 0 & -1 \end{bmatrix} \begin{pmatrix} X \\ Y \\ Z \\ z_i \\ w_i \end{pmatrix} \tag{4.34}$$

At this stage, equation (4.34) still can not be computed because there are only 4 equations with 5 unknown. If we consider pixel coordinate (x_R, y_R) from right image and (x_L, y_L) from left image that have a projection to the same 3D world point and either pixel coordinate obtained from computation by NSSD matching algorithm. Let the camera projection matrix of the left image and the right image be *PL* and *PR* respectively, then

$$\begin{pmatrix} -PL_{14} \\ -PL_{24} \\ -PL_{34} \\ -PL_{44} \\ -PR_{14} \\ -PR_{24} \\ -PR_{34} \\ -PR_{44} \end{pmatrix} = \begin{bmatrix} PL_{11} & PL_{12} & PL_{13} & -x_L & 0 & 0 & 0 \\ PL_{21} & PL_{22} & PL_{23} & -y_L & 0 & 0 & 0 \\ PL_{31} & PL_{32} & PL_{33} & -1 & 0 & 0 & 0 \\ PL_{41} & PL_{42} & PL_{43} & 0 & -1 & 0 & 0 \\ PR_{11} & PR_{12} & PR_{13} & 0 & 0 & -x_R & 0 \\ PR_{21} & PR_{22} & PR_{23} & 0 & 0 & -y_R & 0 \\ PR_{31} & PR_{32} & PR_{33} & 0 & 0 & -1 & 0 \\ PR_{41} & PR_{42} & PR_{43} & 0 & 0 & 0 & -1 \end{bmatrix} \begin{pmatrix} X \\ Y \\ Z \\ z_{Li} \\ w_{Li} \\ z_{Ri} \\ w_{Ri} \end{pmatrix} \tag{4.35}$$

Now we have two projections of the same 3D point (there are 8 equations with 7 unknown). The 3D projection point (X,Y,Z,1) can be recovered using least squares technique applied to equation (4.35).

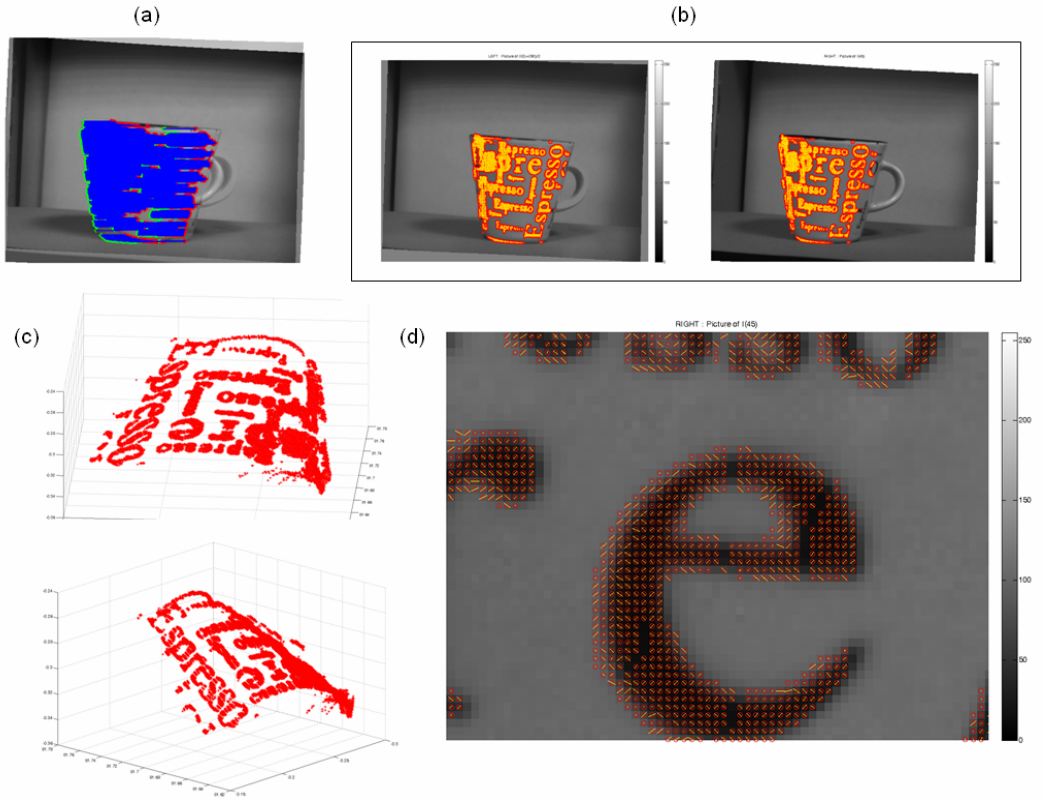

Figure 4.41 3D Reconstruction result and Angle of Polarization Extraction for all pixel matching, (a) Overlay inlier RANSAC result, (b) and (d) visualization of angle of polarization in left and right camera and zoom view of right camera (c) 3D reconstruction result.

In the first experiment, to observe the performance of our triangulation algorithm, we tried to extract all points in the stereo images rather than using a feature detector algorithm. All points from the left and right image are matches using NSSD algorithm, then the results are validated using RANSAC to eliminate outliers. After extracting polarization information, a 3D reconstruction computation is performs. The result can be seen in Figure 4.41.

Visually, the results are satisfying. The next experiment is based-on using a SIFT feature detector before the matching step and using a class of image data that gave the best results to improve the matching result (class data 1 - explained in 4.4.2.2). Then, the system is tested for 5 polarizer scenes (0°, 10°,20°, 30° and 45°). Reconstruction results can be seen from Figure 4.42 to Figure 4.46.

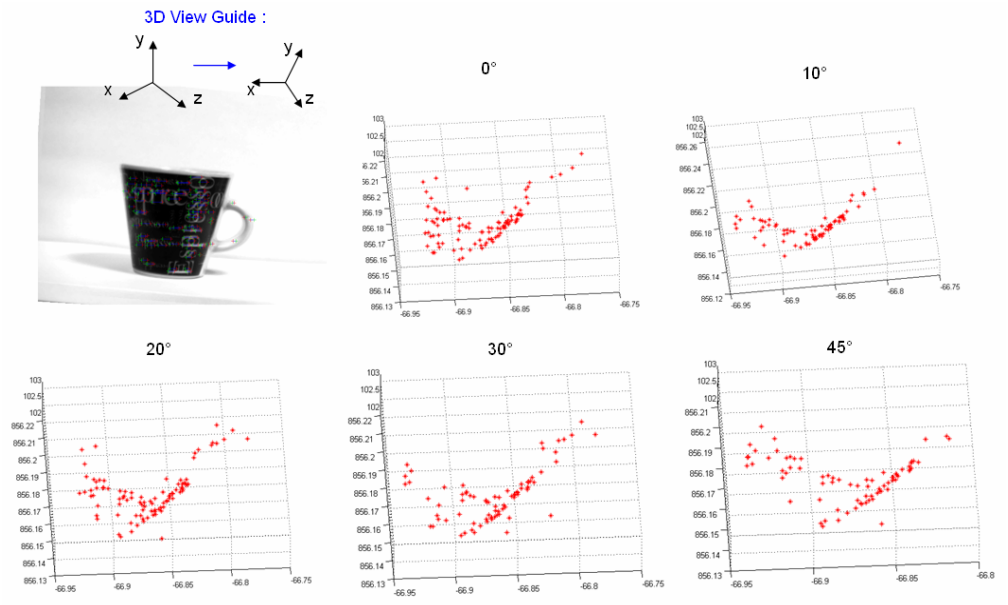

Figure 4.42 3D Reconstruction result Scene 1 with different polarizer orientation Scenes

For each of the reconstructed 3D scene, it appears that the condition of incoming lights have direct impact to the result, for example the polarizer with orientation 0° giving more correct extracted points than others.

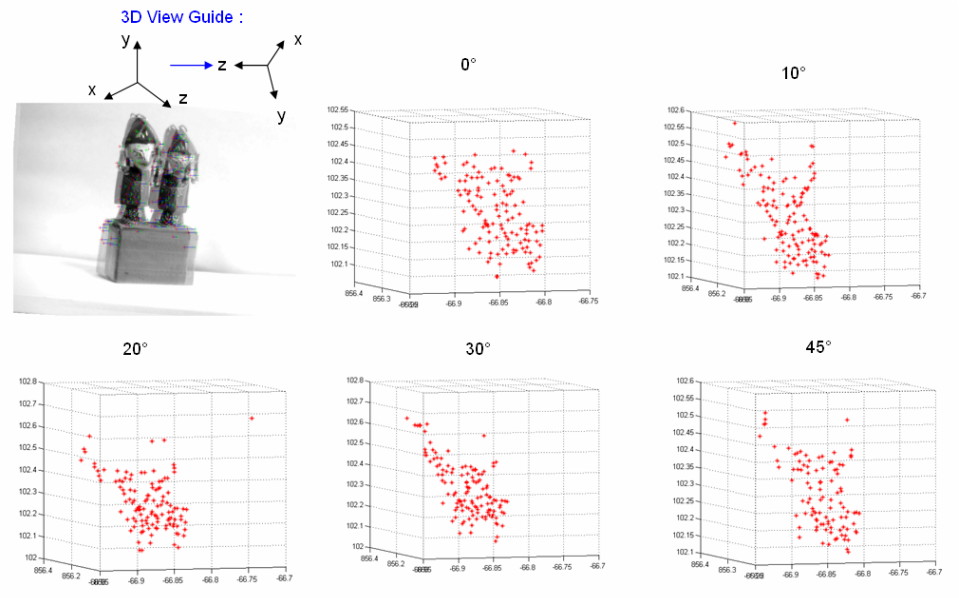

Figure 4.43 3D Reconstruction result Scene 2 with different polarizer orientation Scenes

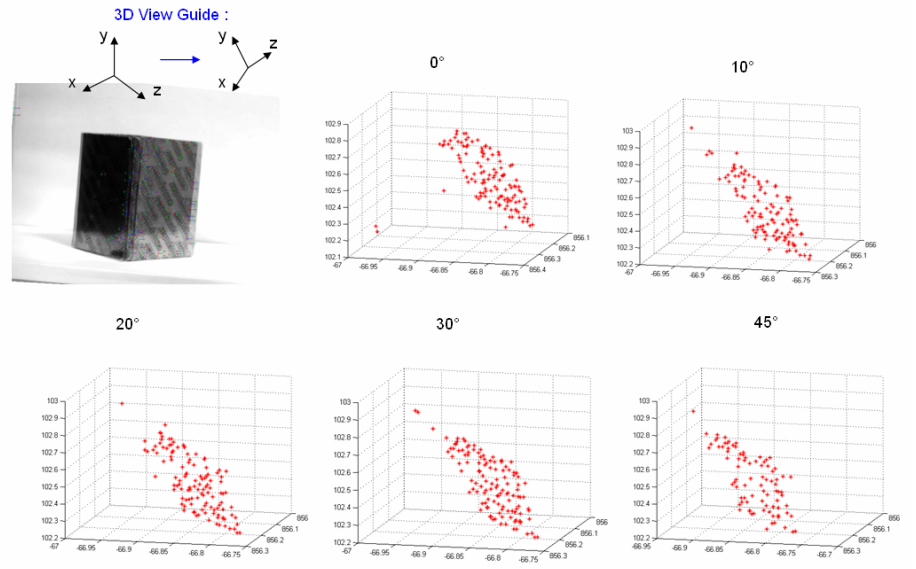

Figure 4.44 3D Reconstruction result Scene 3 with different polarizer orientation Scenes

Thus based on that, in our stereoscopic Polarization imaging system, we need distinguish a different approaches to use polarized images from acquisition, either for computation of 3D reconstruction and extract polarization information. In order to enhance quantity of reconstructed 3D point we use a polarizer pol1 with an orientation at 0° in both the left and on the right camera (class data 1 – in case we know there are not incident light in

90°) or class data 4 for all scenes of incident light. However, to extract the polarization we use polarized images 0° left, 0° right, 90° left and 45° right.

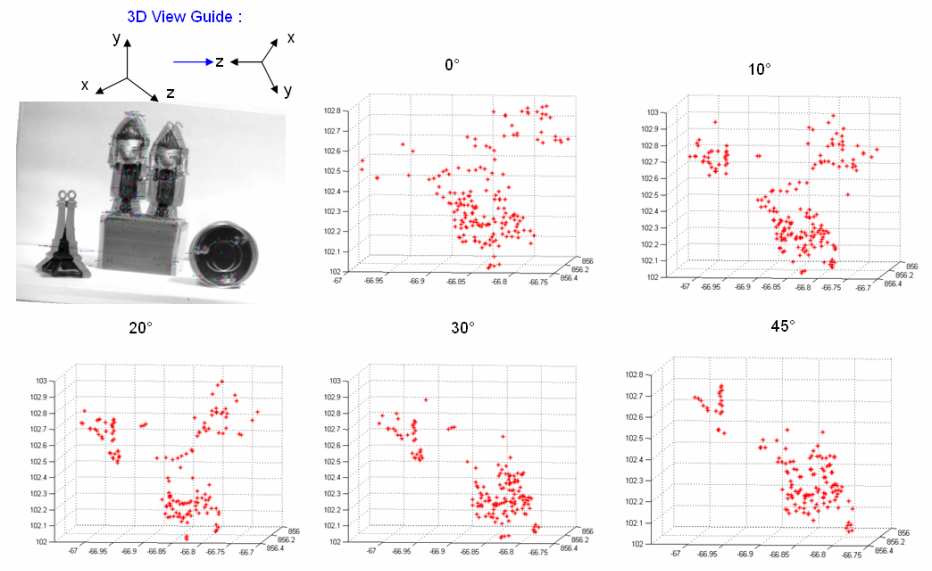

Figure 4.45 3D Reconstruction result Scene 4 with different polarizer orientation Scenes

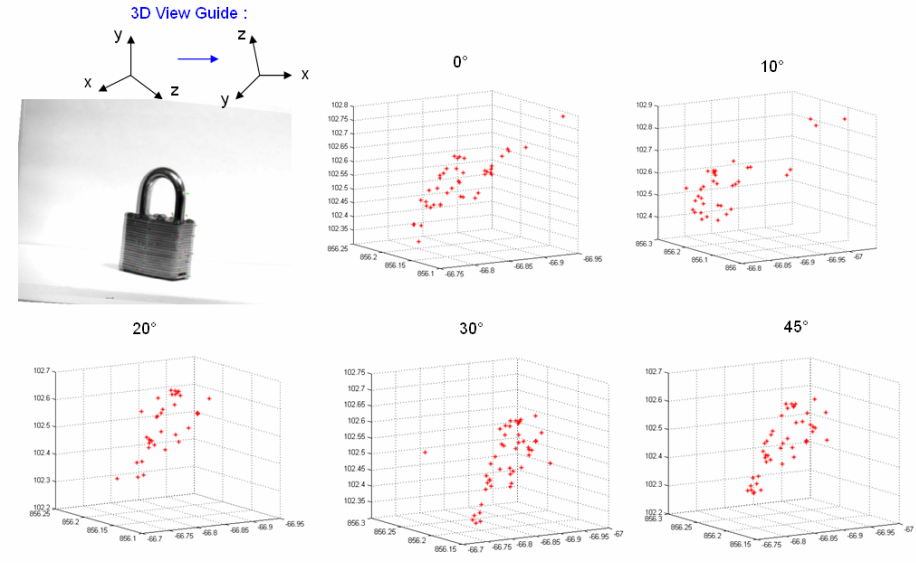

Figure 4.46 3D Reconstruction result Scene 5 with different polarizer orientation Scenes

Visually, the 3D reconstruction from our system can be performs. According to the presented result above, not all objects give a good result. This problem does not stem from our method, but in the type of materials / objects that have been used, because some

other experiment found the object that can give a good result. For current, we claimed that our method is good for 3D reconstruction based-on material select:

- If the material/object/shape have a complex pattern
- If the scenes have more texture

Other than that, the reconstructed 3D points still need to be increased in quantity.

4.6 Conclusion

The main advantage of this method is the simplicity of installation. The setup only takes two general CCD cameras with a liquid crystal polarizer rotator in front of each stereo camera. Each image is taken twice sequentially to get four polarized images (0° in left and right, 45° in right and 90° in left). The important issues to get the polarization component with accuracy, depends on the stereo point matching results from the extracted features in the previous step.

We have presented a simple but novel technique for extracting polarization state component from points correspondence using a pair of calibrated polarization cameras. Our stereo polarization system designed with liquid crystal polarizers in front of camera can capture 4 polarized images with different orientations (α) of the polarizer. Experiments show that our method gives good performance in complex background. However, to achieve the best results, the system components, including the active illumination source, have to be thoroughly calibrated.

Chapter 5
Conclusion and Perspectives

This chapter contains a summary and conclusions of the stereoscopic polarization imaging system research. It also provides some suggestions to improve the prototype and to extend applications to robotics.

5.1 Conclusion

In this work, a new stereoscopic imaging system sensitive to polarization has been developed. The aim was to propose a simple and low cost prototype that can be able to both have some stereoscopic capabilities and to measure the polarization parameters of light.

The thesis firstly reminds basis on polarization vision and introduces the scope and objectives of the work. Then, all the concepts related to polarization imaging were discussed in detail. After reminding the Stokes and Mueller Formalism used to design our set up, a state of art about the polarization imaging system is presented. In robotics or remote sensing, imaging systems have been restricted only to the radiance aspect of electromagnetic radiation. The importance of polarization measurements is finally recognized and the thesis describes some methods that can be used based on bio-inspired models. The key idea of our new system is to develop a simple stereovision system that has some polarization capabilities. Since, in nature the light can be partially lineraly polarized, the prototype has to measure only three parameters, light intensity, degree of polarization and angle of polarization. To get a quite simple system, two optical devices, based on liquid crystal, were placed in front of the two cameras. Therefore, the first and

the second camera can respectively measure the light intensity seen through a polarizer oriented at 0°-90°, and 0°- 45°. The acquisition step provides four images that must be combined to both enable an efficient matching of interest points and an appropriate estimation of the polarization state. The main contributions of this work can be sum up as:

- Polarization calibration: in addition to the geometric calibration process required in stereo vision, we developed a polarization calibration step to ensure that the angle of the liquid crystal polarizer is well estimated and to set the same reference for the two cameras. Moreover, since the extinction coefficients are slightly different a factor can be deduced to properly estimate the polarization parameters.
- Stereo Matching evaluation: the standard techniques of stereo-matching algorithms were studied in detailed to estimate their sensitivity to the polarization effects. Different scenarios were created to choose the one that is less sensitive to this phenomenon. In addition, an optimized combination of the four images has been set up.
- Stereopolarization Prototype: the system was developed and tested on various real scenes. It shows how polarization estimation can be applied for the 3D points that match.

5.2 Perspective

In this work, the following strong assumption was made: the based line between the two cameras is relatively short regarding the distance between the system and the scene. Therefore, the images from the two cameras can be directly combined to get the polarization state of the light reflected by the object. For close objects this assumption is not valid since it means that the polarization state of the light reflected by an object can be seen as an isotropic phenomenon. The shape from polarization methods show that the polarization parameters depend on the incidence angle and consequently on the reflection angle. Our proposed technique can be improved by including an estimation of the object normals after the 3D reconstruction in order to adjust the polarization parameter computation.

Another improvement can be done for the matching process. Indeed, since there is a sinusoidal relationship between the light intensity measured by the cameras for the four angles, some matching algorithm can be improved and adapted to the presented problem. For the methods based on feature extraction, the parameters can be enriched by the polarization information to get better scores during the matching process. In addition, methods such as Speeded Up Robust Features (SURF) [Bay et al. (2008)] or extended SIFT method can be investigated.

Finally, applications in robotics of such a "stereo-polarization" system must be fully investigated since the polarization sensitivity provides useful information for various tasks. For instance, it can be used as a sky compass in aerial robotics to estimate the pose of the robot. For autonomous terrestrial robots, one can apply polarization vision to detect reflecting surfaces such as water to avoid strong damages.

This work has published in three international conferences ([Iqbal et al. (2009)], [Iqbal et al. (2010a)], [Iqbal et al. (2010b)]) and published in an International Journal by SERSC (Science & Engineering Research Support Society) [Iqbal et al. (2011)].

References

[Ahmad and Takakura (2007)] J. Ahmad and Y. Takakura. Improving segmentation maps using polarization imaging. In *Image Processing, 2007. ICIP 2007. IEEE International Conference*, volume 1, pages I –281 –I –284, 16 2007-oct. 19 2007.

[Ainouz et al. (2006)] S. Ainouz, J. Zallat, and A. d. Martino. Clustering and colour preview of polarization-encoded images. In *14th European Signal Processing Conference (EUSIPCO 2006)*, Florence, Italy, September 2006.

[Ainouz et al. (2008)] S. Ainouz, O. Morel, and F. Meriaudeau. Geometric-based segmentation of polarization-encoded images. *Signal-Image Technologies and Internet-Based System, International IEEE Conference on*, 0: 375–381, 2008.

[Andreou and Kalayjian (2002)] A. Andreou and Z. Kalayjian. Polarization imaging: principles and integrated polarimeters. *Sensors Journal, IEEE*, 2 (6): 566 – 576, dec 2002. ISSN 1530-437X.

[Arcoptix (2009)] T. Arcoptix. Overview liquid crystal for polarization imaging. Website product Information, May 2009. URL http://www.arcoptix.ch/-Polarization_products.htm.

[Atkinson and Hancock (2005)] G. Atkinson and E. Hancock. Multi-view surface reconstruction using polarization. In *Computer Vision, 2005. ICCV 2005. Tenth IEEE International Conference on*, volume 1, pages 309 – 316 Vol. 1, oct. 2005.

[Atkinson and Hancock (2007)] G. Atkinson and E. Hancock. Shape estimation using polarization and shading from two views. *Pattern Analysis and Machine Intelligence, IEEE Transactions on*, 29 (11): 2001 –2017, nov. 2007. ISSN 0162-8828.

[Banks et al. (1997)] J. E. Banks, M. Bennamoun, K. Kubik, and P. Corke. A taxonomy of image matching techniques for stereo vision. Technical report, Queensland

University of Technology, Brisbane, Brisbane, 1997. URL http://eprints.qut.edu.au/40202/.

[Barta and Horváth (2004)] A. Barta and G. Horváth. Why is it advantageous for animals to detect celestial polarization in the ultraviolet? skylight polarization under clouds and canopies is strongest in the uv. *Journal of Theorical Biology*, 226 (4): 429–437, 2004.

[Bay et al. (2008)] H. Bay, A. Ess, T. Tuytelaars, and L. Van Gool. Surf: Speeded up robust features. *Computer Vision and Image Understanding (CVIU)*, 110 (3): 346–359, September 2008.

[Bensinger (1981)] C. Bensinger. *The Video Guide Second Edition*. Video-info publication, 1981. URL http://videopreservation.conservation-us.org/vid_guide/-front/front.html.

[Bobick and Intille (1999)] A. F. Bobick and S. S. Intille. Large occlusion stereo. *International Journal on Computer Vision (IJCV)*, 33 (3): 181–200, 1999.

[Bossanovatech (2010a)] T. Bossanovatech. Overview polarization camera ; bossanova salsa. Website product Information, February 2010. URL http://-www.bossanovatech.com/salsa.htm.

[Bossanovatech (2010b)] T. Bossanovatech. Overview polarization camera ; bossanova samba. Website product Information, February 2010. URL http://-www.bossanovatech.com/samba.htm.

[Bouguet (2008)] J.-Y. Bouguet. Matlab camera calibration toolbox. Website Caltech.edu, February 2008. URL http://www.vision.caltech.edu/bouguetj/calib doc/index.html.

[Boykov et al. (1997)] Y. Boykov, O. Veksler, and R. Zabih. Disparity component matching for visual correspondence. In *Proceedings of International Conference on Computer Vision and Pattern Recognition*, page 470–475, 1997.

[Brown et al. (2003)] M. Brown, D. Burschka, and G. Hager. Advances in computational stereo. *Pattern Analysis and Machine Intelligence, IEEE Transactions on*, 25 (8): 993 – 1008, aug. 2003. ISSN 0162-8828.

[Brunet and Chao (2004)] T. Brunet and L. Chao. Uncalibrated stereo vision. Technical report, University of Wisconsin - Madison, 2004.

[Cavallaro and Maggio (2011)] A. Cavallaro and E. Maggio. *Video tracking : theory and practice*. John Wiley Inc, 2011.

[Chiou et al. (2009)] R. N. Chiou, M. N., and T. Cronin. A biological quarter-wave retarder with excellent achromaticity in the visible wavelength region. *Nature Photonics*, 3 (11): 641–644, 2009.

[Choi et al. (2009)] S. Choi, T. Kim, and W. Yu. Performance evaluation of ransac family. *Performance Evaluation*, 24 (3): 1–12, 2009.

[Coulson (1989)] K. L. Coulson. *Polarization and intensity of light in the atmosphere*. A. Deepak Publishing, 1989.

[Cronin et al. (1994)] T. Cronin, N. Shashar, and L. Wolff. Portable imaging polarimeters. In *Pattern Recognition - Conference Computer Vision Image Processing, Proceedings of the 12th IAPR International Conference*, volume 1, pages 606 –609 vol.1, oct 1994.

[Cronin and Shashar (2001)] T. W. Cronin and N. Shashar. The linearly polarized light field in clear, tropical marine waters: Spatial and temporal variation of light intensity, degree of polarization and e-vector angle. *The Journal of Experimental Biology*, 204: 2461–2467, 2001.

[d'Angelo and Wohler (2005)] P. d'Angelo and C. Wohler. 3d reconstruction of metallic surfaces by photopolarimetric analysis. In *14th Scandinavian Image Analysis Conference, SCIA 2005*, volume 3540, pages 689–698, 2005.

[Demos et al. (2005)] S. Demos, R. Bold, R. White, and R. Ramsamooj. Investigation of near-infrared autofluorescence imaging for the detection of breast cancer. *Selected Topics in Quantum Electronics, IEEE Journal of*, 11 (4): 791 – 798, july-aug. 2005. ISSN 1077-260X.

[Drbohlav and Sara (2001)] O. Drbohlav and R. Sara. Unambiguous determination of shape from photometric stereo with unknown light sources. In *Computer Vision, 2001. ICCV 2001. Proceedings. Eighth IEEE International Conference on*, volume 1, pages 581 –586 vol.1, 2001.

[Equinox (2010)] T. Equinox. Overview equinox 3ccd multispectral/polarimetric camera. Website product Information, February 2010. URL http://-www.equinoxsensors.com/products.html.

[Faugeras (1993)] O. Faugeras. *Three-Dimensional Computer Vision: a Geometric Viewpoint*. MIT press, 1993.

[Ferraton et al. (2008)] M. Ferraton, C. Stolz, and F. Meriaudeau. Surface reconstruction of transparent objects by polarization imaging. In *Signal Image Technology and Internet Based Systems, 2008. SITIS '08. IEEE International Conference on*, pages 474 –479, 30 2008-dec. 3 2008.

[Fischler and Bolles (1981)] M. A. Fischler and R. C. Bolles. Random sample consensus: A paradigm for model fitting with applications to image analysis and automated cartography. *Communications of the ACM*, 24: 381–395, June 1981.

[Fluxdata (2009)] T. Fluxdata. Overview polarization camera ; fluxdata fd-1665 3ccd. Website product Information, September 2009. URL http://www.fluxdata.com/-products/fd-1665-polarization-camera/.

[Fusiello et al. (2000)] A. Fusiello, E. Trucco, A. Verri, and R. Verri. A compact algorithm for rectification of stereo pairs. *Machine Vision and Applications Springer Journal*, 12 (1): 16–22, July 2000.

[Gruev et al. (2009)] V. Gruev, J. Van der Spiegel, and N. Engheta. Advances in integrated polarization image sensors. In *Life Science Systems and Applications Workshop, 2009. LiSSA 2009. IEEE/NIH*, pages 62 –65, april 2009.

[Gu et al. (2010)] X. Gu, T. Cheng, D. Xie, Z. Li, T. Yu, D. Li, and Y. Qiao. Aerosol retrieval over cities using an airborne directional polarimetric camera. *SPIE Newsroom*, 2010.

[Hanlon et al. (1999)] R. T. Hanlon, M. Maxwell, N. Shashar, E. R. Loew, and K. L. Boyle. An ethogram of body patterning behavior in the biomedically and commercially valuable squid loligo pealei off cape cod, massachusetts. *Biological Bulletin*, 197: 49–62, 1999.

[Harris and Stephens (1988)] C. Harris and M. Stephens. A combined corner and edge detection. In *The Fourth Alvey Vision Conference, Manchester, UK*, page 147–151, 1988.

[Hartley and Zisserman (2000)] R. Hartley and A. Zisserman. *Multiple View Geometry in Computer Vision*. Cambridge Univ. Press, 2000.

[Hawryshyn (2000)] C. W. Hawryshyn. Ultraviolet polarization vision in fishes: possible mechanisms for coding e-vector. *Philosophical Transactions of the Royal Society of London - Series Biological Sciences*, 355 (1401): 1187–1190, 2000.

[Horvath (1995)] G. Horvath. Reflection-polarization patterns at flat water surfaces and their relevance for insect polarization vision. *Journal of Theoretical Biology*, 175 (1): 27–37, July 1995. ISSN 0022-5193.

[Hovarth (2003)] G. Hovarth. *Polarization Pattern in Nature ; Imaging Polarimetry with Atmospheric Optical and Biological Applications*. PhD thesis, Loránd Eötvös University, 2003.

[Iqbal et al. (2009)] M. Iqbal, O. Morel, and F. Meriaudeau. A survey on outdoor water hazards detection. In *the 5th International Conference on Information & Communication Technology and Systems (ICTS)*, 2009.

[Iqbal et al. (2010a)] M. Iqbal, O. Morel, and F. Meriaudeau. Choosing local matching score method for stereo matching based-on polarization imaging. In *Computer and Automation Engineering (ICCAE), 2010 The 2nd International Conference on*, volume 2, pages 334 –338, feb. 2010. doi: 10.1109/ICCAE.2010.5451536.

[Iqbal et al. (2010b)] M. Iqbal, O. Morel, and F. Meriaudeau. Extract information of polarization imaging from local matching stereo. In *Intelligent and Advanced Systems (ICIAS), 2010 International Conference on*, pages 1 –6, june 2010.

[Iqbal et al. (2011)] M. Iqbal, F. Mériaudeau, and O. Morel. Polarization stereoscopic imaging prototype. *International Journal of Signal Processing, Image Processing and Pattern Recognition (IJSIP) SERSC*, 4 (3), September 2011.

[Jacques et al. (2002)] S. L. Jacques, J. C. Ramella-Roman, and K. Lee. Imaging skin pathology with polarized light. *Biomedical Optic*, 7: 329, 2002.

[Kalayjian et al. (1997)] J. Kalayjian, A. Andreou, and L. Wolff. 1d polarisation contrast retina. In *Electronics Letter 2nd Edition*, volume 33, pages 38 –40, jan 1997.

[Kalayjian and Andreou (1999)] Z. Kalayjian and A. Andreou. A silicon retina for polarization contrast vision. In *Neural Networks, 1999. IJCNN '99. International Joint Conference on*, volume 4, pages 2329 –2332 vol.4, 1999.

[Kalayjian et al. (1996)] Z. Kalayjian, A. G. Andreou, L. Wolff, and N. Sheppard. A polarization contrast retina using patterned iodine-doped pva film. In *Solid-State Circuits Conference, 1996. ESSCIRC '96. Proceedings of the 22nd European*, pages 308 –311, sept. 1996.

[Kanade and Okutomi (1994)] T. Kanade and M. Okutomi. A stereo matching algorithm with an adaptive window: Theory and experiment. *IEEE Transactions on Pattern Analysis and Machine Intelligence*, 16 (9): 920–932, September 1994.

[Karpel and Schechner (2004)] N. Karpel and Y. Y. Schechner. Portable polarimetric underwater imaging system with a linear response. In *SPIE 5432 Polarization: Measurement, Analysis and Remote Sensing VI*, pages 106–115, 2004.

[Koshikawa and Shirai (1987)] K. Koshikawa and Y. Shirai. A model-based recognition of glossy objects using their polarimetrical properties. *Advanced Robotics*, 2: 137–147, 1987.

[Lambrinos et al. (2000)] D. Lambrinos, R. Moller, T. Labhart, R. Pfeifer, and R. Wehner. A mobile robot employing insect strategies for navigation. *Robotics and Autonomous Systems*, 30 (1-2): 39–64, 2000.

[Lane and Thacker (1998)] R. Lane and N. Thacker. Tutorial: Overview of stereo matching research. Technical Report Tina Memo Internal No. 1994-001, Imaging Science and Biomedical Engineering Division, Medical School, University of Manchester, 1998. URL www.tina-vision.net.

[Lin and Lee (1997)] S. Lin and S. W. Lee. Detection of specularity using stereo in color and polarization space. *Computer Vision and Image Understanding*, 65 (2 - Article IV960577): 336–346, February 1997.

[Lin et al. (2004)] S.-S. Lin, K. Yemelyanov, J. Pugh, E.N., and N. Engheta. Polarization enhanced visual surveillance techniques. In *Networking, Sensing and Control, 2004 IEEE International Conference on*, volume 1, pages 216 – 221 Vol.1, march 2004.

[Liou (1980)] K.-N. Liou. An introduction to athmospheric radiation. *International geophysics Academic Press*, 26, 1980. New York.

[Loop and Zhang (1999)] C. Loop and Z. Zhang. Computing rectifying homographies for stereo vision. In *Computer Vision and Pattern Recognition, 1999. IEEE Computer Society Conference on.*, volume 1, pages 2 vol. (xxiii+637+663), 1999.

[Lowe (2004)] D. G. Lowe. Distinctive image features from scale-invariant keypoints. *International Journal of Computer Vision*, 60 (2): 91–110., November 2004.

[Marshall and Shashar (1999)] C. T. W. Marshall, N. J. and N. Shashar. Behavioural evidence for polarisation vision in stomatopods reveals a potential channel for communication. *Current Biology Elsevier Science Ltd*, 9: 755–758, 1999.

[McGuire and Matusik (2006)] M. McGuire and W. Matusik. Real-time triangulation matting using passive polarization. In *SIGGRAPH Sketch*, 2006.

[Miyazaki et al. (2003)] D. Miyazaki, M. Kagesawa, and K. Ikeuchi. Polarization-based transparent surface modeling from two views. *Proceeding IEEE International Conference of Computer Vision*, 89: 1381—1386, 2003.

[Miyazaki et al. (2004)] D. Miyazaki, M. Kagesawa, and K. Ikeuchi. Transparent surface modeling from a pair of polarization images. *Pattern Analysis and Machine Intelligence, IEEE Transactions on*, 26 (1): 73 –82, jan. 2004. ISSN 0162-8828.

[Miyazaki et al. (2005)] D. Miyazaki, N. Takashima, A. Yoshida, E. Harashima, and K. Ikeuchi. Polarization-based shape estimation of transparent objects by using raytracing and plzt camera. In *Proc. SPIE*, volume 5888, 2005.

[Miyazaki et al. (2009)] D. Miyazaki, M. Ammar, R. Kawakami, and K. Ikeuchi. Estimating sunlight polarization using a fish-eye lens. *IPSJ Transactions on Computer Vision and Applications*, 1: 288–300, 2009.

[Mizera et al. (2001)] F. Mizera, B. Bernáth, G. Kriska, and G. Horváth. Stereo videopolarimetry: measuring and visualizing polarization patterns in three dimensions. *Journal of Imaging Science and Technology*, 45: 393–399, 2001.

[Moravec (1977)] H. Moravec. Towards automatic visual obstacle avoidance. In *The 5th International Joint Conference on Artificial Intelligence, Cambridge, MA*, 1977.

[Morel (2005)] O. Morel. *Environnement actif pour la reconstruction tridimensionnelle de surfaces métalliques spéculaires par imagerie polarimétrique*. PhD thesis, Université de Bourgogne, 2005. URL http://tel.archives-ouvertes.fr/tel-00514534/-fr/.

[Morel et al. (2005)] O. Morel, F. Meriaudeau, C. Stolz, and P. Gorria. Polarization imaging applied to 3d reconstruction of specular metallic surfaces. In *SPIE Electronic Imaging - Machine Vision Applications in Industrial Inspection XIII, Electronic Imaging*, volume 5679, pages 178–186, 2005.

[Morel et al. (2006)] O. Morel, C. Stolz, F. Meriaudeau, and P. Gorria. Active lighting applied to three-dimensional reconstruction of specular metallic surfaces by polarization imaging. *Appl. Opt.*, 45 (17): 4062–4068, Jun 2006.

[Morel et al. (2007)] O. Morel, R. Seulin, and D. Fofi. Measurement of the three-dimensional mirror parameters by polarization imaging applied to catadioptric camera calibration. In *IEEE/SPIE 8th International Conference on Quality Control by Artificial Vision (QCAV'2007)*, 2007. URL http://vision.u-bourgogne.fr/le2i/-user_data/publications/morel07b.pdf.

[Nave (2011)] R. Nave. Prism for polarization. Web Publishing, 2 2011. URL http://-hyperphysics.phy-astr.gsu.edu/hbase/phyopt/polpri.html#c1.

[Nishiwaki et al. (2006)] K. Nishiwaki, N. Kondo, Q. Kise, M Zhang, T. Grift, L. Tian, and K. Ting. Feasibility of using polarizing filters to reduce halation effects during image acquisition in the field. Technical report, ASABE Paper No. 063009. St. Joseph, Mich.: ASABE., 2006.

[Photonic (2009)] T. Photonic. Overview polarization camera ; pi-100 photonic-lattice. Website product Information, September 2009. URL http://www.photonic-lattice.com/en/Pol_Camera0.html.

[Rahmann (1999)] S. Rahmann. Inferring 3d scene structure from a single polarization image. In *Conference on Polarization and Color Techniques in Industrial*

Inspection, volume 3826 of SPIE Proceedings, Munich, Germany, pages 22–33, June 1999. URL http://lmb.informatik.uni-freiburg.de/people/rahmann/.

[Rahmann (2000)] S. Rahmann. Polarization images: a geometric interpretation for shape analysis. volume 3, pages 542–546, Barcelona, Spain, September 2000. URL http://lmb.informatik.uni-freiburg.de/people/rahmann/.

[Rahmann (2003)] S. Rahmann. Reconstruction of quadrics from two polarization views. In *Iberian Conference on Pattern Recognition and Image Analysis (IbPRIA03), Springer, LNCS 2652, Mallorca, Spain*, pages 810–820, June 2003. URL http://-lmb.informatik.uni-freiburg.de/people/rahmann/.

[Rahmann and Canterakis (2001)] S. Rahmann and N. Canterakis. Reconstruction of specular surfaces using polarization imaging. In *Computer Vision and Pattern Recognition, 2001. CVPR 2001. Proceedings of the 2001 IEEE Computer Society Conference on*, volume 1, pages I–149 – I–155 vol.1, 2001.

[Ramella-Roman et al. (2003)] J. C. Ramella-Roman, K. Lee, S. A. Prahl, and S. L. Jacques. Polarized light imaging with a handheld camera. In V. V. Tuchin, editor, *SPIE Saratov Fall Meeting 2002: Optical Technologies in Biophysics and Medicine IV*, volume 5068, 2003.

[Rankin and Matthies (2008)] A. Rankin and L. Matthies. Daytime mud detection for unmanned ground vehicle autonomous navigation. In *The 26th Army Science Conference*, December 2008.

[Rantoson et al. (2009)] R. Rantoson, C. Stolz, D. Fofi, and F. Meriaudeau. 3d reconstruction by polarimetric imaging method based on perspective model. *SPIE Europe Optical Metrology*, 15, june 2009.

[Sabbah et al. (2006)] S. Sabbah, A. Barta, J. Gal, G. Horvath, and N. Shashar. Experimental and theoretical study of skylight polarization transmitted through snell's window of a flat water surface. *J. Opt. Soc. Am. A*, 23 (8): 1978–1988, Aug 2006.

[Sadjadi and Chun (1996)] F. Sadjadi and C. Chun. Improved feature classification by means of a polarimetric ir imaging sensor. In *Geoscience and Remote Sensing*

Symposium, 1996. IGARSS '96. 'Remote Sensing for a Sustainable Future.', International, volume 1, pages 396 –398 vol.1, may 1996.

[Saito et al. (1999a)] M. Saito, Y. Sato, K. Ikeuchi, and H. Kashiwagi. Measurement of surface orientations of transparent objects using polarization in highlight. In *Computer Vision and Pattern Recognition, 1999. IEEE Computer Society Conference on.*, volume 1, page 386 Vol. 1, 1999.

[Saito et al. (1999b)] M. Saito, Y. Sato, K. Ikeuchi, and H. Kashiwagi. Measurement of surface orientations of transparent objects using polarization in highlight. 16 (9): 2286–2293, September 1999.

[Sarafraz et al. (2009)] A. Sarafraz, S. Negahdaripour, and Y. Schechner. Enhancing images in scattering media utilizing stereovision and polarization. In *Applications of Computer Vision (WACV), 2009 Workshop on*, pages 1 –8, dec. 2009.

[Scharstein and Szeliski (2008)] D. Scharstein and R. Szeliski. Stereo vision research page. Website Research, 2008. URL http://vision.middlebury.edu/stereo/.

[Schechner and Karpel (2005)] Y. Schechner and N. Karpel. Recovery of underwater visibility and structure by polarization analysis. *Oceanic Engineering, IEEE Journal of*, 30 (3): 570 –587, july 2005. ISSN 0364-9059.

[Schechner et al. (2001)] Y. Y. Schechner, S. G. Narasimhan, and S. K. Nayar. Instant dehazing of images using polarization. In *Proceding IEEE CVPR*, volume Vol. I, pages 325–332, 2001.

[Schechner et al. (2003)] Y. Y. Schechner, S. G. Narasimhan, and S. K. Nayar. Polarization-based vision through haze. *Applied Optics - Special issue about Light and Color in the Open Air.*, 42, No. 3: pp. 511–525, 2003.

[Shamaraz and Masroor (2005)] F. Shamaraz and I. Masroor. Imaging of biological tissues with optical coherence tomography system using jones-mueller calculus. *SPIE Optical Coherence Tomography and Coherence Techniques II*, 5861: 237–244, 2005.

[Shashar and Cronin (1996)] N. Shashar and T. W. Cronin. Polarization contrast vision in octopus. *The Journal of Experimental Biology*, 199: 999–1004, 1996.

[Shashar et al. (2000)] N. Shashar, R. Hagan, J. G. Boal, and R. T. Hanlon. Cuttlefish use polarization sensitivity in predation on silvery fish. *Vision Research*, 40 (1): 71 – 75, 2000. ISSN 0042-6989.

[Shtykov and Vija (2003)] N. Shtykov and J. K. Vija. Measurement of the polarization profile across a surface-stabilized ferroelectric liquid crystal cell using the pyroelectric laser-intensity-modulation method. *Journal of Applied Physics*, 93 (1): 159–164, 2003.

[Shurcliff (1980)] W. A. Shurcliff. *Polarized Light : Production and Use*. Oxford university press, London, 1980.

[Srinivasan (2011)] M. V. Srinivasan. Honeybees as a model for the study of visually guided flight, navigation, and biologically inspired robotics. *Physiol Rev*, 91 (2): 413–60, 2011. ISSN 1522-1210. URL http://www.biomedsearch.com/nih/-Honeybees-as-model-study-visually/21527730.html.

[Szeliski and Scharstein (2002)] R. Szeliski and D. Scharstein. Symmetric sub-pixel stereo matching. In *7th European Conference on Computer Vision*, volume volume 2, page 525–540, Copenhagen, Denmark, May 2002.

[Szeliski and Zabih (1999)] R. Szeliski and R. Zabih. An experimental comparison of stereo algorithms. *Vision Algorithms: Theory and Practice*, (1883): 1–19, 1999.

[Terrier and Devlaminck (2000)] P. Terrier and V. Devlaminck. A device to classify surface orientation from polarization images. In *Image Processing, 2000. Proceedings. 2000 International Conference*, volume 2, pages 495 –498 vol.2, sept. 2000.

[Ulrich (2008)] I. Ulrich. Cmu 1394 digital camera driver. Website Product, March 2008. URL http://www.cs.cmu.edu/~iwan/1394/.

[Usher et al. (2001)] K. Usher, P. Corke, , and P. Ridley. A camera as a polarised light compass: Preliminary experiments. In *the Australian Conference on Robotics and Automation, Sydney, Australia*, pages 116–120, November 2001.

[Vedel et al. (2010)] M. Vedel, N. Lechocinski, and S. Breugnot. Compact and robust linear stokes polarization camera. *EPJ Web of Conferences*, 5: 01005, 2010.

[Wehner (2001)] R. Wehner. Polarization vision - a uniform sensory capacity? *J Exp Biol*, 204 (14): 2589–2596, 2001.

[Wolff (1989)] L. Wolff. Using polarization to separate reflection components. In *Computer Vision and Pattern Recognition, 1989. Proceedings CVPR '89., IEEE Computer Society Conference on*, pages 363 –369, jun 1989.

[Wolff (1990a)] L. Wolff. Polarization-based material classification from specular reflection. *Pattern Analysis and Machine Intelligence, IEEE Transactions on*, 12 (11): 1059 –1071, nov 1990. ISSN 0162-8828.

[Wolff et al. (1997)] L. Wolff, T. Mancini, P. Pouliquen, and A. Andreou. Liquid crystal polarization camera. volume 13, pages 195 –203, apr 1997.

[Wolff et al. (1998)] L. Wolff, A. Lundberg, and R. Tang. Image understanding from thermal emission polarization. In *Computer Vision and Pattern Recognition, 1998. Proceedings. 1998 IEEE Computer Society Conference on*, pages 625 –631, jun 1998.

[Wolff (1990b)] L. B. Wolff. Surface orientation from two-camera stereo with polarizers. In D. J. Svetkoff, editor, *Society of Photo-Optical Instrumentation Engineers (SPIE) Conference Series*, volume 1194 of *Presented at the Society of Photo-Optical Instrumentation Engineers (SPIE) Conference*, pages 287–297, April 1990.

[Wolff (1994)] L. B. Wolff. Polarization camera for computer vision with a beam splitter. *J. Opt. Soc. Am. A*, 11 (11): 2935–2945, Nov 1994.

[Wolff and Andreou (1995)] L. B. Wolff and A. G. Andreou. Polarization camera sensors. *Image and Vision Computing*, 13 (6): 497 – 510, 1995. ISSN 0262-8856.

[Wolff and Boult (1991)] L. B. Wolff and T. E. Boult. Constraining object features using a polarization reflectance model. 13 (7): 635–657, July 1991.

[Wolff and Kurlander (1990)] L. B. Wolff and D. J. Kurlander. Ray tracing with polarization parameters. *IEEE Comput. Graph. Appl.*, 10: 44–55, November 1990. ISSN 0272-1716.

[Woollam (2011)] J. A. Woollam. Tutorial light materials part 1. Website J.A. Woollam Ellipsometry Solution, May 2011. URL http://www.jawoollam.com/tutorial_2.html.

[Xie et al. (2007)] B. Xie, Z. Xiang, H. Pan, and J. Liu. Polarization-based water hazards detection for autonomous off-road navigation. In *Intelligent Robots and Systems, 2007. IROS 2007. IEEE/RSJ International Conference on*, pages 3186 –3190, oct. 2007.

[Xie (1997)] M. Xie. Automatic feature matching in uncalibrated stereo vision through the use of color. *Robotics and Autonomous Systems*, 21 (4): 355 – 364, 1997. ISSN 0921-8890.

[Xuan et al. (2007)] J. Xuan, U. Klimach, H. Zhao, Q. Chen, Y. Zou, and Y. Wang. Improved diagnostics using polarization imaging and artificial neural networks. *Journal of Biomedical Imaging*, 2007 (2): 1–9, 2007. ISSN 1687-4188.

[Zabih and Woodfill (1994)] R. Zabih and J. Woodfill. Non-parametric local transforms for computing visual correspondence. In *Proc. of the Third European Conference*, volume 2, pages 151–158, 1994.

[Zhang and Kambhamettu (2002)] Y. Zhang and C. Kambhamettu. Stereo matching with segmentation-based cooperation. In *Proceedings 7th European Conference on Computer Vision*, volume 2, page 556–571, Copenhagen, Denmark, May 2002.

[Zhou et al. (2007)] B. Zhou, J. Xuan, H. Zhao, G. Chepko, M. Freedman, and K. Y. Zou. Polarization imaging for breast cancer diagnosis using texture analysis and svm. In *Life Science Systems and Applications Workshop, 2007. LISA 2007. IEEE/NIH*, pages 217 –220, nov. 2007.

Appendix A

Allied Vision Technology Camera Guppy F-080B/C

Specification :

Feature	**Specification**
Image device Type	1/3 (diag. 6 mm) progressive scan SONY IT CCD ICX204AL/AK with HAD microlens
Effective chip size	4.8 mm x 3.6 mm
Cell size	4.65 µm x 4.65 µm
Lens mount	• C-Mount: 17.526 mm (in air), Ø 25.4 mm (32 tpi), mechanical flange back to filter distance: 9.5 mm • CS-Mount: 12.526 mm (in air), Ø 25.4 mm (32 tpi), mechanical flange back distance: 8 mm
Picture size (max.)	1032 x 778 (Format_7 Mode_0)
ADC	12 bit
Frame rates	3.75 fps; 7.5 fps; 15 fps; 30 fps variable frame rates in Format_7 up to 30 fps
Gain control	Manual: 0-24 dB (0.035 dB/step); auto gain (select. AOI)
Shutter speed	54 µs …67,108,864 µs (~67s); auto shutter (select. AOI)
External trigger shutter	• Trigger_Mode_0, Trigger_Mode_1, advanced feature: • Trigger_Mode_15 (bulk); image transfer by command; trigger delay
Look-up table	One, user programmable (10 bit → 8 bit); gamma (0.5)
Smart functions	• AGC (auto gain control), AEC (auto exposure control), LUT (look-up table) only color: AWB (auto white balance) • One configurable input, three configurable outputs, RS-232 port (serial port, IIDC V1.31)
Transfer rate	100 Mbit/s, 200 Mbit/s, 400 Mbit/s
Digital interface	IEEE 1394a IIDC V1.3

Feature	Specification
Power requirements	DC 8 V - 36 V via IEEE 1394 cable or 8-pin HIROSE
Power consumption	Less than 2 watt (@ 12 V DC)
Dimensions	48.2 mm x 30 mm x 30 mm (L x W x H); without tripod and lens
Mass	50 g (without lens)
Operating temperature	+ 5 °C ... + 45 °C housing temperature (without condensation)
Storage temperature	- 10 °C ... + 60 °C ambient temperature (without condensation)
Regulations	FCC Class B, CE, RoHS (2002/95/EC)
Standard accessories	• b/w: C/CS-Mount with built-in protection glass • color: C/CS-Mount with built-in IR cut filter
Optional accessories	• Board level OEM version • b/w: C/CS-Mount: IR cut filter / IR pass filter available as CSMount adapter. • color: C/CS-Mount: protection glass available as CS-Mount adapter.
Software packages	• AVT FirePackage (SDK and Viewer, 100% control the bus) • AVT Direct FirePackage (SDK and Viewer, compatible to DirectX and WDM) • AVT Fire4Linux (SDK and Viewer, compatible to RedHat and Suse Distributions)

Block Diagram of AVT CCD Camera :

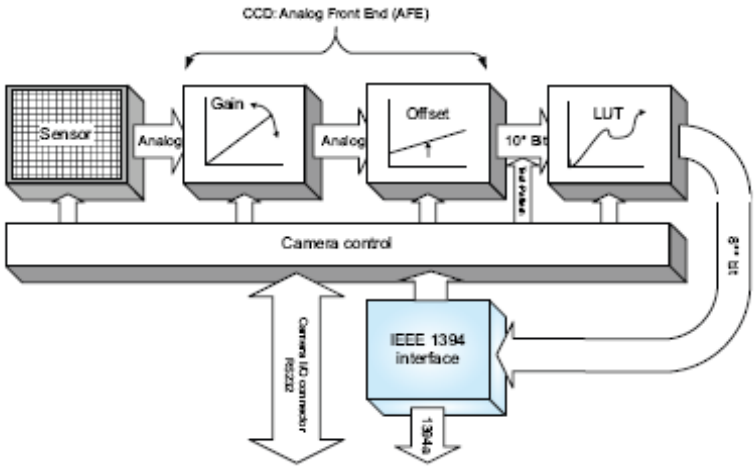

Fig. 1: Block diagram CCD b/w camera

Frame Rates :

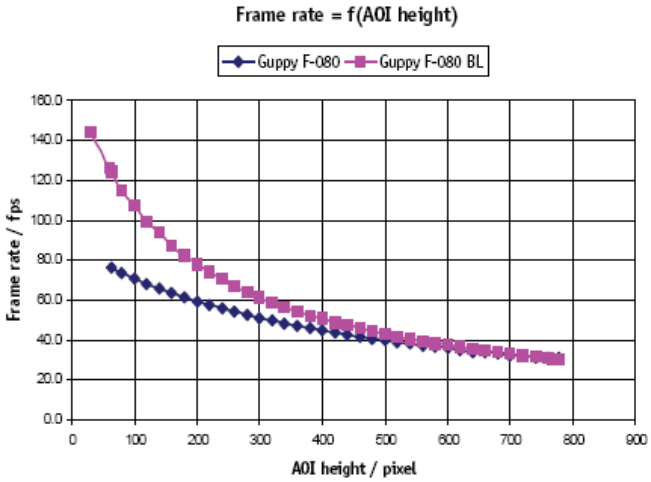

Fig. 2: Frame rates GUPPY F-080 and board level versions

Video Format, Modes and bandwidth :

Format	Mode	Resolution	Color mode	60 fps	30 fps	15 fps	7.5 fps	3.75 fps	1.875 fps
0	0	160 x 120	YUV444						
	1	320 x 240	YUV422						
	2	640 x 480	YUV411						
	3	640 x 480	YUV422						
	4	640 x 480	RGB8						
	5	640 x 480	MONO8		x x*	x x*	x x*	x x*	
	6	640 x 480	MONO16						
1	0	800 x 600	YUV422						
	1	800 x 600	RGB8						
	2	800 x 600	MONO8		x x*	x x*	x x*		
	3	1024 x 768	YUV422						
	4	1024 x 768	RGB8						
	5	1024 x 768	MONO8		x x*	x x*	x x*	x x*	
	6	800 x 600	MONO16						
	7	1024 x 768	MONO16						
7	0	1032 x 778	MONO8	@30 fps					
		1032 x 778	Raw8	@30 fps					
	1								
	2								
	3								

Camera Interface :

The IEEE 1394a plug is designed for industrial use and has the following pin assignment as per specification:

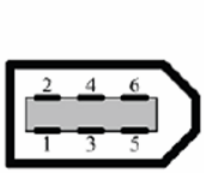

Pin	Signal
1	Cable power
2	Cable GND
3	TPB-
4	TPB+
5	TPA-
6	TPA+

Fig. 3 : IEEE 1394 (FireWire) Interface

Sensor Position Accuracy of AVT Camera :

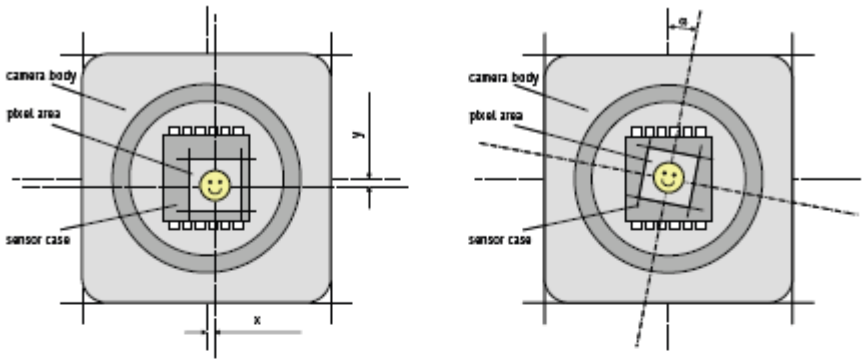

AVT Guppy Series

Method of Positioning:	Automated mechanical alignment of sensor into camera front module. (lens mount front flange)		
Reference points:	Sensor: Center of pixel area (photo sensitive cells). Camera: Center of camera front flange (outer case edges).		
Accuracy:	x/y:	+/- 0.25mm	(Sensor shift)
	z:	+50 / -100µm	(for SN > 84254727, optical back focal length)
		+0 / -100µm	(for SN > 252138124, optical back focal length)
	α:	+/- 1°	(Sensor rotation)

AVT Marlin, Oscar, Dolphin, Pike, Stingray

Method of Positioning:	Optical alignment of photo sensitive sensor area into camera front module. (lens mount front flange)		
Reference points:	Sensor: Center of pixel area (photo sensitive cells). Camera: Center of camera front flange (outer case edges).		
Accuracy:	x/y:	+/- 0.1mm	(Sensor shift)
	z:	+0 / -50µm	(Optical back focal length)
	α:	+/- 0.5°	(Sensor rotation)

Note: x/y - tolerances between c-Mount hole and pixel area may be higher.

Spectral Sensitivity :

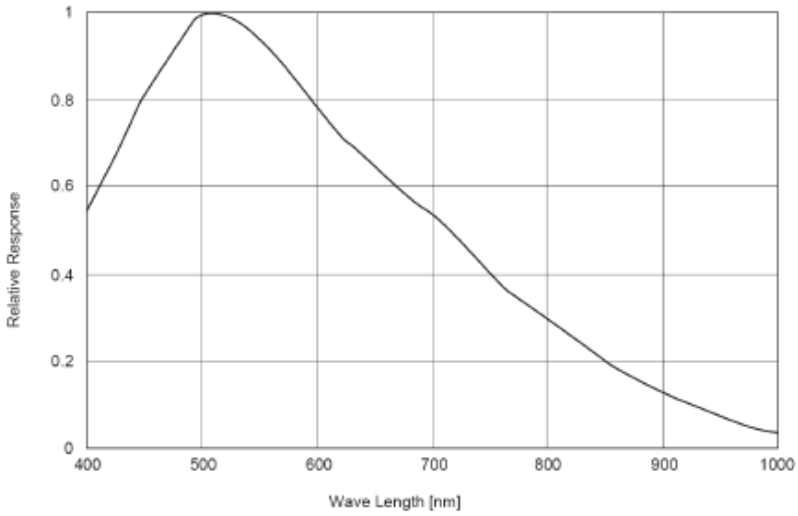

Fig. 4 : Spectral sensitivity of Guppy F-080B without cut filter and optics

Lens Mount :

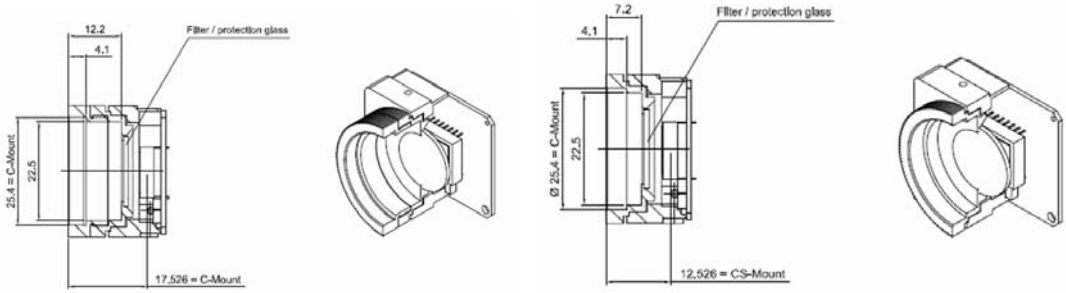

Fig. 5: Guppy C-Mount (left) and CS-Mount (right) dimensions

Information :

Allied Vision Technologies Germany

Taschenweg 2A, D-07646 Stadtroda, Germany

e-mail: info@alliedvisiontec.com , Tel.: +49 (0)36428 6770 Fax: +49 (0)36428 677-28

Appendix B

ARCoptix Achromatic switchable polarization rotator

Specification :

Twist	45° or 90° (custom twist possible)
Twist accuracy	±1°
Output ellipticity	Between 0.1 and 10% (depending of the model and the wavelength)
wavelength range	350-1800 nm
Active area	10 mm or 20mm (diam.)
Transmission	> 85% (VIS)
retarder material	Nematic Liquid-Crystal
Substrates	Glass
wavefront distortion	< lamda/4
temperature range	15°-35°
Anti-reflection	Coating Broadband VIS
Retardance temperature dependency	About 0.5%/°C (wavelength dependent)
Housing size	25 mm in diam. 15mm deep

Transmission :

Total transmission of the TN cells (including losses due to reflections) is given by the graph below. For lower absorption losses Anti-reflection coatings are necessary. The transmission is identical for all the models.

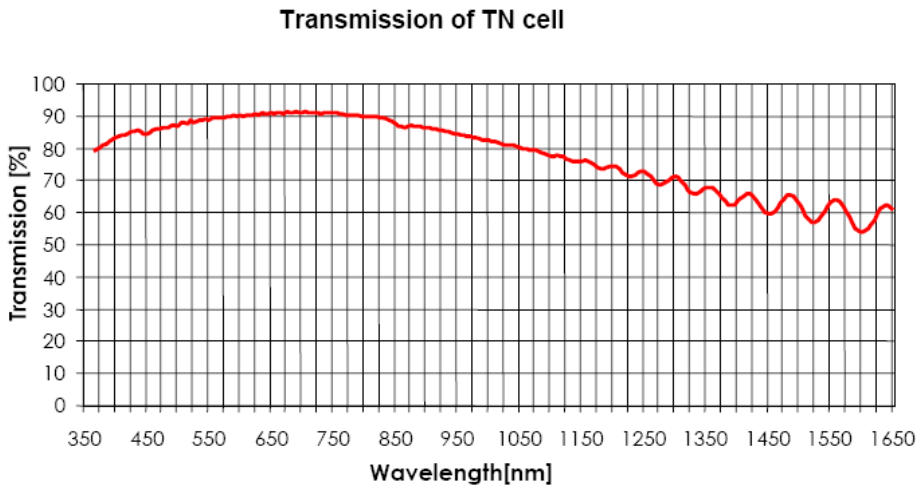

Fig. 1: Transmission of the TN cell (all models) without polarizers.

Rotatory efficiency:

As explained in the previous section, the rotatory efficiency can be quantified by measuring the transmission of the TN cell when it placed between two ideal parallel polarizers.

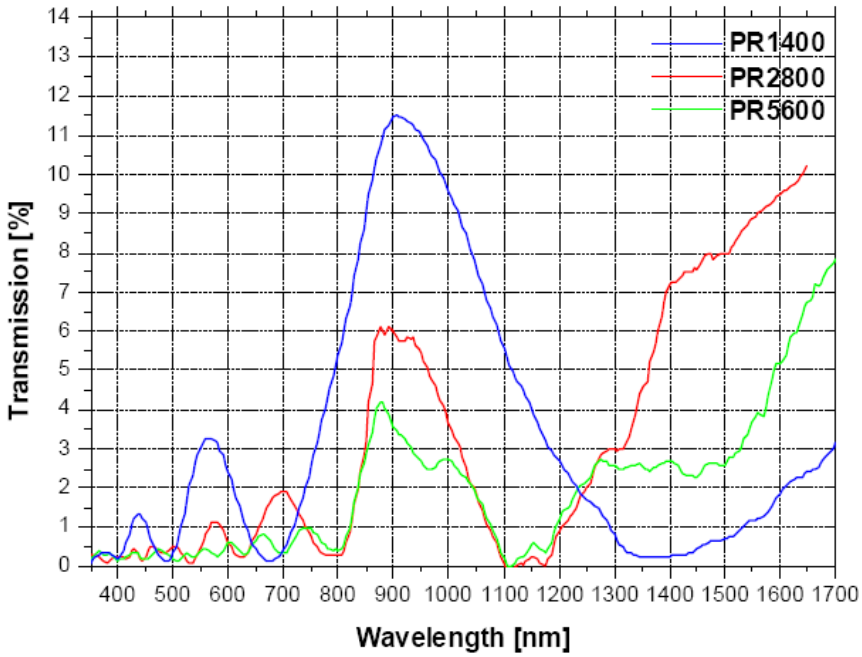

Fig 2: Measured transmission (when placed between two Glan-Thomson polarizers) for the three standard models In summary the (extinction ratio) for the three standard models

Types of products:

Type of Product	Field of application	Properties
45° and 90° high end polarization rotators (scientific grade)	Scientific applications	No spacers over the aperture. Minimal wavefront distortion (λ/4) and AR coating
Industrial large series cells (industrial grade)	Industrial applications	Cost effective, industrial quality, compact, some wavefront distortion and spacers distributed over the aperture
Custom made	Scientificindustrial application	Optimized for minimal switching time, specific angle of rotation, specific size, specific wavelength.

In summary the (extinction ratio) for the three standard models :

Model	Mean Extinction ratio 350-800nm	Switching time
PR1400	4%	25ms
PR2800	2% (1/500 at 633nm)	70ms
PR5600	Below 1%	150ms

Electrical connection:

The phase shifter must be connected to an alternative power supply providing a square wave of minimal ±6 V. The frequency of the bias must ideally be around 100 Hz and there should be a polarity inversion. LC driver can be supplied by ARCoptix if necessary.

Electrical driving:

The polarization converter needs to be connected to an alternative (AC) power supply producing a square wave signal with change of polarity (oscillating between positive and negative bias). To drive the polarization rotator there are essentially two options:

1) Use the Arcoptix digital LC Driver that has two independent outputs that are computer controlled via USB and optimized for liquid crystal device driving (see figure 2). It generates a square signal of 1.6 KHz with variable amplitude between 0V and 9V. The LC driver produces a highly stable signal with a precision of 1mV. However only two levels are relevant for driving the cell 0V and 9V (e.g.

minimal and maximal value) for switching off and on the TN cell. External trigger can be obtained on demand.

2) Use a standard labor generator with square wave signal. The should be somewhere around 0.1-1 kHz and the amplitude should be variable between 0 and 5V (almost no current).

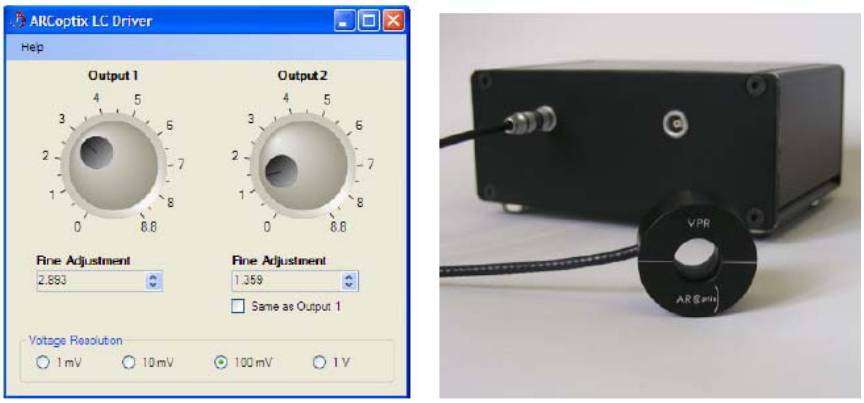

Fig 3: LC Driver with two independent outputs that are computer controlled via USB.

Housing:

The Housing (for scientific grade only) is made of anodized aluminum. It has a diameter of 25mm. The optical axis is indicated by a stripe.

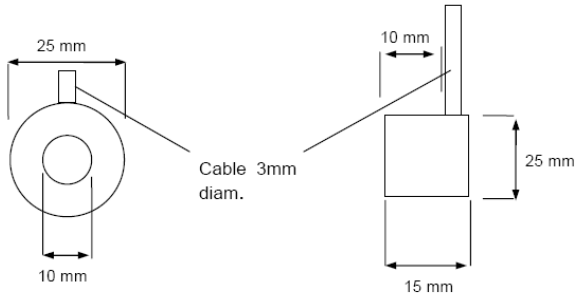

Fig 4: Housing Illustration

Information :

ARCoptix S.A

Trois-portes 18, 2000 Neuchâtel, Switzerland

Mail: info@arcoptix.com, Tel: ++41 32 731 04 66